EXAMINING RIBONUCLEASES AND G-QUADRUPLEX BINDING PROTEINS AS REGULATORS OF GENE EXPRESSION IN *S. VENEZUELAE*

EXAMINING RIBONUCLEASES AND G-QUADRUPLEX BINDING PROTEINS AS REGULATORS OF GENE EXPRESSION IN *S. VENEZUELAE*

By: EMMA MULHOLLAND, B.Arts.Sc.

A Thesis Submitted to the School of Graduate Studies in Partial Fulfillment of the Requirements for the Degree Master of Science

McMaster University MASTER OF SCIENCE (2020) Hamilton, Ontario (Biology)

TITLE: Examining ribonucleases and G-quadruplex binding proteins as regulators of gene expression in S*. venezuelae*

AUTHOR: Emma Mulholland, B.Arts.Sc. (McMaster University)

SUPERVISOR: Dr. Marie Elliot

NUMBER OF PAGES: xiii, 95

Abstract

Controlling when genes are expressed is critical for the growth of an organism. Studying gene expression regulation in *Streptomyces* presents an opportunity to better understand how these complex bacteria develop and how they control their impressive biosynthetic capabilities. In this work we investigated the potential role of a G-quadruplex binding protein, and two ribonucleases (RNases) in regulating gene expression in *Streptomyces venezuelae.* G-quadruplexes are structures that form in DNA or RNA molecules. Depending on their location in DNA, G-quadruplexes can increase or decrease the expression of nearby genes and the stability of a G-quadruplex structure can be affected by G-quadruplex binding proteins. We probed the ability of a G-quadruplex-associated protein from *S. venezuelae*, TrmB (a tRNA-methyltransferase), to bind and methylate G-quadruplexes and prevent the formation of these structures. We were unable to conclude that TrmB bound or methylated G-quadruplex structures or motifs. RNases are enzymes that cleave RNA molecules and have important roles in controlling cellular RNA levels, and thus gene expression. We investigated the roles of RNase J and RNase III in *S. venezuelae*. Both of these RNases impact development and specialized metabolism in *Streptomyces.* We found that the RNase J mutant was unable to grow properly on classical medium containing glycerol. We also documented small RNA fragments that were unique to the RNase J mutant and sought to identify them. To better understand the RNase J and RNase III strains, we conducted RNA-sequencing of wild type *S. venezuelae* and mutant strains lacking RNase III or RNase J. Comparisons between each mutant and the wild type strain revealed significant changes in genes related to nitrogen assimilation, phosphate uptake, and specialized metabolite production in both the RNase III and RNase J mutant. Together these results contribute to our understanding of the diverse regulatory features that exist in *S. venezuelae*.

Acknowledgements

Firstly, an immense thank-you to my supervisor, Dr. Marie Elliot. For the past four years you have shown me what it means to be a dedicated and engaged scientist, educator, and mentor. The integrity and enthusiasm you bring to every aspect of your work is a source of daily inspiration. When the world turned upside down six months ago, I felt anxious, but knowing that you had the back of everyone in our lab meant that one thing I wasn't worried about was my work. I will be forever grateful. Thank you as well to my committee members, Dr. Turlough Finan and Dr. Yingfu Li for your guidance and direction on this project.

To my parents—who have driven the route from Waterloo to Hamilton so many times now that they could probably do it with their eyes closed—thank you (and please don't test my theory). Thank you for your love and encouragement in all its forms: text messages, weekend visits, frozen meals, and hugs are just a few things that come to mind. Thank you, Sarah, for being the best quarantine and thesis-writing roommate. Also, to Adrian, Maverick, Marco, Katelyn, Paulina, Leah, and Michelle: we might not be in the same house, or city, anymore but you have been with me on every step of this journey since first year. Thank you for keeping me smiling.

Finally, thank you to all the members past and present of the Elliot lab, especially those who welcomed me into the lab as a nervous undergraduate. To Savannah Colameco—you are the coolest, smartest person I have ever met and to this day I ask myself "what would Savannah do?" when I don't know the answer. To Dr. Hindra, Dr. Michelle Williams, and Dr. Tina Netzker— the three of you are science superheroes, thanks for putting up with all my questions. To Xiafei Zhang—thanks for the guidance and the laughs and for showing me how to be a good TA. When I leave you can annex my space and really have the largest bench in the lab. To Matt Zambri— I'm sorry for all the puns (but I'm also not sorry enough to stop telling them). To Meghan Pepler—learning in a lab meeting about how fish "deposit" bacteria on their eggs will forever

remain a highlight of my academic experience. Lastly, to Evan Shepherdson—thanks for always laughing at my bad jokes and then making me feel better by telling a worse one. It has been a joy and a privilege to work with you all over the past three years.

Table of Contents

List of Figures

List of Tables

List of Abbreviations

×	times
Δ	deletion
°	degree
α	alpha
γ	gamma
µ	micro
µg	microgram
µL	microlitre
µM	micromolar
A	adenine
C	cytosine
CD	circular dichroism
cm	centimeter
dH_20	distilled water
DNA	deoxyribonucleic acid
DNase	deoxyribonuclease
dNTP	deoxy nucleoside triphosphate
EMSA	electrophoretic mobility shift assay
g	gravity
G	guanine
gDNA	genomic DNA
GQ	G-quadruplex
h	hour
IPTG	isopropyl β-D-1-thiogalactopyranoside
kb	kilobase
LB	lysogeny broth
M	molar
mCi	millicurie
mg	milligram
min	minute
mL	millilitre
mM	millimolar
mRNA	messenger RNA
MYM	maltose-yeast extract-malt extract
MYMG	maltose-yeast extract-malt extract-glycerol
N	any nucleotide
NF H_20	nuclease free water
nm	nanometer
nM	nanomolar
OD	optical density

P^{32}	phosphorus-32 isotope
P-adj	adjusted P-value
PCR	polymerase chain reaction
pmol	picomole
RNA	ribonucleic acid
RNase	ribonuclease
rnc	*RNase III* (gene denotation)
rnj	*RNase J* (gene denotation)
RPM	revolutions per minute
rRNA	ribosomal RNA
RT	reverse transcription
SDS	sodium dodecyl sulfate
SFM	soy flour-mannitol
T	thymine
tRNA	transfer RNA
U	unit
UTR	untranslated region
UV	ultraviolet
V	volt
W	watt
WT	wild type
YP	yeast-peptone

1. Introduction

1.1 Regulation of gene expression

Organisms live in complex environments and can encounter many different environmental stimuli throughout their life. They need to respond to these stimuli in order to survive and organisms can accomplish this is by altering their gene expression patterns. Bacteria, like all living things, are capable of fine-tuning gene expression through a combination of different regulatory mechanisms, including transcriptional, post-transcriptional, translational, and post-translational regulation.

Transcriptional regulation is a process that increases or decreases the transcription of a gene into RNA. The transcription level of a gene can be influenced by the structure and composition of its promoter, the presence or absence of various transcription factors, and other elements such as sigma factors and small molecules (1–4).

Post-transcriptional regulation alters the stability of a transcribed RNA molecule. This can be mediated by modifications to an RNA molecule, such as adenylation, or through changes that can promote or prevent degradation of the RNA, like the binding of sRNAs (5, 6). sRNAs are small, non-coding RNA molecules. An sRNA bound to a target RNA molecule can increase the stability of the molecule by blocking ribonuclease (RNase) access to that molecule or it may decrease the stability by recruiting RNases (7, 8). sRNAs can also have a role in translational regulation by binding mRNA molecules and causing a conformation change that unblocks previously occluded translation initiation sites (9). Structures in an RNA molecule can function similarly to sRNAs by occluding or opening sites that are important for translation initiation (10). Translation can also be affected by the composition of the emerging peptide which, under certain circumstances, can interact with the ribosome and cause ribosome stalling (11).

Finally, gene expression can be affected post-translationally through protein modifications that alter the function and stability of proteins. For example, the addition of different small peptide tags to a protein can direct that protein for secretion or cause it to be targeted for degradation (12, 13). Through these various regulatory strategies, bacteria can adjust their levels of gene expression to effectively respond to changes in their environment.

All of these methods of regulation are interrelated and connected in bacteria. For example, the transcriptional regulator GlnR controls the expression of nitrogen assimilation genes in *Streptomyces* by activating or repressing its various target genes, with GlnR itself being regulated post-translationally through phosphorylation (14, 15). This work is focused on primarily understanding mechanisms of post-transcriptional regulation mediated through RNases and nucleic acid structures in *Streptomyces*.

1.2 *Streptomyces* introduction

1.2.1 Classical *Streptomyces* life cycle

From a microbiological perspective, soil is a dynamic and highly competitive environment. Soil-dwelling bacteria must therefore be particularly adept at responding to their environment and be well prepared to face a wide variety of environmental stressors. One type of soil-dwelling bacteria is *Streptomyces*, a genus of Gram-positive bacteria known for its remarkable biosynthetic capabilities and complex life cycle.

The classical model of the *Streptomyces* life cycle begins with spore germination, when a spore reaches a favourable growth environment (Figure 1.1). Following germination, a network of branching hyphae develops during vegetative growth; these hyphae can extend throughout the growth medium. Various environmental and developmental cues then trigger the emergence of aerial hyphae, which grow up and away from the colony as non-branching hyphae (16). The start of aerial growth coincides with the production of various specialized metabolites by *Streptomyces* within the

vegetative mycelium. The final stage of the life cycle is sporulation, which occurs when the aerial hyphae are subdivided and form chains of spores. The aerial hyphae are first partitioned into chains of pre-spore compartments that each contain one copy of the genome. These compartments mature into dormant spores with thick cell walls and, in *Streptomyces venezuelae*, green pigment is deposited into the walls of this spore coat (16). The spores are subsequently dispersed into the environment, allowing the cycle to begin again. Although many streptomycetes have been studied and characterized, *S. venezuelae* is an excellent model organism for this genus because, unlike other *Streptomyces* species, it grows quickly and well-dispersed in liquid medium and fully differentiates through each life stage, facilitating rapid analysis of growth and development in liquid culture.

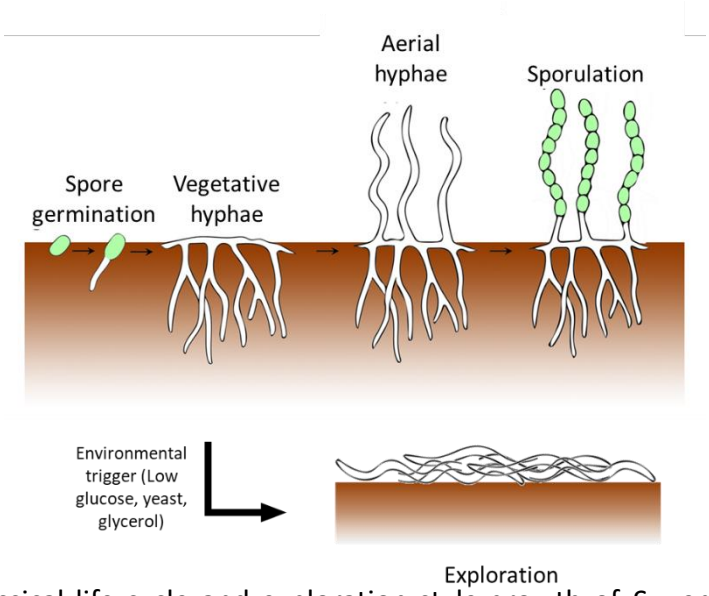

Figure 1.1. Classical life cycle and exploration-style growth of *S. venezuelae*. In the classical life cycle, *S. venezuelae* begins as a spore that then germinates and grows into a network of branching, vegetative hyphae. Non-branching aerial hyphae then emerge from the vegetative mycelium. These aerial hyphae are then sub-divided into spores which, when mature, are dispersed into the environment. Under particular growth conditions, *S. venezuelae* shifts from the classical model of growth to 'exploration', where it grows rapidly outwards as non-branching vegetative hyphae instead of going through full vegetative, aerial, and sporulation stages of growth. (Modified from 17).

1.2.2 Exploration as an alternative mode of growth in *Streptomyces*

In addition to the classical life cycle described above, several *Streptomyces* species, including *S. venezuelae,* can adopt an alternative form of growth called "exploration" (17). In exploratory growth, *Streptomyces* colonies grow rapidly outwards as non-branching, vegetative hyphae, contrary to the more stationary development associated with the classical life cycle (Figure 1.1). Exploration can be triggered on solid medium by different conditions, including co-culture with *Saccharomyces cerevisiae* or growth on a low glucose medium (17). Recent work has shown that the addition of glycerol to the classic *Streptomyces* growth medium, maltose-yeast extract-malt extract (MYM), can also promote exploration in *S. venezuelae* (Shepherdson, unpublished). When grown on MYM medium with glycerol (MYMG), *S. venezuelae* grows rapidly outwards as in exploration, but the central region of the colony still progresses through aerial growth and sporulation as in the classical model of growth (Shepherdson, unpublished).

1.2.3 Biosynthetic capabilities and silent gene clusters in *Streptomyces*

Over two-thirds of naturally derived antibiotics come from various *Streptomyces* species, making them an important biomedical resource (18). *Streptomyces* are also the source of anti-cancer drugs, anti-fungal agents, and herbicides; the genetic underpinning of these compounds are the biosynthetic gene clusters contained in the genomes of *Streptomyces* species. Whole genome sequencing has revealed that these bacteria have the potential to produce many more bioactive natural products than are currently documented in the lab (19). While one species may only produce one or two compounds when grown under laboratory conditions, it may contain 20 to 40 predicted biosynthetic gene clusters, the majority of which are transcriptionally inactive (19). Understanding why these gene clusters are silent and how they might be regulated will help unlock the full biosynthetic potential of these bacteria.

1.3 Gene expression regulation in *Streptomyces* is complex and multifaceted

1.3.1 Comparison of nitrogen assimilation regulation between *E. coli* and *Streptomyces*

Streptomyces contain the genes for many of the same regulatory systems found in other bacteria, but these systems are not identical in *Streptomyces*. An example is the Ntr system, which regulates nitrogen assimilation in many Gram-negative bacteria and has been extensively studied in *Escherichia coli* (20). In general, cells assimilate nitrogen by incorporating ammonium through the production of glutamine and glutamate via the enzymes glutamine synthetase, glutamate synthase, and glutamate dehydrogenase (Figure 1.2) (20). The activity level of these enzymes depends on the availability of

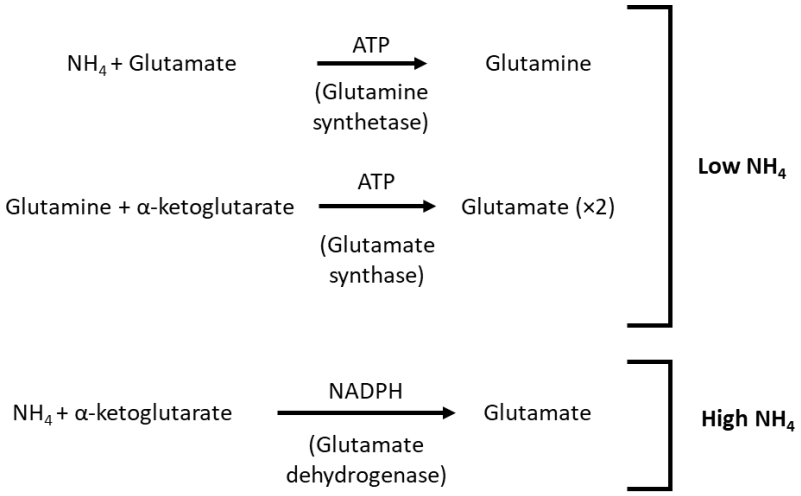

Figure 1.2. Schematic showing the predominant nitrogen assimilation pathways in bacteria at different NH_4 concentrations. (Modified from 21 and 23).

nitrogen: in high-nitrogen environments, the enzyme glutamate dehydrogenase adds ammonium directly to α-ketoglutarate to produce one molecule of glutamate, which can then be converted to glutamine by glutamine synthetase (21). In low-nitrogen environments, glutamine synthetase adds ammonium to glutamate to make glutamine, while glutamine, alongside α-ketoglutarate, can in turn be used by glutamate synthase to produce two molecules of glutamate (21). In this system, glutamine synthetase (GSI) is of particular importance and its activity is directly regulated through the Ntr system.

1.3.1.1 Transcriptional and post-translational regulation of glutamine synthetase in *E. coli*

In *E. coli* GSI is regulated both transcriptionally and post-translationally. The two-component system NtrB/NtrC senses nitrogen abundance through GlnD and the P_{II} protein (encoded by *glnB* and *glnK,* respectively), and in nitrogen-limited conditions can activate transcription of the gene encoding GSI, *glnA* (21). Glutamine synthetase is also regulated post-translationally through adenylation by the protein GlnE (22). GlnE adenylates GSI under high nitrogen conditions, making it less active, and removes the adenyl group under low nitrogen conditions (22). In *E. coli* GlnE itself is further regulated through a pathway that also includes various post-translational modifications of GlnD and the P_{II} protein (23).

1.3.1.2 Transcriptional and post-translational regulation of glutamine synthetase in *Streptomyces*

Streptomyces contains homologues of many of the Ntr system genes found in *E. coli* and other bacteria, but their corresponding proteins do not seem to have the same relationships and roles (23). Most of the work on nitrogen assimilation in *Streptomyces* has been done in *Streptomyces coelicolor*, but the same genes are present in *S. venezuelae* and it is reasonable for now to postulate that the systems in the two streptomycetes behave similarly. *S. coelicolor* contains five glutamine synthetase genes: *glnA,* a homolog of the GSI-encoding *glnA* found in *E. coli*; *glnII*, a gene encoding a glutamine synthetase more closely related to those found in plants; and *glnA2, glnA3,* and *glnA4* which encode three other glutamine synthetase-like products (24). Notably, only *glnA* and *glnII* encode functional glutamine synthetase enzymes (24). *S. venezuelae* contains the same complement of glutamine synthetase genes but lacks *glnA3*. *S. coelicolor* and *S. venezuelae* also contains homologs to several other Ntr regulatory genes found in *E. coli,* including *glnK, glnD* and *glnE*. In *S. coelicolor,* GSI is similarly adenylated by GlnE in a nitrogen dependent manner, but the upstream regulatory pathway that controls GlnE is different (22, 23).

The other significant difference between the nitrogen assimilation system in *E. coli* and *Streptomyces* is how the transcription of nitrogen assimilation genes is regulated. As described above, *E. coli* and related bacteria control transcription of nitrogen assimilation operons through a two-component system composed of a sensor histidine kinase (NtrB) and a transcriptional regulator (NtrC) (20). However, in *Streptomyces,* the global transcriptional regulator of nitrogen regulation is GlnR. GlnR is an orphaned OmpR-like response regulator that controls several nitrogen assimilation related genes and operons in both *S. coelicolor* and *S. venezuelae* (14). Genes bound and activated or repressed by GlnR include *glnA, glnII, nirB, gdhA,* and *amtB,* whose gene products are all related to nitrogen assimilation (25, 26). Under nitrogen-limiting conditions, GlnR activates genes involved in nitrogen uptake and assimilation and represses those that are active under nitrogen abundant conditions (23). A sensor kinase partner for GlnR has not yet been identified, but GlnR can be phosphorylated on serine and threonine residues *in vivo* and this phosphorylation is dependent on nitrogen availability and affects the ability of GlnR to bind target promoters: at high nitrogen concentrations, GlnR is phosphorylated and cannot bind its target genes, while at low nitrogen concentrations, GlnR is not phosphorylated and can bind DNA (15).

1.3.2 Pathways that regulate metabolism are interconnected in *Streptomyces*

The GlnR regulatory process is further complicated by the network of connections between other regulators in *Streptomyces* such as AfsR, PhoP, and MtrA (Figure 1.3). One regulatory pathway that has a particularly significant impact on the GlnR regulon is the phosphate uptake system. In *Streptomyces,* phosphate uptake is controlled by the two-component system PhoRP (27, 28). PhoP is phosphorylated by

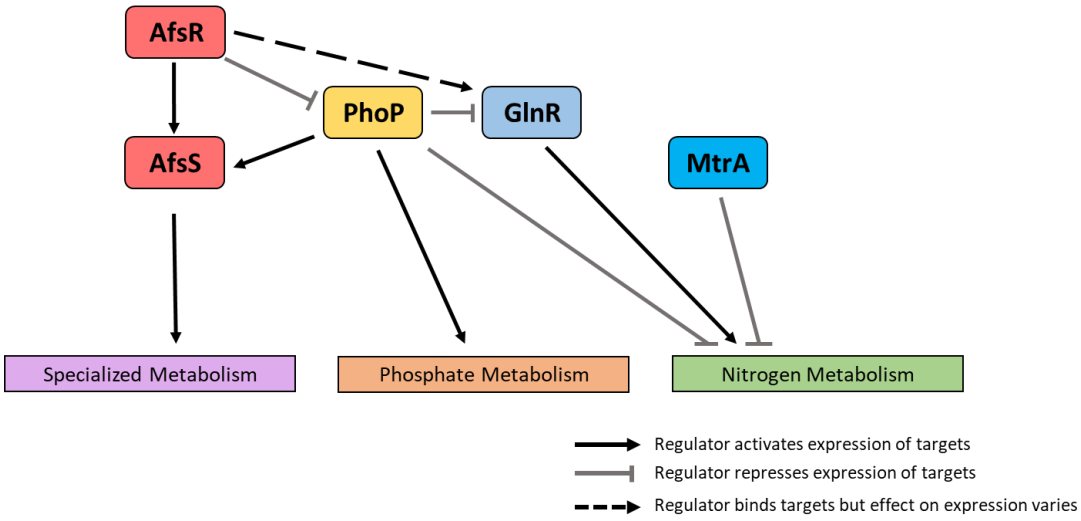

Figure 1.3. Simplified schematic showing the connections between metabolic regulators in *Streptomyces.* (Modified from 28).

PhoR and is then able to bind and activate genes in the *pho* regulon (29). PhoP binding sites have been identified in the promoter region of *glnR* itself, as well as in several GlnR target genes including *glnA, glnII,* and *amtB* (30). In the *glnA* and *glnII* promoters, the PhoP and GlnR binding sites overlap and each regulator competes for binding, while the recognition sites are further apart in the *amtB* promoter region (31). Furthermore, reporter assays have shown that the *glnA, glnII, amtB,* and *glnR* promoters are more active in a Δ*phoP* mutant compared with the wild type, with the implication that PhoP can repress expression of both *glnR* and genes in the GlnR regulon (30).

Two additional regulators connected to phosphate and nitrogen metabolism in *Streptomyces* are MtrA and AfsR. MtrA is part of a two-component system with the kinase MtrB. Under nitrogen-rich conditions, phosphorylated MtrA competes with GlnR to bind the promoters of several GlnR regulated genes and represses their expression (32). AfsR is a regulator that responds to *S*-adenosylmethionine concentrations through phosphorylation by the Ser-Thr kinase AfsK (33, 34). AfsR represses *phoRP* expression and competes with PhoP for binding to the *glnR* promoter, adding another layer of complexity to the network of metabolic regulators in *Streptomyces* (35, 36).

The regulation of nitrogen assimilation is a good example of how different regulatory methods and pathways can be intertwined in bacteria. And while many of the genes and gene products from regulatory systems in other bacteria are also present in *Streptomyces*, it is clear that there are significant differences in how these processes work in *Streptomyces.* These differences highlight the need for further study of regulatory mechanisms in these organisms.

1.4 Ribonucleases are important regulators of gene expression

Ribonucleases (RNases) are major mediators of post-transcriptional gene regulation: these enzymes cleave and degrade RNA. RNases can act as endonucleases and cleave RNA in the middle of the molecule, or as exonucleases and degrade RNA molecules progressively from one end (21). They are found in all forms of life and have varied targets and functions, but overall are critical for helping cells respond rapidly to their environment (37). RNase III, RNase J, and/or RNase E work together to process precursor rRNA and tRNA molecules into their mature forms and, alongside RNase Y, are also major degraders of mRNA (38, 39). In *E. coli,* the RNases YbeY and RNase R help ensure cellular functioning by targeting and degrading defective 70S ribosomes (40). In a similar quality control role, RNase J can remove stalled RNA polymerase units from DNA through a ‘torpedo’ mechanism (41). PNPase, a 3’-5’ RNase can also add or remove poly(A) tails from RNA molecules, which affects the stability of the transcript (42). *S.*

venezuelae encodes many different RNases, including RNase E, RNase J, RNase III, RNase H, YbeY, and PNPase, but two of particular interest are RNase III and RNase J. Previous work in *S. coelicolor* and *S. venezuelae* has shown that these RNases have a role in development and specialized metabolism, making them a relevant research focus for understanding RNase-mediated regulation in *Streptomyces* (43, 44).

1.4.1 Overview of RNase J

RNase J is a dual endonuclease and 5'-3' exoribonuclease. RNase J was first characterized in *Bacillus subtilis* as being the first bacterial ribonuclease with 5'-3' directionality (45). In *B. subtilis* there are two RNase J proteins, RNase J1 and RNase J2, which dimerize to form the full RNase J1/J2 protein (46). The two proteins share high protein sequence similarity, but the majority of ribonucleolytic activity has been attributed to RNase J1 (46). Further study revealed that at least one copy of RNase J is found in many bacteria and that it has a role in rRNA processing and general RNA degradation, similar to RNase E (47, 48). Organisms that contain RNase E typically lack RNase J and vice versa but intriguingly, the actinobacteria are an exception as they contain both RNase E and RNase J (49). The presence of both enzymes suggests that RNase J and E may have different roles in *Streptomyces* and its relatives than in other model organisms.

In *B. subtilis* RNase J plays an important role in processing the 5' end of pre-16S rRNA and is also important for mRNA degradation (45, 50, 51). The primary activity for RNase J is as a 5'-3' exonuclease that targets monophosphorylated RNA transcripts (46). These monophosphorylated transcripts can arise from previous cleavage events, by *e.g.* RNase III, RNase E, or RNase J (in an endonuclease capacity). The dual endo/exonuclease behaviour of RNase J depends both on the abundance of enzyme and substrate, and on the phosphorylation state of the substrate (52). Monophosphorylated 5' ends favours exonucleolytic activity, while triphosphorylated 5' ends favour endonucleolytic activity; a high concentration of RNase J is also required for endonucleolytic activity (52).

1.4.2 RNase J in *Streptomyces*

The RNase J homolog in *S. venezuelae* is encoded by *vnz_26680*. RNase J is nonessential in two model species of the *Streptomyces* genus, *S. coelicolor* and *S. venezuelae,* but the deletion of the gene coding for RNase J (*rnj*) from either of these species impacts antibiotic production and development (44, 53). In *S. coelicolor,* deleting *rnj* delays the production of actinorhodin, leads to the overproduction of undecylprodigiosin, and decreases the production of calcium-dependent antibiotic (53). In *S. venezuelae,* an Δ*rnj* strain develops slower when growing in liquid medium compared to the wild type strain, with sporulation delayed by several hours (44). Contrary to what has been shown in *B. subtilis*, RNase J does not appear to have a role in processing the 5' end of 16S rRNA in *S. venezuelae* (44). The *S. venezuelae* Δ*rnj* mutant also exhibits reduced production of the antibiotic jadomycin B and has impaired ribosomes, demonstrated by an abundance of translationally inactive 100S ribosome dimers (44). Although the specific pathways through which RNase J regulates these functions are still unclear in *Streptomyces,* it is clear that RNase J has an important role in the development and metabolism of *S. venezuelae*.

1.4.3 Overview of RNase III

RNase III (encoded in *S. venezuelae* by *vnz_26040*) is an endonuclease that targets dsRNA (54). Diverse forms of the RNase III protein are found in organisms ranging from bacteria to mammals (55). Domain organization may vary across these different RNase III proteins, but the central defining feature is the presence of the RNase III Domain (55). RNase III from bacteria and yeast possess an N-terminal endonuclease domain and a C-terminal dsRNA binding domain (56). In *E. coli*, RNase III has an important role in processing precursor rRNA and tRNA, and in sRNA-mediated regulation. RNase III liberates precursor rRNA and tRNA molecules from their progenitor transcripts by cleaving the double stranded hairpin structures that separate the respective molecules in their precursor transcripts (57). The released precursor tRNAs,

16S, 23S and 5S rRNAs are then further processed at their 5′ and 3′ termini to maturation (58). As a dsRNA targeting ribonuclease, RNase III is also involved in degrading RNA that is targeted by *cis*- or *trans*-encoded small regulatory RNAs. For example, in *Salmonella typhimurium,* RNase III mediates the degradation of the trans-encoded sRNA MicA and its target *ompA* mRNA*,* where *ompA* encodes an outer membrane pore (59).

1.4.4. RNase III in *Streptomyces*

The *Streptomyces* homolog of RNase III was first characterized in *S. coelicolor* for its ability to restore antibiotic production to a mutant *S. coelicolor* strain that was defective in antibiotic production (43). In *S. coelicolor*, deleting the gene encoding RNase III (*rnc* or *absB*) results in a loss of actinorhodin and undecylprodigiosin production; disrupting the catalytic ability of RNase III had the same effect, demonstrating that the endonuclease activity of RNase III is required for antibiotic production (60). A similar effect is seen in *S. venezuelae,* where the loss of *rnc* from the *S. venezuelae* genome results in decreased jadomycin B production. Non-functional 100S ribosomes also accumulate in *S. venezuelae* Δ*rnc* strains, while primer extension assays show that the absence of RNase III leads to the misprocessing of the 5′ pre-23S rRNA site (44). Collectively, these data show that RNase III has an important role in *Streptomyces* development and metabolism but, as with RNase J, the specific mechanism(s) and pathways remains unclear, although rRNA misprocessing and general ribosome impairment may be one influencing factor (44).

1.5 G-quadruplexes as regulatory elements

Beyond ribonucleases, another mechanism by which gene regulation at the transcriptional and post-transcriptional/translational level can be achieved is through the formation of structures within DNA or RNA. An intriguing example of this phenomenon are G-quadruplexes (Figure 1.4). These structures are formed from repeated tracts of guanine residues in nucleic acids and can occur within or between

molecules of DNA and RNA (61). The typical consensus sequence for a GQ structure is $G_3N_{1-7}G_3N_{1-7}G_3N_{1-7}G_3$, although significant variability is possible in the number of G residues and intervening spacer lengths. GQ structures form at these sequences when the guanine residues form planar G-quartets with each other through Hoogsteen base pairing (Figure 1.4). These G-quartets then stack on top of one another to form a structure known as a G-quadruplex (GQ) (61).

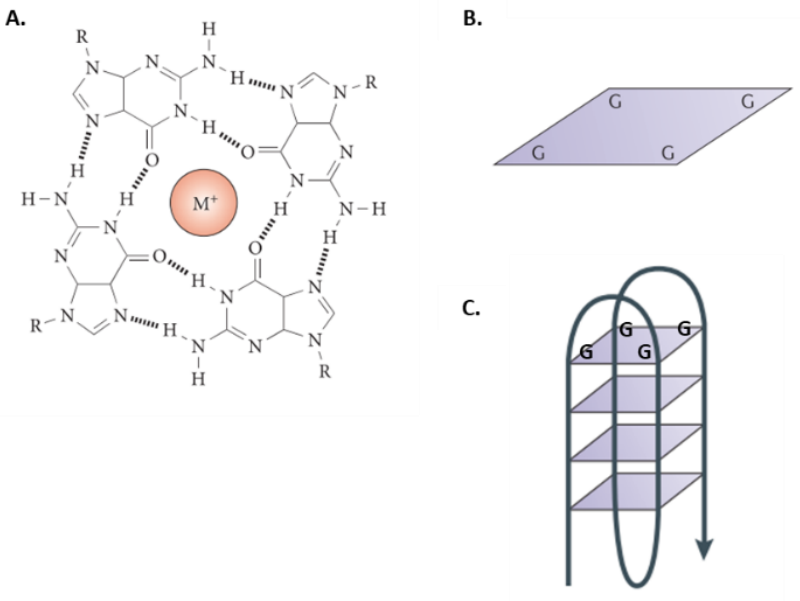

Figure 1.4. Schematic of G-quadruplex structures. **A.** Diagram showing the Hoogsteen interactions (dashed lines) between four guanine molecules to form a G-quartet, stabilized by a central metal ion. **B.** Four guanine molecules aligned in a square planar conformation to form a G-quartet. **C.** Diagram of an intramolecular G-quadruplex formed by the stacking of four G-quartets. (Modified from 61).

1.5.1 G-quadruplexes in eukaryotic and bacterial systems

GQs can have diverse effects depending on where they form in the genome or RNA transcripts. For example, GQs can act as roadblocks to polymerase machinery in DNA, a fact that has been exploited to detect GQ structures using polymerase stop assays (62).

Conversely, GQs can also stabilize regions of nucleic acids and increase expression from genes (63). Until recently, GQs have been predominantly studied in eukaryotic systems, where they have been implicated in a wide range of biological functions including splicing, transcription termination, and recombination (64). Of particular interest in eukaryotes is the connection between GQs and cancer. GQs are abundant in the telomeres of eukaryotic cells and can block the activity of the telomere-extending enzyme telomerase, thus preventing the extension of telomeres through the action of GQ-stabilizing ligands may represent a therapeutic option for cancer treatment (65).

GQ structures and motifs have become a topic of interest more recently in bacterial systems. GQ structures have now been implicated as regulatory features that can modulate metabolism, recombination, and general gene expression in bacteria (64). In *Paracoccus denitificans*, stabilizing a GQ structure upstream of nitrogen assimilation regulatory genes leads to decreased expression of the corresponding downstream genes (66). RecA, a key recombination protein, can bind *in vitro* to a GQ structure found upstream of a gene involved in pilin formation in *Neisseria gonorrhoeae*, implying a potential role for GQ structures in mediating antigen variation of the pilin sequence (67). Further work utilizing reporter assays and fluorescent probes specific for GQ structures in RNA has revealed that the presence of GQ structures in the coding sequences of various mRNA transcripts in *E. coli* and *Pseudomonas aeruginosa* can also affect gene expression levels (63).

1.5.2 G-quadruplexes in *Streptomyces*

Because GQ sequences are rich in G-residues, there are increased opportunities for their occurrence in organisms with high genomic GC content. Thus, one important question is how GC-rich organisms might utilize, or mediate, the formation of these structures in their nucleic acids. The average GC-content of *Streptomyces* bacterial genomes is ~70%, and previous work has shown that the genomes of several bacteria in

this genus are enriched for GQ motifs; more than twice the number of expected GQ motifs have been detected for several *Streptomyces* species (68). Of these sequences, over 20% are located in intergenic regions where they have the potential to exert regulatory effects on the adjacent genes (68). Further analysis in *S. venezuelae* and *S. coelicolor* showed that the presence of GQ motifs in the 5' UTR can have varying effects on the downstream gene, depending on the position of the motif relative to the start codon, the strand of the motif, and the structure and composition of the motif itself (68).

1.5.2.1 Identification of a potential G-quadruplex binding protein

Given the potential regulatory effects of these structures, organisms likely have ways of modulating how and when GQ structures can form *in vivo* and they may control GQ formation through GQ-binding compounds. From *S. venezuelae,* the enzyme TrmB, a tRNA-methyltransferase, interacts with GQ DNA structures *in vitro* (68). In *E. coli* and *B. subtilis,* TrmB catalyzes the formation of *N*7-methylguanosine (m7G) at position 46 in tRNA molecules (69). The N7 position in guanine is the position involved in forming the Hoogsteen bonds that hold together the planar quartets of a G-quadruplex structure (61). If the N7 position was blocked, potentially by a methyl group added by TrmB, this could prevent the formation of a GQ structure at that motif (70). Although TrmB is annotated as an RNA-associated protein, it is conceivable that it may also interact with DNA. For example, there is evidence that two methyltransferases in humans target both DNA and RNA (71). The possibility that modifications in DNA, such as those potentially caused by TrmB, could affect the regulation of gene expression in bacteria by preventing the formation of GQ structures, is an exciting hypothesis for investigation.

2. Objectives

With their hidden biosynthetic potential, complex life cycle, and GC-rich genomes, *Streptomyces* are different from other model organisms in which RNases and G-quadruplexes have been studied. Since the progression through their lifecycle and the

activation or repression of their biosynthetic clusters are primarily mediated through changes in gene expression, understanding the myriad of ways that *Streptomyces* controls gene expression is of paramount importance. Although we know that RNases have important regulatory roles in controlling growth and specialized metabolism in *Streptomyces*, it is unclear how they specifically impact these processes at a mechanistic level. And while G-quadruplexes have recently been understood to have regulatory roles in bacteria as well as eukaryotes, minimal work has been done on them in GC-rich organisms like the streptomycetes, despite the increased potential for their occurrence. How might *Streptomyces* utilize RNases or G-quadruplexes to regulate gene expression throughout their life cycle and control their morphological differentiation and specialized metabolism?

This work aims to investigate how global transcript levels change in RNase mutants and to identify specific functions or pathways in *S. venezuelae* that are impacted by RNase J and/or RNase III. A second aim of this work is to probe the role of G-quadruplexes in GC-rich *S. venezuelae,* with a focus on investigating potential interactions between G-quadruplex structures and the tRNA-methyltransferase protein, TrmB.

To this end, the objectives of this work are to:

1) Develop an understanding of the changes that occur at the transcript level for Δ*rnj* and Δ*rnc* strains of *S. venezuelae* relative to the wild type and probe impacted genes/pathways to determine if transcripts that change in expression are direct targets for either RNase.
2) Determine whether TrmB can bind and methylate G-quadruplex structures and prevent their formation in DNA.

3. Methods and Materials

3.1 Plasmids, bacterial growth conditions, and strain maintenance

Complete lists of the strains and plasmid constructs used in this work are found in Table 3.1 and Table 3.2. All liquid cultures were grown shaking at 200 RPM. Unless otherwise noted, *S. venezuelae* cultures were grown in maltose-yeast extract-malt extract medium (MYM) at 30°C, while *E. coli* cultures were grown in either Lysogeny Broth (LB) or Super Optimal Broth (SOB) at 37°C. When antibiotics were included in the growth medium, they were used at the following final concentrations: nalidixic acid (20 µg/mL), kanamycin (50 µg/mL *E. coli*; 25 µg/mL *S. venezuelae*), chloramphenicol (25 µg/mL), ampicillin (100 µg/mL), apramycin (50 µg/mL), hygromycin B (50 µg/mL).

Spore stocks of *S. venezuelae* strains were produced by suspending a single *S. venezuelae* colony in 100 µL of sterile dH_2O and then dividing the suspension in half and spreading it on two MYM agar plates to create a lawn. The plates were incubated at 30°C for 3-4 days. The accumulated biomass was harvested from the plates using a sterile metal spatula and placed in 5 mL of sterile dH_2O. The samples were then sonicated in a water bath sonicator for 5-10 minutes to disrupt spores from the remaining biomass. The suspension was passed through a sterile syringe containing cotton to filter out the mycelial mass and the filtered solution was centrifuged for 5 min at 2,200 ×*g*. The remaining liquid was decanted and the spores were resuspended in 400 µL of sterile 40%$_{v/v}$ glycerol. Glycerol spore stocks were then stored at -20°C.

E. coli stocks were prepared by mixing 500 µL of culture with an equal volume of sterile 40%$_{v/v}$ glycerol before then being stored at -80°C.

Table 3.1: Bacterial strains used in this work

Species	Strain	Description	Reference
E. coli	DH5α	General cloning	Invitrogen
	BW25113/pIJ790	ReDirect recombination strain.	(72)
	ET12567/pUZ8002	Methylation deficient strain, carrying a conjugation helper plasmid, for conjugating DNA into *Streptomyces.*	(73)
	Rosetta2	Overexpression of recombinant *Streptomyces* proteins.	Novagen
S. venezuelae	NRRL B-65442	Wild type.	(74)
	WT+pIJ82	Wild type with pIJ82 vector.	(44)
	WT+pMS82	Wild type with pMS82 vector.	From M. Zambri
	Δ*rnj*	RNase J deletion mutant.	(44)
	Δ*rnj*+pIJ82	RNase J deletion mutant with empty vector.	(44)
	Δ*rnj*+pIJ82::*rnj*	Complemented RNase J deletion mutant.	(44)
	Δ*rnc*	RNase III deletion mutant.	(44)
	3×FLAG-rnc	FLAG-tagged RNase III construct in wild type *S. venezuelae* background.	This work
	Δ*rnc+3×FLAG-rncE132Q*	FLAG-tagged catalytically inactive RNase III construct in RNase III mutant background.	This work
	Δ*rnc+3×FLAG-rnc*	FLAG-tagged RNase III construct in RNase III mutant background.	This work
	3×FLAG-rnj	FLAG-tagged RNase J construct in wild type *S. venezuelae* background.	This work
	Δ*rnj+3×FLAG-rnjH86A*	FLAG-tagged catalytically inactive RNase J construct in RNase J mutant background.	This work

Species	Strain	Description	Reference
	Δ*rnj::3×FLAG-rnj*	FLAG-tagged RNase J construct in RNase J mutant background.	This work
	Δ*nnaR*	*nnaR* deletion mutant in wild type *S. venezuelae* background.	This work
	Δ*rnj*Δ*nnaR*	*nnaR* deletion in RNase J mutant background.	This work
	Δ*rnc*Δ*nnaR*	*nnaR* deletion in RNase III mutant background.	This work

Table 3.2: Cosmids and plasmids used in this work

Plasmid/Cosmid	Description	Reference
pET15b	Overexpression vector	Novagen
pET15b + *sven_3866*	Overexpression of TrmB	(68)
pRARE2	Contains tRNAs for 7 rare codons in *E. coli*	Novagen
pIJ82	Integrating vector for *Streptomyces*	Gift from H. Kieser
pIJ82 + *rnj*	Complementation vector for *rnj* mutant	(44)
pUC57	Vector for synthesized *FLAG*-tag products	GenScript
pUC57 + *3×FLAG-rnj*H86A	pUC57 with *rnj* promoter and gene for FLAG-tagged RNase J H86A	GenScript
pUC57 + *3×FLAG-rnc*E132Q	pUC57 with RNase III promoter and gene for FLAG-tagged RNase III E132Q	GenScript
pMS82	Integrative vector for *Streptomyces*	(75)
pMS82 + *3×FLAG-rnj*H86A	Construct for integration of gene for FLAG-tagged RNase J H86A into *Streptomyces*	This work
pMS82 + *3×FLAG-rnc*E132Q	Construct for integration of gene for FLAG-tagged RNase III E132Q into *Streptomyces*	This work
pMS82 + *3×FLAG-rnj*	Construct for integration of gene for FLAG-tagged RNase J into *Streptomyces*	This work
pMS82 + *3×FLAG-rnc*	Construct for integration of gene for FLAG-tagged RNase III into *Streptomyces*	This work
Sv-5-A04	Wild type cosmid containing *nnaR*	Gift from M. Bibb and M. Buttner
Sv-5-A04 *vnz_13340::hygoriT*	Modified cosmid for creation of *S. venezuelae nnaR* mutant	This work

3.2 General molecular techniques

3.2.1 *S. venezuelae* growth curves

Ten millilitres of liquid MYM medium were inoculated with 10 µL of a spore stock and grown overnight. Each strain was then sub-cultured from the overnight culture to a starting OD_{600} of 0.05 and grown in either a 500 mL or 3.6 L baffled flask. Starting at 10 hours post-induction, the OD_{600} value of each culture was measured every 2 hours until 24 hours of growth was reached. To ensure that spectrophotometer readings fell between 0.1 and 1, samples were diluted 1:10 in liquid MYM before measuring. The developmental stage of the strain was tracked using light microscopy.

3.2.2 Polymerase chain reactions (PCR)

PCRs were conducted using 20 µL reactions with either NEB Phusion® High Fidelity DNA Polymerase or with NEB 2× Taq Master Mix. Reaction mixtures and conditions were as summarized in Table 3.3. When colony PCR was conducted on *E. coli* cells, a small portion of the colony was transferred to individual reaction tubes in lieu of template DNA. When colony PCR was conducted on *S. venezuelae* cells, a colony was patched to solid MYM medium and a portion of the biomass from this patch was resuspended in 30 µL of nuclease free water and boiled at 95°C for 15 minutes to lyse the cells. The solution was centrifuged at 13,000 ×*g* to pellet the cell debris and 1 µL of the supernatant was used in subsequent PCR reactions. PCR products were visualized on a 1% agarose gel and purified with either the PureLink™ PCR Purification Kit (Invitrogen) or via gel extraction with the NEB Monarch®DNA Gel Extraction Kit, following the manufacturer's instructions.

Table 3.3: Polymerase chain reaction conditions

Polymerase	Reaction Conditions	Cycling Conditions
2× Taq Master Mix (NEB)	1× Taq Master Mix 5% DMSO 0.3 µM Forward Primer 0.3 µM Reverse Primer Template DNA (1-5 ng) or Colony Nuclease free water to 20 µL/rxn	1) 95°C for 3 minutes 2) 95°C for 30 seconds 3) 45-65°C for 30 seconds 4) 72°C for 1 minute/kb 5) Repeat 2-4 34 × 6) 72°C for 5 minutes
Phusion (NEB)	1× Phusion GC Buffer 5% DMSO 0.2 mM dNTPs 0.5 µM Forward Primer 0.5 µM Reverse Primer Template DNA (1-5ng) Nuclease free water to 20 µL/rxn	1) 98°C for 3 minutes 2) 98°C for 10 seconds 3) 45-65°C for 30 seconds 4) 72°C for 30 seconds/kb 5) Repeat 2-4 34× 6) 72°C for 5 minutes

3.2.3 Extraction of DNA from *E. coli* cells

Plasmids were extracted from cultures of *E. coli* cells using the PureLink™Quick Plasmid Miniprep Kit (Invitrogen), according to the manufacturer's instructions.

Cosmid DNA was extracted from *E. coli* cultures. Cell pellets were resuspended in 500 µL of ice-cold Solution I (50 mM Tris pH 8, 55.5 mM glucose, 10 mM EDTA), after which 1 mL of Solution II (200 mM NaOH, $1\%_{w/v}$ SDS) was added to each sample. The samples were mixed by inverting the sample tubes before leaving the suspension on ice for 5 minutes for cells to lyse. Solution III (CH_3COOK/CH_3COOH 5M, pH 4.80) was then added to each sample (750 µL). The samples were left on ice for another 5 minutes, and then centrifuged at 7,800 ×*g* for 10 minutes at 4°C. The supernatant was transferred to a fresh tube and an equal volume of phenol:chloroform:isoamyl alcohol (50:50:1, pH 7.6) was added to each sample. The samples were vortexed, and then centrifuged at 2,200 ×*g* for 5 minutes. The aqueous phase of each sample was recovered and DNA was precipitated from the sample with the addition of 2 volumes of $95\%_{v/v}$ ethanol and 0.1 volume of CH_3COONa/CH_3COOH buffer (5M, pH 5.2). The samples were left to precipitate at -20°C for at least 30 minutes and then they were centrifuged at 7,800 ×*g*

for 30 minutes at 4°C. The resulting pellet was washed with 70%$_{v/v}$ ethanol and resuspended in ~100 µL of nuclease free water. Recovered cosmid and plasmid DNA integrity was checked by running 5 µL of each purified sample on a 1% agarose gel.

When necessary, co-extracted RNA from cosmid isolations was digested by RNase A. Between 10-50 µL of purified cosmid were diluted to 300 µL, to which 10 µL of RNase A (10 µg/mL) were then added. The resulting solution was incubated at 37°C for 1-2 hours to remove RNA, after which the remaining DNA was purified through an additional phenol:chloroform extraction and precipitation step.

3.2.4 Restriction digestion and dephosphorylation of DNA

DNA digestion reactions were carried out in 50 µL reactions with 30 U of the appropriate restriction enzyme (*Kpn*I, *Bam*HI, *Eco*RI, *Nde*I, *Xho*I, *Hind*III or *Xba*I) in its corresponding buffer (NEB). The reactions were left to incubate in a water bath at 37°C. After 1 hour, an additional 30 U of enzyme were added to the reaction. When required, DNA was dephosphorylated by adding 10 U of calf intestinal phosphatase (NEB) directly to the digestion reaction and incubating the reaction at 37°C for an additional hour. The reactions were purified either with the PureLink™ PCR Purification Kit (Invitrogen) or via gel extraction after being run on a 1% agarose gel (NEB Monarch® DNA Gel Extraction Kit).

3.2.5 Electroporation of DNA into *E. coli*

E. coli cells were sub-cultured in liquid SOB medium until an OD_{600} of 0.4-0.6 was reached, after which cells were washed three times with cold 10%$_{v/v}$ glycerol. DNA was electroporated into electro-competent *E. coli* cells using a BioRad MicroPulser on the EC2 setting. Shocked cells were recovered for 1 hour at either 37°C or 30°C in LB or SOB medium, and then spread on an appropriate agar medium (including antibiotics for selection of DNA uptake) and grown overnight at 37°C or 30°C.

3.2.6 Heat shock transformation

DNA was transformed into competent *E. coli* (Subcloning Efficiency™ DH5α Competent Cells, ThermoFisher). Two microlitres of DNA were added to 50 µL of cells and left on ice for 15 minutes. Cells were then heat shocked at 37°C for 30 seconds and immediately cooled on ice for 2 minutes. Cells were recovered in 1 mL of liquid LB medium for 1 hour at 30°C or 37°C and were then plated to solid LB medium plates containing the appropriate antibiotic selection.

3.2.7 DNA Ligation

Insert and vector DNA for ligation were digested as described above and vector DNA was dephosphorylated. Insert and vector DNA were mixed in a 3:1 molar ratio in 1×T4 DNA Ligation Buffer (Roche) with 5 U of T4 DNA ligase (Roche). Samples were left at room temperature for five minutes, after which 2 µL of the reaction were added to competent *E. coli* cells for heat shock transformation.

3.2.8 Labelling of DNA with P^{32}

Oligonucleotides were radiolabelled for northern blotting or for use in G-quadruplex formation assays. The oligos were labelled at the 5' end in reactions containing oligonucleotide (0.1 µM), 10 U of T4 polynucleotide kinase (NEB), 1×T4 polynucleotide kinase buffer, and 5 µL of [γ-^{32}P]ATP (Perkin Elmer, 0.4 mCi/mL). The reaction was brought to 20 µL with nuclease-free water. The reactions were incubated at 37°C for 30 minutes and the oligonucleotide was purified using the PureLink™ PCR Purification Kit (Invitrogen) or NucAway spin columns (Ambion), following the manufacturer's instructions.

3.2.9 Conjugation of DNA into *S. venezuelae*

Constructs for introduction to *S. venezuelae* were introduced via the *E. coli* ET12567/pUZ8002-containing strain. The construct was transformed via electroporation into electro-competent *E. coli* 12567/pUZ8002 cells and grown overnight. The cells were then washed 3 times with liquid LB medium, followed by resuspension in 500 µL of SOB

or LB. Separately, 20 µL of *S. venezuelae* spores were suspended in 500 µL of liquid 2× yeast extract-tryptone (2×YT) medium. The washed *E. coli* cells were then mixed with the *S. venezuelae* spore suspension and briefly centrifuged. The remaining liquid was removed and the cells were resuspended in approximately 50 µL of 2×YT and plated to soy flour-mannitol (SFM) agar plates. After 4-8 hours of incubation at 30°C, the plates were overlaid with nalidixic acid and the construct-specific selective antibiotic. The plates were then left to incubate at 30°C until single colonies appeared (usually after 3-4 days).

3.4 Total RNA-extraction and purification from *S. venezuelae*

To extract RNA, *S. venezuelae* cells were grown in liquid culture until the desired time point was reached. Cells were collected in Falcon tubes and the cell pellets were either stored at -80°C or were placed on ice for immediate RNA extraction.

Cells were lysed by vortexing the pellets for 2 minutes with an approximately equal volume of sterile glass beads and 5 mL of cold lysis solution (4M guanidine thiocyanate, 25 mM trisodium citrate, 0.5%$_{v/v}$ sodium *N*-lauroylsarcosinate, 0.8%$_{v/v}$ β-mercaptoethanol). An equal volume of phenol:chloroform:isoamyl alcohol (50:50:1, pH 4.6) was then added to the lysate and samples were vortexed on and off in thirty second intervals to emulsify the solutions. Samples were then centrifuged at 7,800 ×*g* and the aqueous phase containing the RNA was recovered. Samples were treated twice more with equal volumes of phenol:chloroform:isoamyl alcohol. After the final treatment and recovery of the aqueous phase, total RNA was precipitated by adding an equal volume of cold isopropanol (100%) and 0.1 volume of sodium acetate buffer (3 M, pH 6). The samples were inverted several times to mix and then left overnight at -20°C. Following precipitation, the samples were centrifuged at 8,870 ×*g* (4°C) for 30 minutes. The RNA pellets were washed once with cold 70%$_{v/v}$ ethanol and then left to air dry for 10 minutes. The pellets were resuspended in 100 µL of nuclease free water once dry. After

resuspension, 2 µL of the total RNA was separated on a 2% agarose gel to assess integrity.

3.4.1 DNase treatment, determination of RNA concentration, and confirmation of DNA-free RNA samples

Fifty microlitres of total RNA was DNase treated post-extraction. The sample was diluted to a total volume of 390 µL in nuclease free water, at which point 50 µL of TURBO DNase Buffer (10×) and 20 U of TURBO DNase enzyme were added to bring the final volume to 500 µL (Fisher Scientific). The sample was incubated in a 37°C water bath for 1 hour, then an additional 10 U of DNase enzyme was added and the sample was left at 37°C for another hour. Total RNA was extracted from the reaction mixture with phenol:chloroform:isoamyl alcohol (50:50:1, pH=4.6). The aqueous and organic layers were separated by centrifugation and the aqueous layer containing the RNA was recovered. The phenol:chloroform extraction was repeated once, after which the RNA was precipitated and dried as described above. The final RNA pellet was resuspended in 50 µL of nuclease free water. Two microlitres of DNase-treated total RNA were separated on a 2% agarose gel to assess integrity.

The concentration of the DNase-treated RNA was determined using a NanoDrop spectrophotometer. One and a half microlitres of a 1:10 dilution of each sample was tested at a time and each sample was tested in technical triplicate. The arithmetic mean of the three replicates was taken as the concentration for the sample.

PCR was used to confirm that each total RNA sample was DNA-free. Primers for the gene *sven_4897* (Table 3.4) were used in a standard Taq PCR reaction (Table 3.3), with 0.5 µg of total RNA included as template. One reaction with genomic DNA as template was included as a positive control. If no product was observed from the RNA-template PCR reactions (but was detected in the genomic DNA-containing reaction), this indicated that all extraneous DNA had been properly digested and removed during the DNase treatment.

3.4.2 Gel extraction of RNA bands

To extract a specific band from an RNA sample, total RNA was run on a denaturing acrylamide gel (6M urea, 6% acrylamide) then the desired RNA bands were visualized and marked using UV shadowing. The marked region of the gel was cut out from the rest of the gel, crushed, and then incubated in buffer (200 mM NaCl, 10 mM Tris, 1 mM EDTA, pH 8) at 37 °C for 30 minutes. The solution was centrifuged at 13,000 ×*g* for 5 minutes and the supernatant was recovered. This crush-soak process was repeated three times with the gel pellet, and the supernatant was collected each time. RNA was then precipitated from the supernatant as described above in the extraction of total RNA from cells.

3.5 RNA-sequencing and analysis

RNA was extracted and purified for RNA-sequencing, as described in section 3.4, from wild type, Δ*rnj* and Δ*rnc* strains at vegetative, fragmentation, and sporulation stages of growth in liquid MYM culture. Two biological replicates were collected for each strain and stage of growth. Early/vegetative samples were collected at 10 hours for wild type and the Δ*rnc* strain, and at 12 hours for the Δ*rnj* strain. Mid-stage/fragmenting samples were collected at 14 hours for wild type and the Δ*rnc* strain, and at 18 hours for the Δ*rnj* strain. Late-stage/sporulating samples were collected at 20 hours for the Δ*rnc* strain and at 24 hours for the Δ*rnj* strain. The replicates used for the wild type sporulation time point were collected at 18 hours. RNA-sequencing was conducted by the MOBIX facility at McMaster University. Sequencing was done using paired-end technology on the Illumina MiSeq v3 platform.

Downstream analysis of the RNA-sequencing data was completed using the Galaxy platform. Illumina adapter sequences were trimmed off of the raw reads using the Trimmomatic program and the quality of trimmed reads was assessed using FastQC (76, 77). Reads were then aligned to the *S. venezuelae* NRRL B-65442 genome (NCBI accession: NZ_CP018074.1) using the BowTie2 program and the aligned files were sorted

using SamTools (78, 79). The aligned reads were visualized using the Integrated Genomics Viewer (80). The number of reads aligning to genomic features were counted using the HTseq-count program for each replicate (81). The HTseq-count tables were then normalized and used for differential transcript level analysis with the program DESeq2 (82). Differential transcript abundance was assessed by comparing transcript reads for wild type and the Δ*rnj* or Δ*rnc* mutant strains at each time point.

3.5.1 RT-PCR and semi-quantitative PCR analysis

cDNA libraries were generated from RNA samples using the NEB LunaScript™ RT SuperMix Kit. To confirm there was no contaminating DNA in the RNA samples, a negative control ("-RT") reaction with no reverse transcriptase enzyme was also run for each sample. One microgram of RNA was used for each reaction with 4 µL of reverse transcriptase (+ or -) master mix and nuclease free water to bring the total volume to 20 µL per reaction. The reactions were run with the following conditions: 25°C for 2 minutes (primer annealing), 55°C for 10 minutes (reverse transcription activity), and 95 °C for 1 minute (enzyme inactivation).

For semi-quantitative PCR, 2 µL of cDNA were added as template from the reverse transcribed samples and -RT reaction, along with primers for amplifying selected genes of interest that were differentially expressed in the RNA-sequencing data: *nasA* (*vnz_11080*)*, nirB* (*vnz_11140*)*, nnaR* (*vnz_13340*)*,* and *amtB* (*vnz_26110*) (Table 3.4). Primers for *rpoB* were used as a loading/input control (Table 3.4). Reactions containing gDNA or nuclease-free water as template were also included with each primer set as a positive and negative control, respectively. Samples were amplified using standard Taq PCR conditions, but with the number of amplification cycles adjusted so that observations were made during the linear stage of amplification. Ten microlitres of each product were separated on a 2% agarose gel containing ethidium bromide.

3.6 Northern blotting

We used northern blotting to identify potential sRNA candidates. Five micrograms of each RNA sample for analysis were heated to 95°C for 5 minutes and then loaded and separated on a denaturing polyacrylamide gel (6M urea, 6% acrylamide). The separated RNA was then transferred to a nylon membrane (Zeta-Probe Blotting Membrane, Bio-Rad) using the Trans-Blot® SD Semi-Dry Electrophoretic Transfer Cell (Bio-Rad). RNA was chemically cross-linked to the membrane using a solution of 1-ethyl-3-(3-dimethylaminopropyl) carbodiimide (0.16 M in 0.13 M 1-methylimidazole, pH 8) and incubated at 55°C for 2 hours (83). Oligonucleotide probes to targets of interest (Table 3.4) were 5′ end-labelled with [γ-32]P ATP and the membrane was incubated overnight at 42°C in approximately 30 mL of ULTRAhyb®-Oligo Hybridization Buffer (Ambion) that contained 25 µL of labelled probe. Excess probe was washed off the membrane through a series of washes with low (300 mM NaCl, 30 mM citrate, 0.1%$_{w/v}$ SDS) and high (30 mM NaCl, 3 mM citrate, 0.1%$_{w/v}$ SDS) stringency buffer, before the membrane was exposed to a phosphor screen and then visualized using a phosphorimager.

3.7 Creation of FLAG-tagged RNase variants

Constructs of catalytically inactive RNase J and RNase III under the expression of their native promoter were synthesized by GenScript. The constructs contained a copy of the native promoter, as determined through transcription start sequencing data (generous gift from M. Buttner), followed by an N-terminal 3× FLAG tag , a three glycine residue linker, followed by the sequence for either the catalytically inactive RNase J (H86A) or RNase III (E132Q), and the native terminator sequence (50, 84). The constructs were cloned following PCR amplification, digestion with *Kpn*I and *Hind*III, and ligation into the integrating vector pMS82. The constructs were confirmed with sequencing and were then conjugated into the wild type and cognate RNase mutant strains of *S. venezuelae*.

PCR site-directed mutagenesis was used to revert the point mutations in the catalytically inactive RNase strains. Primers with mutations to revert the point mutations (Table 3.4) were used to amplify the gene product region of each construct. This region was then combined with the PCR product of the promoter and FLAG-tag region through overlap-extension PCR. The final PCR product of the promoter-FLAG tag-linker-revertant gene was then cloned into pMS82, which was sequenced to confirm the reversion. The pMS82-revertant gene construct was then conjugated into wild type *S. venezuelae* and the appropriate RNase mutants.

3.7.1 Western blotting

We used western blotting to confirm the expression of the FLAG-tagged proteins in *S. venezuelae*. Forty to eighty micrograms of total protein extract from each sample were run on a 12% SDS-denaturing polyacrylamide gel for 1 hour at 150 V. The proteins were transferred to a methanol-activated PVDF membrane (Amersham Bioscience) using the Bio-Rad Trans-Blot® SD Semi-Dry Electrophoretic Transfer Cell with 1× transfer buffer (48 mM Tris, 39 mM glycine, 1.28 mM SDS, 20%$_{(v/v)}$ MeOH) for 1 hour and 15 minutes at 15 V. The membrane was blocked for at least one hour with 6% blocking solution (6 g of skim milk powder in 100 mL of Tris buffered saline with 0.1% $_{(v/v)}$ Tween (TBS-T)). The membrane was washed twice with TBS-T for 10 seconds and then 6.6 µL of Anti-FLAG® Rb antibody (Sigma-Aldrich) were added to 10 mL of blocking solution and the membrane was left shaking in the solution overnight at 4°C. The membrane was washed several times with TBS-T following primary antibody incubation, after which 3.3 µL of secondary antibody (Pierce™ Gt anti-Rb IgG Superclonal™ secondary antibody HRP conjugate) were added to 10 mL of blocking solution. The membrane was then incubated in the solution at room temperature, shaking for at least 2 hours. FLAG-tagged protein was detected using the Amersham™ ECL™ Western Blotting Detection Reagents (Fisher) according to the manufacturer's instructions, followed by visualization with X-ray film exposure.

3.8 TrmB overexpression and purification

The overexpression construct for 6×His-tagged TrmB (Table 3.2) was transformed into competent Rosetta2 cells (Table 3.1) via electroporation. An overnight culture was grown from a single colony, which was then sub-cultured in liquid LB medium or Terrific Broth and grown to an OD_{600} of 0.6. At this point, a 1 mL pre-induction sample was taken. Protein induction was then initiated by adding IPTG to a final concentration of 1 mM. Cells were grown for a further 4 hours, shaking at 37°C, after which they were collected by centrifugation and stored at -80°C.

Recombinant protein was purified by His-tagged Ni-affinity purification. Cells were resuspended in 5 mL of cold, filter-sterilized lysis solution (300 mM NaCl, 50 mM NaH_2PO_4, 10 mM imidazole, pH 8, with one Roche cOmplete EDTA-Free Protease Inhibitor Tablet per 10 mL) and then lysed by sonication (Branson Sonifier Cell Disruptor350, 20× 30 second pulses at 50% duty cycle, output control=4). The resulting cell lysate was centrifuged at 11,000 ×*g* for one hour. The supernatant was then removed and mixed with 1 mL of Ni-NTA agarose resin (HisPur™ Ni-NTA Resin, Thermo Scientific) and left to shake for 1 hour at 4°C. The Ni-NTA cell supernatant mixture was loaded onto a chromatography column and washed with lysis buffer containing increasing concentrations of imidazole (20 mM-30 mM). His-tagged protein was eluted from the column with concentrations of 70 mM-500 mM imidazole. The eluted protein was dialyzed against storage buffer (5 mM Tris-HCl pH 8.5, 50 mM NaCl, 10% glycerol) and stored in 150 µL aliquots at -80°C. Protein samples were separated on a 12% SDS-PAG at 150 V for 1 hour and were visualized by Coomassie staining. When necessary, protein concentration was determined using the Bradford assay (85).

3.9 Electrophoretic mobility shift assays (EMSAs)

We used EMSAs to test the ability of TrmB to bind to G-quadruplex structures. The 5' P^{32}-labelled oligo (1 nM) and purified TrmB protein (0.2 µM to 2 µM), were mixed together and the reaction brought to 20 µL with TrmB storage buffer before being

incubated at room temperature for 30 minutes. For experimental reactions, the oligo 'GQ probe 1' was used, while the oligo 'GQ probe 1 mut' was used as the negative control as it did not form G-quadruplex structures (Table 3.4). Four microlitres of 6× bromophenol blue loading dye (1.2 M sucrose, 3.73 mM bromophenol blue) were added to each reaction and 20 µL of each sample were run on a 10% polyacrylamide gel in 0.5× TBE buffer for 30 minutes at 150 V. The gel was wrapped in cling film, exposed to a phosphor screen, and visualized using a phosphorimager.

3. 10 GQ-formation assays

3.10.1 Circular dichroism (CD) spectroscopy

Circular dichroism (CD) spectroscopy was used to confirm the ability of experimental oligonucleotides to form G-quadruplexes (those listed as GQ probe in Table 3.4) and later to test for the presence of G-quadruplex structures in oligonucleotides. Oligonucleotides that were tested for G-quadruplex formation were prepared for CD by heating the DNA (1 µM or 10 µM) in reactions brought to a total volume of 300 µL with GQ folding buffer (100 mM KCl, 50 mM Tris-HCl, pH 7.4). The samples were heated at 95°C for 5 minutes and then slow-cooled overnight in the heating block to allow the formation of G-quadruplex structures. The entire reaction was transferred to a 1 cm quartz cuvette and spectra were measured and recorded between 220 and 320 nm at 1 nm intervals, in technical triplicate. The same process was done for a DNA-free blank sample, and the values for the blank were subtracted from the experimental sample values.

3.10.2 CD based-GQ formation assays

To determine if TrmB could prevent the formation of G-quadruplex structures through methylation, test oligonucleotides were incubated in methylation buffer with purified TrmB. The DNA was then extracted and folded, and CD spectroscopy was used to determine whether G-quadruplex structures were present in the experimental and control samples. The procedure was based on kinetic experiments with *Aquifex aeolicus* TrmB (86). The experimental process is outlined in Figure 3.1.

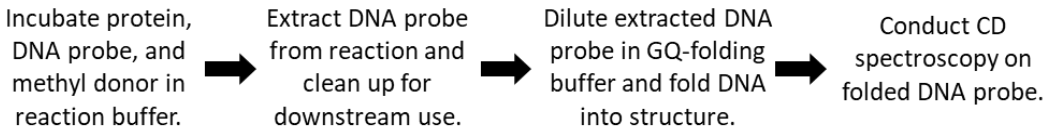

Figure 3.1. Experimental protocol flowchart of CD-based GQ-formation assays.

The oligonucleotide probe (10 µM), either GQ probe 1 or GQ probe 1 mut (Table 3.4), was added, together with 0.3 µg of purified TrmB and S-adenosyl methionine (20 µM), to methylation buffer (50 mM Tris-HCl pH 7.6, 5 mM $MgCl_2$, 6 mM β-mercaptoethanol, 50 mM KCl) and incubated at 30°C for 30 minutes. The DNA was then purified via phenol:chloroform extraction, as described in section 3.2.3. The purified DNA was resuspended in nuclease free water and diluted to 300 µL in GQ folding buffer then folded, before being tested using CD spectroscopy, as described in section 3.10.1. The final results were analyzed in Excel.

3.10.3 Piperidine-based GQ formation assays

To investigate if TrmB was capable of methylating G-quadruplex sequences in DNA, test oligonucleotides were incubated with purified TrmB, before being subjected to piperidine treatment, which breaks DNA at methylated guanine residues. Larger versions of the probes used in the CD based GQ formation assays were used for the piperidine tests (GQ probe 1 +39nt and GQ Probe 60nt_2). The larger nucleotide probes were created by adding 18 nucleotides to the 5’ end of the original probe and 21

nucleotides to the 3′ end. The additional nucleotides were taken from previously designed oligos that had been confirmed to not form any other structures (68). An outline of this experimental protocol is shown in Figure 3.2.

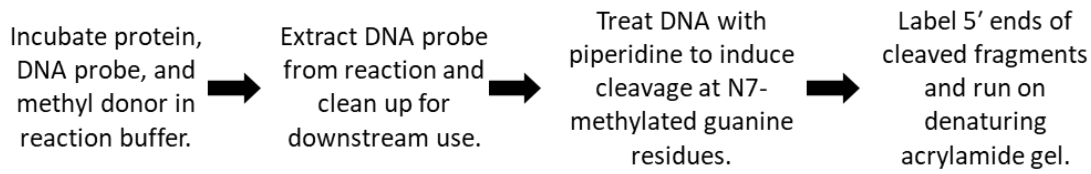

Figure 3.2. Experimental protocol flowchart of piperidine cleavage GQ-formation assays.

Two hundred picomoles of the experimental oligonucleotide probe (GQ probe 1 +39nt, Table 3.4) were incubated with 0.3 µg of TrmB and S-adenosyl methionine (20 µM) in methylation buffer (described above) for 30 minutes at 30°C. The DNA was purified using phenol:chloroform extraction and was precipitated as described in section 3.2.3, with the addition of 0.5 µg of glycogen to aid precipitation. As a positive control, one reaction was incubated at room temperature for 30 minutes in a 0.4%$_{v/v}$ solution of dimethyl sulfate (DMS) to methylate all guanine residues. The precipitated DMS or protein-treated DNA was resuspended in 100 µL of 10%$_{v/v}$ piperidine solution in nuclease-free water and heated at 90°C for 30 minutes to induce breakage at any methylated guanine residues. The DNA was again collected via precipitation with glycogen and ethanol and then resuspended in 20 µL of nuclease-free water. The fragments were then 5′ end-labelled with [γ-^{32}P]ATP as described above. Five to ten microlitres from the labelling reaction were then separated on a 6% denaturing polyacrylamide gel (6 M urea) for 30-60 minutes at 60 W. The gel was then transferred to filter paper and was visualized using a phosphorimager.

Table 3.4: Oligonucleotides used in this study

Name	Sequence*	Description
GQ probe 1	TTT TTT GGG AGG GCG GGA GGG	GQ probe for EMSAs
GQ probe 1 mut	TTT TTT GGG AGA GCG AGA GGG	Negative control GQ probe for EMSAs
GQ probe 1 +39nt	GCT TTA TCC AGT GAT CTC TTT TTT GGG AGG GCG GGA GGG CAA ATT AGA ACA TAC TGT AAA	Extended GQ probe for EMSAs/CD
GQ Probe 1 +39nt_mut	GCT TTA TCC AGT GAT CTC TTT TTT GGG AGA GCG AGA GGG CAA ATT AGA ACA TAC TGT AAA	Mutated extended GQ probe for EMSAs/CD
GQ Probe 60nt_2	GCT TTA TCC AGT GAT CTC TTT TTT GAG AGA GCG AGA GAG CAA ATT AGA ACA TAC TGT AAA	New mutated version of GQ Probe 1 +39 nt
SVEN_4897 F	ATA T**GG TAC C**GA TCT GGA ACG GCA TCC AGG	Checking RNA for DNA contamination
SVEN_4897 R	ATA T**TC TAG A**CG CGA GGT CCT TGT TCT TGG	Checking RNA for DNA contamination
FLAG-sv5394 F	CAT CAT **AAG CTT** TGG CCC CGT AGG GCA CAG	F primer for amplifying *FLAG-sv5394*
FLAG-sv5394 R	CAT CAT **GGT ACC** CCC GTT CTG GCG GAG C	R primer for amplifying *FLAG-sv5394*
sven_5265 promoter (HindII)-F	ATA T**AA GCT T**GC TAC CAG CAG CAG GAC C	F primer for amplifying *FLAG-sv5265*
sven_5265 (KpnI)-R	ATA T**GG TAC C**GA CAG CGA CTC AAC CCT ACC	R primer for amplifying *FLAG-sv5265*
sv5394H866A_revert_R	GTG GTC CTC ATG GCC GTG CGT G	R primer for reverting H86A mutation -> Wt
sv5394H866A_revert_F	CAC GGC CAT GAG GAC CAC ATC GG	F primer for reverting H86A mutation -> Wt
sv5265E132Q_RevR	GAT CAC CGC TTC AAG GGT GTC	R primer for reverting E132Q mutation ->Wt
sv5252E132Q_RevF	CCC TTG AAG CGG TGA TCG G	F primer for reverting E132Q mutation -> Wt
vnz_11015.north	CTC CCC CGA CTG GAC TCG AAC CAG TAA CC	Probe for *vnz11015* sRNA sequence
vnz_18810.north	GCC CCT CAC GCA CCT GCC AGA GCC GAC CTA CCC	Probe for *vnz18810* sRNA sequence
vnz_15980.north	GGC GGC CGG TCG GGC GTG CTC GGT TCC GGC	Probe for *vnz15980* sRNA sequence

Name	Sequence*	Description
5S rRNA.north	CCT AAC GCT ATG ACC ACC G	Probe for 5S rRNA sequence in northern blots
vnz13340RED_F	CGA GAC CGT CAC GCG TCA CCG TCA GGC TCT GAC CTC ATG *ATT CCG GGG ATC CGT CGA CC*	F primer to amplify hyg cassette for *nnaR* deletion
vnz13340RED_R	ACG CGG GGG CCG TAC GGA GGG GGC GGG CGG CCG GGG TCA *TGT AGG CTG GAG CTG CTT C*	R primer to amplify hyg cassette for *nnaR* deletion
vnz13340int_F	CGC CGC CTC GCT GTT C	Internal primer to check *nnaR* deletion
vnz13340down_R	AGT CCT CGA ACT CGT TGT TGA GC	Reverse primer to check *nnaR* deletion
vnz13340up_F	TCC TTC CAG ACC TCC GGC	Forward primer to check *nnaR* deletion
vnz13340int_R	CGT ACG CCC TTC TCC GC	Reverse internal primer to check *nnaR* deletion
vnz11080qPCR_F	CTG GAG GAC ATC CCG AAG AC	F primer for RT/qPCR for *vnz11080*
vnz11080qPCR_R	TTC AGT TCG GTG AGG TAG CG	R primer for RT/qPCR for *vnz11080*
vnz11140qPCR_F	TGA AGA CAC GGA TCG TGG TG	F primer for RT/qPCR for *vnz11140*
vnz11140qPCR_R	GAG CAG CAC CCT GTT GTA GG	R primer for RT/qPCR for *vnz11140*
vnz13340qPCR_F	GAA GCT GAT CCA GAC GGT GG	F primer for RT/qPCR for *vnz13340*
vnz13340qPCR_R	TCA CCC GTC GTA GGT GGT	R primer for RT/qPCR for *vnz13340*
vnz19350qPCR_F	GAG CTC CTC AAG TAC CTC GC	F primer for RT/qPCR for *vnz19350*
vnz19350qPCR_R	TAG TCG TAC CCC CAC ACC TC	R primer for RT/qPCR for *vnz19350*
vnz26110qPCR_F	CAC CGG GTT CAT GCT CAT CT	F primer for RT/qPCR for *vnz26110*
vnz26110qPCR_R	CAG CAT GTT GAG GGT GGA CT	R primer for RT/qPCR for *vnz26110*
rpoBF2	TCA AGG AGT TCT TCG GCA CC	F primer for RT/qPCR for *rpoB*

Name	Sequence*	Description
rpoBR2	ACC GAT CAG ACC GAT GTT CG	R primer for RT/qPCR for *rpoB*

*Underlined sequences indicate GQ motifs; *italicized* sequences indicate sequences homologous to FRT regions in ReDirect cassette templates; **bolded** sequences indicate restriction enzyme recognition sites (*Kpn*I, *Bam*HI, *Eco*RI, *Nde*I, *Xho*I, *Hind*III or *Xba*I). Oligonucleotides named with 'F' indicate a forward primer and 'R' indicates a reverser primer.

4. Results: TrmB and G-quadruplex interactions

4.1. Introduction

G-quadruplex (GQ) structures are recognized as important regulatory features in nucleic acids in both eukaryotes and bacteria and are particularly relevant in GC-rich organisms like *Streptomyces*, where the probability of a GQ-forming sequence occurring is higher than in an organism with lower GC content. The formation of a GQ in DNA can affect the expression of the surrounding genes, so proteins and small molecules that can bind G-quadruplexes and either stabilize or destabilize them can therefore have a significant regulatory role in organisms (66, 87). TrmB, a tRNA-methyltransferase, was previously identified as a potential GQ-interacting protein in *S. venezuelae* (68). TrmB methylates guanine residues in tRNA at the N7 position, which is one of the two positions involved in the non-canonical interactions between guanines that form the planar G-quartets in GQs. One proposed model for the interaction of TrmB with GQs in *S. venezuelae* was that it may be able to regulate GQ formation by methylating the guanine residues in GQ sequences (68). The goal of this section of work was to confirm whether TrmB could bind GQ structures, and subsequently to determine if TrmB could prevent the formation of GQs structures by methylating the guanine residues.

4.2 Electrophoretic mobility shift assays are inconclusive for TrmB binding with GQ structures

Previous attempts to overexpress *S. venezuelae* TrmB (*vnz_19075*) in *E. coli* for the purposes of testing its ability to bind and/or modify GQ sequences, resulted in inefficient purification and low final protein yields. We solved this issue by optimizing overexpression and purification conditions (Figure 4.1A and B). The resulting purified protein was used in all subsequent assays.

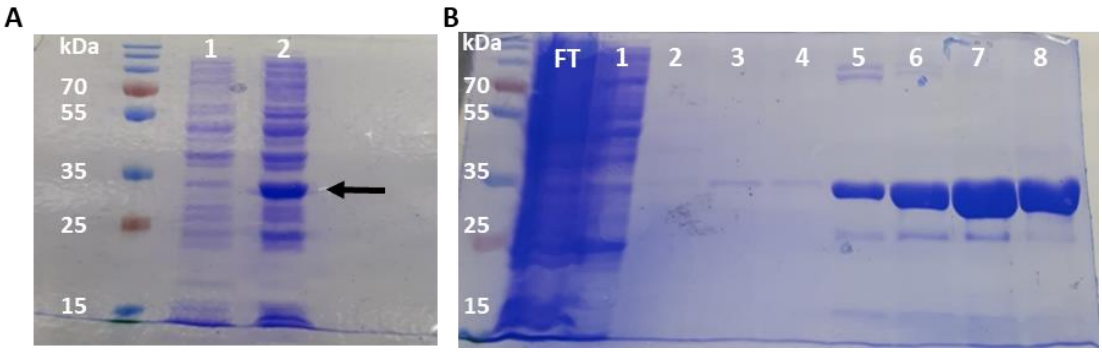

Figure 4.1. SDS-PAGs showing the overexpression and purification of TrmB. Twenty microlitres of each sample were run on a 12% denaturing (SDS) polyacrylamide gel for 90 minutes at 150 V. (**A)** Coomassie stain of pre- (1) and post- (2) induction cell lysate from an *E. coli* strain carrying the TrmB overexpression plasmid. The band corresponding to TrmB is indicated with an arrow. (**B)** Coomassie stain of purified TrmB. TrmB was purified using His-tag affinity chromatography. FT: flow through; lanes 1-8: increasing concentrations of imidazole in buffers used to wash and elute bound protein (lanes 1 and 2, 20 mM; lanes 3 and 4, 30 mM; lane 5, 70 mM; lane 6, 100 mM; lane 7, 150 mM; lane 8, 500 mM).

To test if purified TrmB could bind GQ sequences *in vitro*, we used electrophoretic mobility shift assays (EMSAs) modeled on those conducted previously using TrmB and oligonucleotide probes containing GQ sequences (68). The positive probe (GQ probe 1) contained a GQ sequence of 4 G-tracts, each containing three repeated G residues. Each tract was separated by a single nucleotide spacer. The negative probe (GQ probe 1 mut) possessed the same sequence as the positive probe, but the second and third G-tracts were disrupted by replacing one of the guanine residues with adenine to prevent the formation of GQ structures. The probes were folded into GQ structures and we used CD spectroscopy to confirm that the positive probe formed GQ structures, while the negative probe did not, as evidenced by a peak in the CD signal for the positive probe at 260 nm, and the absence of such a peak in the negative probe (Figure 4.2).

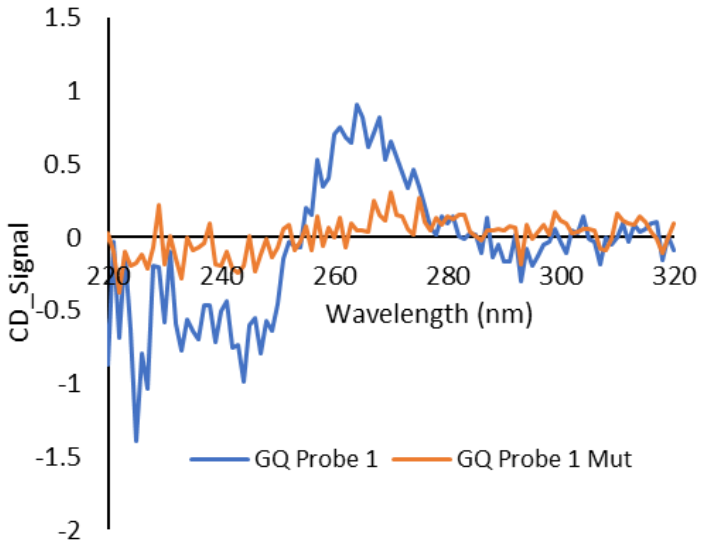

Figure 4.2. CD spectra of positive probe (GQ probe 1; blue) and negative control probe (GQ probe 1 mut; orange), confirming the presence of a GQ structure in the positive probe, but not the negative probe. Probes were diluted to a concentration of 1 µM in GQ-folding buffer and were scanned from 320-220 nm in 1 nm intervals. Each sample was scanned three times and the average of the three values was calculated. Samples were normalized by subtracting the average values of a buffer-only sample scanned across the same wavelengths.

We then used these folded GQ and negative control probes to conduct EMSAs to test the ability of TrmB to bind specifically to the GQ structure. We encountered a number of technical issues while performing these experiments, including inconsistencies in how the folded and labelled probes behaved when separated on polyacrylamide gels. For example, Figure 4.3 shows a representative example of one of several EMSAs that we conducted. The DNA probe (10 nM) was incubated with the indicated concentration of TrmB, and each reaction was loaded to an acrylamide gel. All 10 samples remained stuck in the wells of the gel despite being run at 150 V for 30 min. Additionally, both the positive and negative (mutated) probes were labelled with P^{32} and incubated with TrmB in an identical manner (including same input concentration), yet the GQ/folded probe bands were barely detectable, while the mutant probe bands appeared much more intense. One possible explanation may be that if more folded

probe was lost in the purification process post-labelling, the overall concentration of the positive probe would be lower in the corresponding EMSA reactions, and those bands would appear fainter in the final visualization.

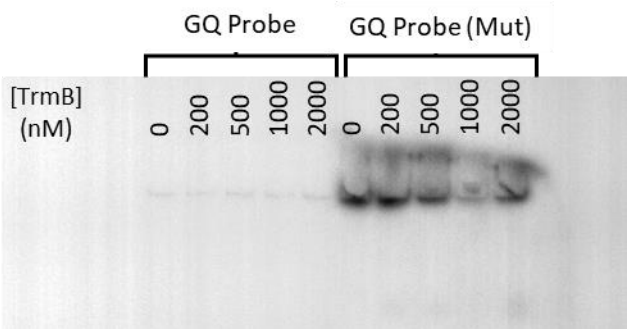

Figure 4.3. EMSA with 5'-end radiolabelled wild type (left) and mutated (Mut; right) GQ probes (10 nM) and indicated concentrations of purified TrmB. Twenty microlitres of each reaction were run on a 6% polyacrylamide gel at 150 V for 30 minutes.

There were also differences in how the folded and unfolded versions of the GQ probe behaved when separated on an acrylamide gel. We tested separating each probe on its own (without protein) on a native polyacrylamide gel. As can be seen in Figure 4.4, the unfolded probe partially ran into the gel while the folded probe remained in the wells. Given the challenges associated with visualizing the folded GQ probes, we were unable to draw meaningful conclusions about the ability of TrmB to bind GQ structures *in vitro* using EMSAs.

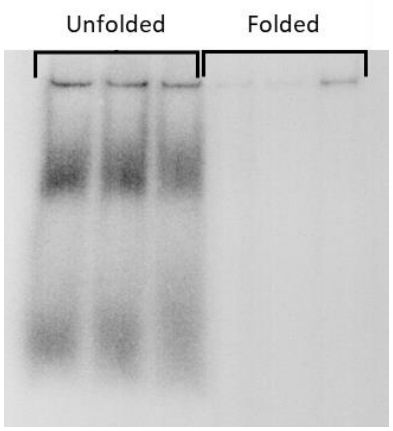

Figure 4.4. Native polyacrylamide gel comparing folded and unfolded GQ probes. Labelled and unfolded positive GQ probe (left; 20 nM, 3 replicates) and labelled and folded positive GQ probe (right; 20 nM, 3 replicates) on a 6% polyacrylamide gel. Twenty microlitres of each sample was run at 150 V for 30 minutes.

4.3. TrmB methylation of GQ sequences remains unclear

Although EMSAs can provide information about whether a protein can bind DNA, they do not provide insight into the nature of that interaction. Given that the major question surrounding TrmB in *S. venezuelae* was whether it could methylate guanine residues and prevent GQ formation, and in light of the technical issues associated with the EMSAs, we switched our focus to probing the specific methylation capabilities of TrmB and its effect on GQ formation using the probes described above. The goal of this work was two-fold: (i) to determine whether TrmB could methylate the GQ probe DNA, and (ii) to determine if this methylation could prevent the downstream formation of GQ structures in the target DNA.

4.3.1. CD spectroscopy does not reveal changes in GQ formation in TrmB samples

We set up *in vitro* methylation reactions with purified TrmB, *S*-adenosyl-methionine as a methyl group donor, and either positive (GQ-forming) or negative (mutated) DNA probes. To ensure that any effects observed were specifically due to the action of the TrmB protein, we conducted the same reactions using the Lsr2 protein (a DNA-binding protein lacking methylation activity) in place of TrmB.

If TrmB can methylate the GQ sequence and prevent GQ formation, then we would expect that the methylated DNA recovered from a reaction with TrmB would be unable to form a GQ structure. The product of the same reaction conducted with Lsr2 instead of TrmB should be capable of forming a GQ structure (since Lsr2 should not interfere with GQ folding). As an additional control, we included reactions using the mutated probe, incubated with either TrmB or Lsr2. The mutated probe should not form GQ structures, irrespective of the protein with which it was incubated. Finally, as a positive control, we included a reaction containing GQ probe alone (no protein), which had been pre-folded into a GQ structure.

We assessed the probe structures following methylation and folding using CD (Figure 4.5). As expected, there was no positive GQ spectrum in either reaction

containing the mutated probe. There were no clear differences in the spectra of the TrmB reactions with either the positive or mutated GQ probe either. It is worth noting, however, that the positive control (probe alone) lacked a strong, positive peak at 260 nm, like that shown in Figure 4.2. The lack of a clear spectrum in these samples may be due to significant losses of DNA from the methylation reactions, which could also have contributed to the unexpected fluctuations seen in the 220-240 nm range of all spectra. Given the lack of expected behaviour from the control reactions, it was not possible to draw any conclusions regarding the ability of TrmB to prevent GQ formation by guanine residue methylation.

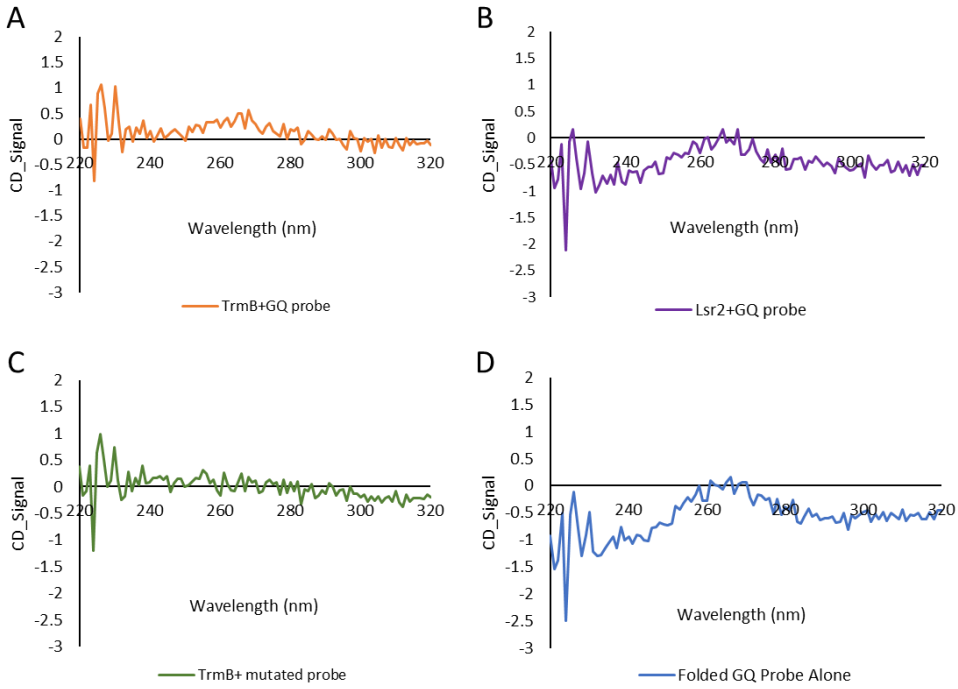

Figure 4.5. CD spectra from DNA recovered from each methylation reaction. Each sample was diluted to 300 µL in GQ folding buffer and measured from 320-220 nm at 1 nm intervals. Each sample was scanned three times and the average of the three values was calculated. Samples were normalized by subtracting the average values of a buffer only sample scanned across the same wavelengths. Spectrum of DNA from **(A)** reaction of TrmB and positive GQ probe; **(B)** reaction of Lsr2 and positive GQ probe; **(C)** reaction of TrmB and the negative (mutated) GQ probe; **(D)** reaction of the pre-folded positive probe alone.

4.3.2. Piperidine treatment does not reveal methylated G residues in TrmB samples

One limitation of CD spectroscopy is that high concentrations and large volumes of DNA are required in order to obtain clear spectra. In our initial experiments (above), methylation reactions were conducted using DNA at a concentration of 10 µM; it was likely that DNA was lost during the subsequent purification steps, and consequently, that the final concentration of DNA used for CD spectroscopy would be lower than the starting amount. We were also using a short DNA probe (21 nt in length) which was more difficult to precipitate and purify compared with larger oligonucleotides. To bypass these problems, we modified the final steps of the methylation assay and used larger oligonucleotide probes. We confirmed the ability of this larger probe (non-mutated sequence) to adopt a GQ structure using CD spectroscopy (Figure 4.6).

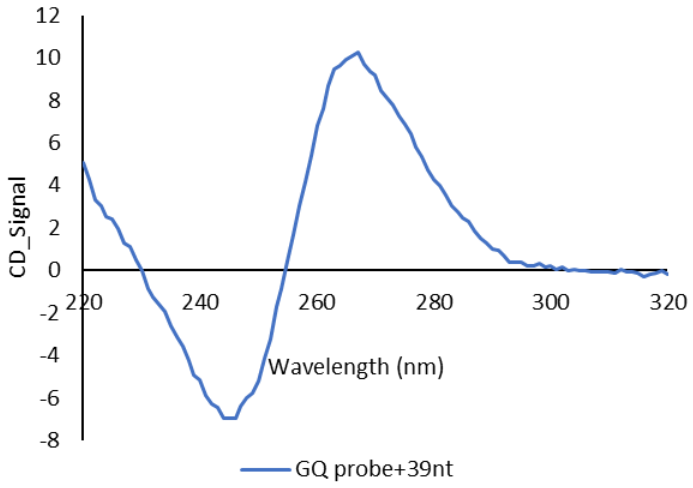

Figure 4.6. CD spectrum of the larger 60 nucleotide unmutated GQ probe. DNA was diluted to 10 µM in GQ folding buffer and CD was conducted from 320-220 nm in 1 nm intervals. Each spectrum was scanned three times and the average of the values was used. A buffer-only sample was used to normalize the experimental spectrum.

Instead of monitoring GQ formation following methylation using CD, we instead opted to employ a piperidine breakage assay. Following methylation, the purified DNA

was treated with piperidine to induce breaks in the DNA at methylated guanine residues and then the fragments were radiolabelled and resolved on a sequencing-length (40 cm) denaturing polyacrylamide gel. For comparison and as a positive control, one DNA sample was treated with dimethyl sulfate (DMS) instead of TrmB, where DMS methylates all guanine residues. As a negative control, we also included a sample where DNA was exposed only to piperidine treatment and no protein or DMS.

In a trial with the positive GQ probe and either DNA and piperidine alone (negative); DNA, DMS and piperidine (positive); and DNA and TrmB/SAM and piperidine (experimental), we observed a cleavage pattern only in the DMS treated example, where 3-4 bands were visible near the bottom of the gel and may correspond to the 5'-most tract of guanines in the GQ probe (Figure 4.7). In the lane with the experimental sample, there were no bands at that location. The highest band visible on the gel in all three samples likely corresponded to the full-length probe. In all three samples, there was also an intense band that appeared in the middle of the gel, indicated with an arrow. We repeated the assay using a range of SAM concentrations and observed similar results to the initial test (Figure 4.8). The same 5' tract appeared intense in the DMS-treated control (indicated by a square bracket in Figure 4.8), and these bands also increased in intensity as SAM concentration increased, suggesting that these residues may be increasingly methylated at higher SAM concentrations. An intense band in the middle of the gel (indicated by an arrow in Figure 4.8) was also seen in all of these samples, regardless of experimental condition, suggesting that the DNA probe may be prone to breakage at that position, irrespective of methylation status.

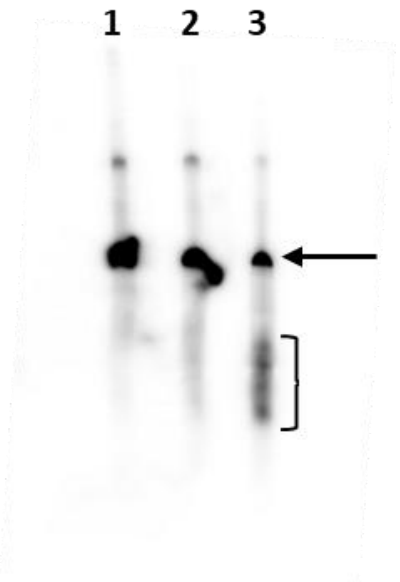

Figure 4.7. Phosphorimage of 5′ end radiolabelled GQ probe DNA from DMS and piperidine treated samples. **(1)** DNA from piperidine-only reaction (negative control); **(2)** DNA from reaction with methylation reaction with TrmB (300 ng) then treated with piperidine; **(3)** DMS and piperidine-treated DNA (positive control). The square bracket indicates the bands that may correspond to a methylated track of guanines in the DNA. The arrow indicates the intense band that appeared in all samples. Ten microlitres of each reaction were run on a 6% acrylamide-urea gel for 35 min at 60 W.

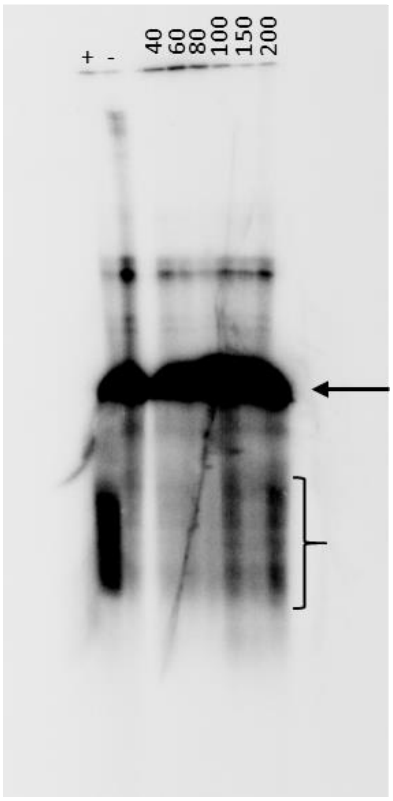

Figure 4.8. Phosphorimage of 5′ end radiolabelled GQ probe DNA treated with DMS and piperidine (+), or piperidine alone (-). Lanes to the right of the negative control show DNA from methylation reactions with TrmB (300 ng) supplemented with increasing concentrations of SAM (40-200 µM). The square bracket indicates the bands that may correspond to a methylated track of guanines in the DNA. The arrow indicates the intense band that appeared in all samples. Ten microlitres of each reaction were run on a 6% acrylamide-urea gel for 35 min at 60 W.

4.5 Conclusions

Previous work showed that TrmB could associate with GQ structures through biotin pulldowns using *S. venezuelae* cell lysate (68). The initial goal of this work was to confirm this interaction *in vitro* and determine if TrmB, an annotated tRNA-methyltransferase, could also methylate DNA sequences like the GQ probe used in the pulldown assay. Methylation of the guanine residues in GQ motifs would affect their ability to form GQ structures, possibly representing a novel mechanism for bacteria to regulate gene expression, as the presence of GQ structures in nucleic acids has been shown to affect the expression of nearby genes. We were unable to show that TrmB could bind the DNA of interest using EMSAs, or demonstrate definitively that TrmB could methylate DNA containing GQ sequences. In summary, answering the question of whether TrmB can bind and methylate GQ sequences will require additional investigation.

5. Results: Phenotypic and transcript abundance changes in Δ*rnj* and Δ*rnc* mutants

5.1 Introduction

RNases are important for a multitude of cellular processes, including rRNA and tRNA maturation, bulk RNA degradation, and RNA quality control (37). In *S. venezuelae,* the deletion of the genes encoding RNase J or RNase III from the genome impacts the development and antibiotic production abilities of the bacteria, but the specific molecular mechanisms underlying these effects remain unclear (44). In this section, we investigated how the loss of either of these RNases affected (i) the growth and development of *S. venezuelae* and (ii) the global transcript levels of *S. venezuelae*.

5.2 Deletion of *rnc* or *rnj* alters the classical development of *S. venezuelae*

My work on RNases in *S. venezuelae* began with validating the developmental phenotypes of two RNase mutant strains of *S. venezuelae*, one lacking the gene encoding RNase J (Δ*rnj*), and one lacking the gene encoding RNase III (Δ*rnc*) (44). We established that in liquid MYM medium, the Δ*rnj* strain was delayed in development and remained mostly vegetative, even after 20-24 hours of growth, at which point the wild type and Δ*rnc* strains had both sporulated completely (Figure 5.1A). On solid MYM medium, the Δ*rnc* strain also displayed a distinctive 'peeling' phenotype, where large portions of the colony peeled away from the medium underneath; this phenotype was not observed for wild type *S. venezuelae* (Figure 5.1B). These results confirm previous reports that RNase III and RNase J are important for the proper growth and development of *S. venezuelae* (44).

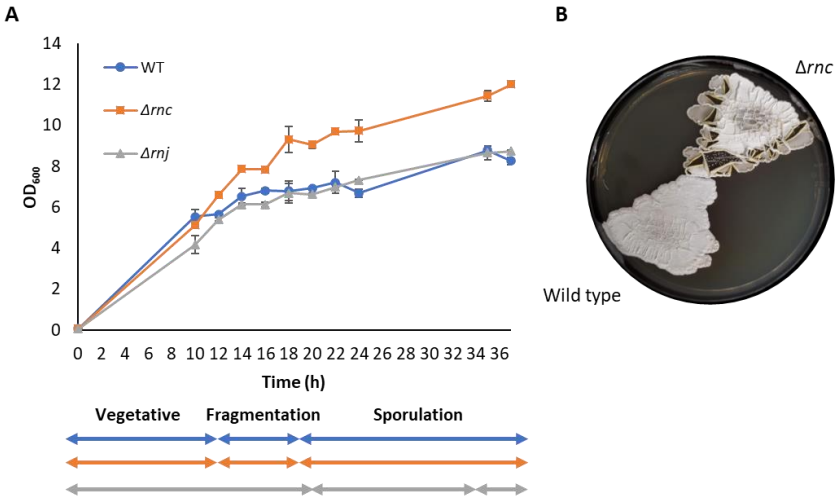

Figure 5.1. Growth of wild type and RNase mutants in liquid and on solid MYM medium. **A.** Growth of wild type *S. venezuelae* and RNase mutants in liquid MYM medium. Strains were inoculated from an overnight culture to a starting OD_{600} of 0.05 and grown shaking at 30°C. OD_{600} was measured using a spectrophotometer and developmental stage was tracked using light microscopy. Error bars represent standard error of three biological replicates. **B.** Growth of wild type *S. venezuelae* and an Δ*rnc* mutant on solid MYM medium. Five microlitres of an overnight culture were streaked on the plate and then grown at 30°C for 3 days.

5.3 The Δ*rnj* mutant fails to explore on MYMG medium

There are a variety of different growth conditions that can trigger the exploration phenotype in *S. venezuelae*. We tested both the Δ*rnc* and Δ*rnj* mutants on several solid media types and conditions that promote exploration in wild type *S. venezuelae*. The most dramatic phenotype was observed when the Δ*rnj* strain was grown on solid MYM-glycerol (MYMG) medium, which is standard MYM medium that has been supplemented with 2% glycerol. Wild type *S. venezuelae* grown on MYMG has a phenotype intermediate of full exploration and classical development, exhibiting rapid outward colony expansion, but at the same time progressing through the classical life cycle stages of vegetative growth, aerial growth, and sporulation within the core regions of the colony (Figure 5.2). On MYMG the Δ*rnj* mutant did not explore and indeed, was impaired in its ability to grow at all. For up to 14 days the mutant colony remained static and undeveloped, while the wild type sporulated and grew rapidly outwards. This phenotype was specific to the Δ*rnj* mutant and could be complemented with the reintroduction of *rnj* on an integrating plasmid (Figure 5.2).

We also noted the frequent occurrence of "escaper" growths out of the main Δ*rnj* colony body after 10+ days of growth on MYMG. Escapers are regions of outgrowth from the main colony body that grow much faster and more robustly than the main colony; they likely represent regions of the colony where suppressor mutations have arisen. We harvested cells from a particularly robust escaper region in a Δ*rnj* +pIJ82 mutant grown on MYMG and showed that the escaper cells maintained their wild type phenotype when re-grown on fresh MYMG medium (Figure 5.3).

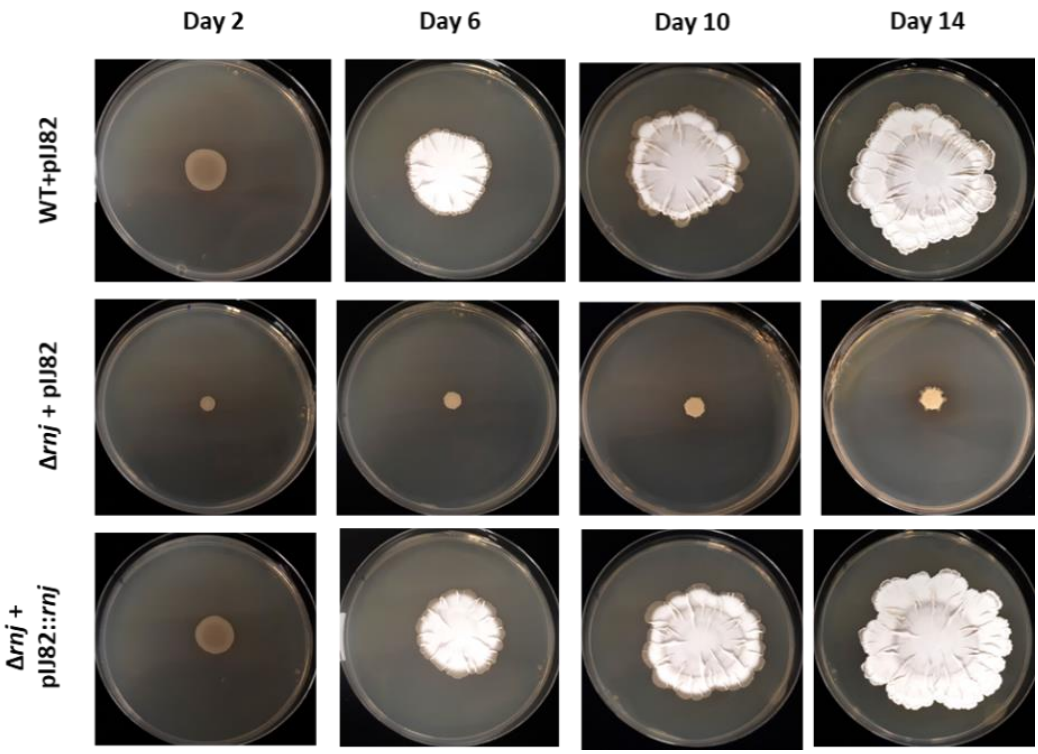

Figure 5.2. Growth of wild type and Δ*rnj* mutants on solid MYMG medium. Liquid cultures of strains were grown shaking overnight at 30°C in MYM medium. Biomass levels were then normalized to the same OD_{600} before 5 µL of each liquid culture were spotted to MYMG plates. Plates were then grown at 30°C for 14 days. Images above are of the same colony across 14 days.

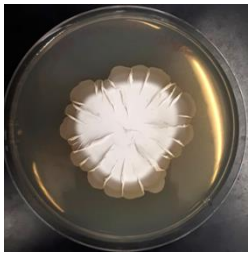

Figure 5.3. Growth of Δ*rnj* + pIJ82 escaper strain on MYMG. Five microlitres of the collected spore stock were spotted on an MYMG plate and grown at 30°C for 6 days.

Another medium which promotes exploration in wild type *S. venezuelae* is solid YP (yeast-peptone) medium. Unlike MYMG, when the Δ*rnj* mutant was grown on YP, it developed faster than the wild type strain, exhibiting the wrinkling pattern characteristic of exploration on YP within 2 days of growth. The Δ*rnj* colonies grown on YP also had a more irregular colony outline compared to the wild type strain which was more uniformly circular. This phenotype could also be complemented by the reintroduction of *rnj* to the mutant (Figure 5.4).

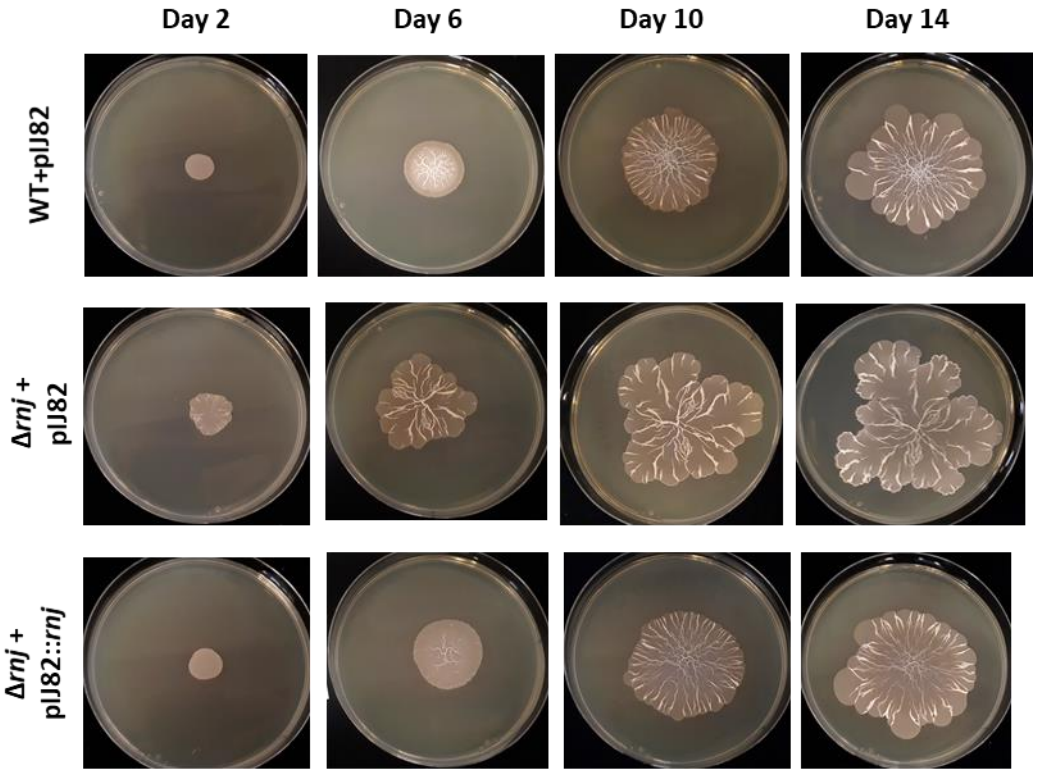

Figure 5.4. Growth of wild type and Δ*rnj* mutants on solid YP medium. Liquid cultures of strains were grown shaking overnight at 30°C in MYM medium. Cultures were then normalized to the same OD_{600} before 5 µL of each liquid culture were spotted to YP plates. Plates were then grown at 30°C for 14 days. Images are of the same colony across 14 days.

5.4 A small RNA is abundant in the Δ*rnj* mutant

When total RNA was extracted from Δ*rnj* mutants and was separated on an agarose gel, we consistently observed an intense band of ~70-100 nt. The band was only present in the Δ*rnj* strain and not the Δ*rnc* strain and complementation of the Δ*rnj* strain caused the band to disappear, suggesting that the band arose specifically as a result of the removal of *rnj* from *S. venezuelae*. We extracted the band and it was sequenced using an sRNA-specific RNA-sequencing protocol. Three potential candidates for the sRNA band were identified based on abundance of reads aligned to regions within these genes: *vnz_11015* (tRNA-Asn), *vnz_18810* (RNA component of the signal recognition particle), and *vnz_15980* (coding sequence of a hypothetical secreted protein). We designed probes for each of these candidate sequences and tested them using northern blots with RNA from wild type and Δ*rnj S. venezuelae,* to determine whether any of

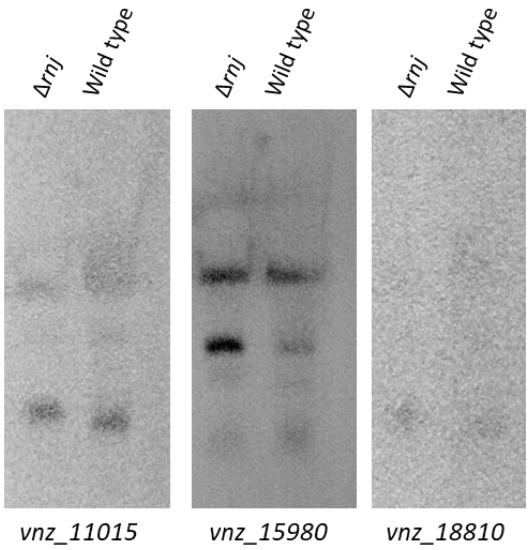

Figure 5.5. Northern blots for potential sRNA candidates in wild type and Δ*rnj S. venezuelae* RNA. Five micrograms of total RNA were run on a 6% denaturing polyacrylamide gel with 6M urea.

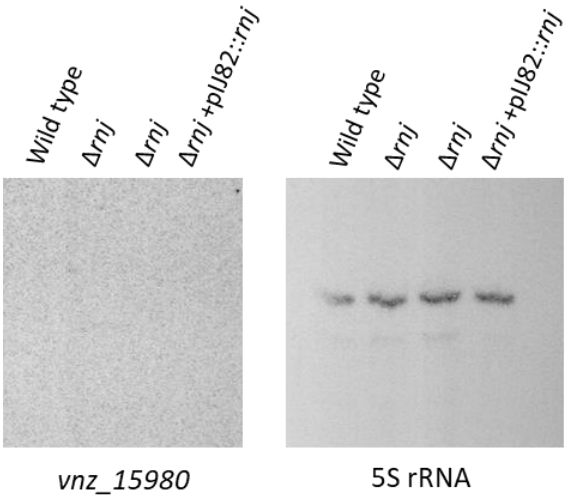

Figure 5.6. Replicate of northern blots for *vnz_15980* in the wild type and Δ*rnj S. venezuelae* RNA. Five micrograms of total RNA were run on a 6% denaturing polyacrylamide gel with 6M urea.

these candidate transcripts were more abundant in the Δ*rnj* mutant compared with the wild type. Blots of *vnz_11015* and *vnz_18810* revealed no difference in abundance between the wild type and Δ*rnj*. A preliminary northern with a probe for *vnz_15980* revealed a band that was more intense in the Δ*rnj* sample compared to the wild type (Figure 5.5), but we were not able to detect this transcript in subsequent blotting experiments, despite the 5S rRNA positive control behaving exactly as expected (Figure 5.6). As such, it seems unlikely that any of these transcripts are responsible for the intense band observed in the extracted Δ*rnj* RNA samples.

5.5 RNA-sequencing reveals global transcript level changes in Δ*rnj* and Δ*rnc* mutants

To understand how transcription levels changed on a global scale in the RNase mutants relative to the wild type, we extracted RNA from the wild type and both Δ*rnj* and Δ*rnc* mutant strains for RNA-sequencing. The strains were grown in liquid MYM medium and cells were collected at timepoints corresponding to the different stages of growth (vegetative growth, hyphal fragmentation, and sporulation). We were unable to successfully extract RNA from the wild type sporulation samples, potentially due to the low abundance and quality of RNA in the spores of wild type *S. venezuelae*. For comparison at the sporulation time point, we used RNA-sequencing data that had been collected from the same wild type strain at 18 hours, representing a late fragmentation/early sporulation timepoint, by Gehrke *et al* (88).

We compared the transcript profiles of each mutant to the wild type at each stage of development (Δ*rnj* vs. wild type at vegetative, Δ*rnj* vs. wild type at fragmentation, etc.), with an initial focus on genes that encode known regulators of development and antibiotic production in *S. venezuelae,* and on specialized metabolic clusters identified in *S. venezuelae* using the antiSMASH program (89). We found a large number of genes with significantly different transcript levels in either mutant relative to

the wild type and, interestingly, found similar trends in the types of genes that had differential transcript abundance in both the Δ*rnj* and Δ*rnc* strains.

We filtered the data for genes that had significantly altered transcript levels based on fold change from wild type to mutant (4-fold or greater), base mean (greater than 50), and adjusted P-value (less than 0.05). In the Δ*rnc* mutant, we identified 1136 genes overall that had significantly changed transcript levels relative to the wild type, representing 15.4% of all annotated genes. The total was less for the Δ*rnj* mutant, in which we identified 893 genes (total) that had significantly changed transcript levels relative to the wild type, or 12.1% of all annotated genes. In the Δ*rnc* data, the timepoints with the highest numbers of genes with altered transcript abundance were vegetative growth (411 genes upregulated) and sporulation (506 genes downregulated). The trend was similar in the Δ*rnj* data with the transcript levels of 304 genes altered during vegetative growth and 282 changed during sporulation. A summary of these changes is in Figure 5.7. The full data set for each RNase mutant is available in Supplemental Files 1 and 2.

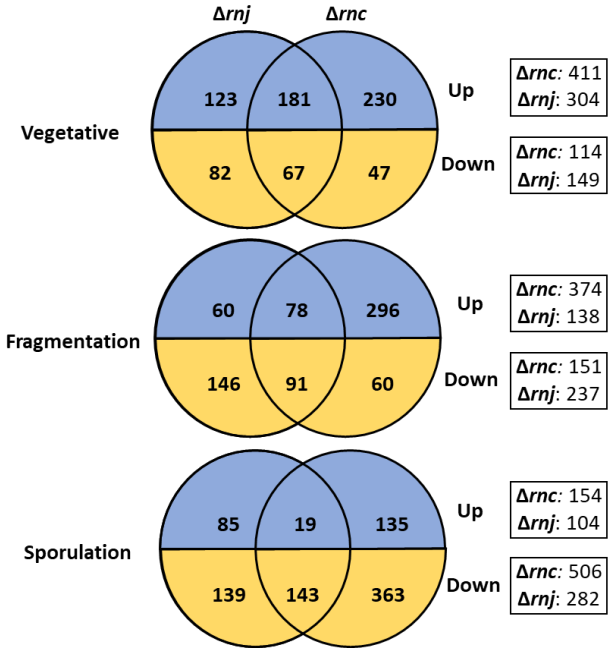

Figure 5.7. Summary of changes in transcript abundance in *S. venezuelae* Δ*rnj* and Δ*rnc* mutants relative to wild type *S. venezuelae*. Changes in transcript levels were analyzed using DESeq2 and the data were filtered for significant changes as described above. Numbers in boxes indicate the total number of genes with significantly altered transcript levels in either mutant at the indicated growth stage. Numbers in the Venn diagram indicate how many of the genes were unique to each mutant or shared between each mutant. The complete RNA-sequencing analysis is available in Supplemental Files 1 and 2.

5.5.1 Deletion of *rnj* or *rnc* affects the transcript levels of regulators of phosphate uptake and specialized metabolism

In examining our RNA-sequencing data, we initially set out to assess the effects of these RNase mutations on the expression of regulators known to impact development and specialized metabolite production in *S. venezuelae* (for a complete list, see "Regulators" in the supplementary data). We found that most regulators did not have significantly altered transcript abundance in either the Δ*rnc* or Δ*rnj* strain, but amongst those that were impacted, the trend was decreased transcript abundance in the mutant relative to the wild type. The regulators that changed the most in the mutants compared to the wild type were *phoR* and *phoP*, which encode a two-component system that regulates phosphate uptake in *S. venezuelae* (29). In both Δ*rnc* and Δ*rnj* mutants, the transcript abundance of these genes was at least 8-fold lower in the mutant relative to the wild type during vegetative growth (Table 5.1 and 5.2). In the Δ*rnj* mutant, we further noted the increased transcript levels of *atrA*, which encodes a TetR- family transcriptional regulator, during vegetative growth and sporulation

Table 5.1: Differential transcript abundance in regulators between wild type and Δ*rnj* at each timepoint[1]

Gene ID	Gene Name	Vegetative	Fragmentation	Sporulation
vnz_15230	*afsR*	-0.22	0.09	0.62
vnz_15235	*afsS*	-0.56	-1.58	0.93
vnz_15890	*lsr2*	-1.48	-0.37	1.02
vnz_19105	*atrA*	**2.32***	1.16	**2.53***
vnz_19350	*glnR*	-1.87	1.51	1.26
vnz_19580	*phoR*	**-3.26***	-1.26	-1.46
vnz_19585	*phoP*	**-3.16***	-0.45	-0.69

[1]Vegetative/Fragmentation/Sporulation columns contain the $\log_2$(Fold Change) values from wild type to the Δ*rnj* mutant at each of those developmental stages. Bolded cells with an asterisk (*) indicate the $\log_2$(FC) value is significant (P-adj <0.05); positive values indicate higher transcript abundance in the mutant strain, while negative values indicate lower transcript abundance in the mutant. Blue highlights indicate a regulator whose transcript abundance increased in the Δ*rnj* mutant and yellow highlights indicate that a regulator whose transcript abundance decreased in the Δ*rnj* mutant. The full data for these genes are available in the supplemental data.

Regulators with altered transcript levels (relative to the wild type) were more abundant in the Δ*rnc* mutant, where we detected significant changes in the transcript levels of the genes *sIHF* (encoding a nucleoid associated protein involved in chromosome organization), *absC* (encoding a MarR family transcriptional regulator), *afsS* (encoding a small regulatory protein that activates antibiotic cluster expression), and *lsr2* (encoding a nucleoid associated protein that is a global regulator of biosynthetic cluster expression) at various stages in development (88, 90–92). *sIHF* and *absC* transcript levels were significantly lower in the Δ*rnc* mutant during sporulation, while *afsS* levels was lower during fragmentation and *lsr2* expression was lower during vegetative growth.

Table 5.2: Differential transcript abundance in regulators between wild type and Δ*rnc* at each timepoint[1]

Gene ID	Gene Name	Vegetative	Fragmentation	Sporulation
vnz_05240	*sIHF*	-0.15	-1.28	**-3.12***
vnz_15230	*afsR*	-1.03	-0.54	-0.12
vnz_15235	*afsS*	-0.07	**-2.33***	-1.17
vnz_15890	*lsr2*	**-2.86***	-0.14	-0.46
vnz_19350	*glnR*	-1.52	-0.63	1.43
vnz_19580	*phoR*	**-3.41***	0.81	**-2.37***
vnz_19585	*phoP*	**-3.43***	1.86	-1.58
vnz_24975	*absC*	-1.93	-0.23	**-2.54***

[1]Vegetative/Fragmentation/Sporulation columns contain the $\log_2$(Fold Change) values from wild type to the Δ*rnc* mutant at each of those developmental stages. Bolded cells with an asterisk (*) indicate the $\log_2$(FC) value is significant (P-adj <0.05); positive values indicate higher transcript abundance in the mutant strain and negative values indicate lower transcript abundance in the mutant. Blue highlights indicate a regulator with increased transcript abundance in the Δ*rnc* mutant and yellow highlights indicate a regulator with decreased transcript abundance in the Δ*rnc* mutant. The full data for these genes are available in the supplemental data.

5.5.2 Genes encoding nitrogen assimilation and phosphate uptake products have altered transcript abundance in the RNase mutants

One of the most obvious changes in both the Δ*rnc* and Δ*rnj* strains, relative to their wild type parent, was the significant increase in transcript abundance of several genes encoding nitrogen assimilation-related products during the later stages of growth, including: the nitrite reductase gene *nirB* and its related operon (*vnz_11140, vnz_11145,* and *vnz_11150*), the nitrate reductase gene *nasA* (*vnz_11080*), the ammonium transporter gene *amtB* and its related operon (*vnz_26110*, *vnz_26115*, and *vnz_26120*), the nitrate transporter gene *narK* (*vnz_13345*), the glutamine synthetase gene *glnII* (*vnz_09185*), and the potential nitrogen regulatory protein gene *nnaR* (*vnz_13340*) (Table 5.3 and 5.4).

We confirmed the differential expression of *nnaR, nirB, amtB,* and *nasA* using semi-quantitative RT-PCR (Figure 5.8). Further investigation revealed that all of the above-listed genes are documented targets (in *S. venezuelae* or *S. coelicolor*) of the global nitrogen regulator, GlnR, which activates the expression of these genes in low nitrogen growth conditions (26, 93). An increase in *glnR* transcript levels (and GlnR protein) in the mutants, relative to the wild type, could account for the increase in the transcript levels of its target genes. However, the only significant increase in *glnR* transcript abundance occurred in the Δ*rnc* strain during sporulation, after the transcript levels of the target genes had increased (Table 5.4). In fact, the transcript abundance of *glnR* was lower in the mutants relative to the wild type during vegetative growth, suggesting that an increase in abundance of *glnR* (and GlnR) alone did not account for the increase in the transcript abundance of the GlnR target genes that we observed.

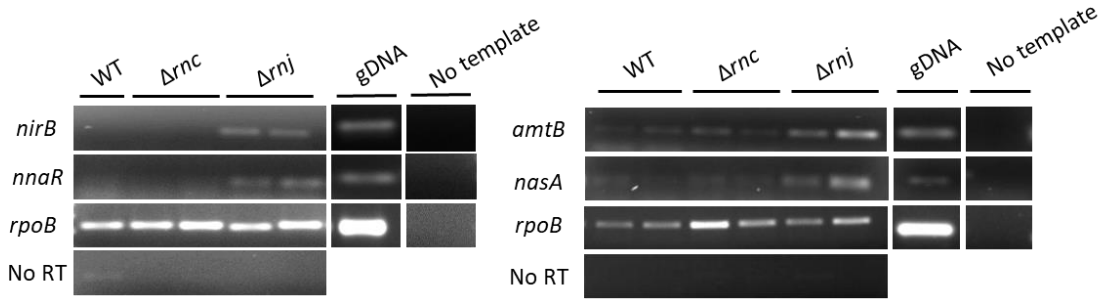

Figure 5.8. Semiquantitative RT-PCR on RNA extracted from wild type and Δ*rnc* or Δ*rnj* mutants during fragmentation. Primers for *rpoB* were used as a positive control, while no reverse transcriptase (–RT) and no template reactions with each set of primers served as negative controls. Ten microlitres from each sample were run on an agarose gel. Pictured samples from the same primer pair reactions were separated on the same agarose gel.

The changes in nitrogen-related genes prompted us to also look at genes involved in the stringent response, specifically the *relA* and *rshA* homologs in *S. venzuelae*. Transcripts for *rshA* were more abundant in both RNase mutants during vegetative growth, then less abundant during the later stages of growth (Table 5.3 and 5.4). There were no significant changes in the transcript levels of *relA* in the RNase mutants.

As previously mentioned, we also found that the genes encoding the two-component system responsible for regulating phosphate uptake, *phoRP*, had significantly lower transcript levels in both the Δ*rnc* and Δ*rnj* strains during vegetative growth. Transcript abundance for several of the regulatory targets of PhoP were also lower in the RNase mutants compared to the wild type during vegetative growth, including the *pst* operon (*vnz_19250-vnz_19265*), which encodes a phosphate ABC transporter; *phoD* (*vnz_08450*), which encodes a secreted alkaline phosphatase; and *phoU* (*vnz_19575*), which encodes a phosphate transport system regulatory protein. PhoP has also been implicated in regulating components of oxidative phosphorylation and, accordingly, we found that transcript abundance for the genes that encode complex I (*nuoA-M/vnz_21055-vnz_21120*) was significantly different in both mutants

compared to the wild type during vegetative growth and fragmentation (Table 5.5 and 5.6) (94).

Since the RNase J mutant grew poorly on MYM medium with glycerol, we also examined the expression of the major TCA cycle enzyme-encoding genes in both of our *S. venezuelae* RNase mutants. Previous research demonstrated that a *B. subtilis* mutant which developed poorly on glycerol-containing medium developed high levels of TCA cycle products (95). We found that there were significant changes in transcript abundance for the genes encoding citrate synthase, aconitase (*acnA*), isocitrate dehydrogenase (*icd*), succinate dehydrogenase (*sdh*), and malate dehydrogenase (*mdh*). All of the genes encoding these products had significantly lower transcript levels during at least one stage of growth in both the Δ*rnj* and Δ*rnc* mutants (Table 5.5 and 5.6).

Table 5.3: Differential transcript abundance in nitrogen assimilation and phosphate uptake genes between wild type and Δ*rnj* strains [1]

Gene ID	Name	Vegetative	Fragmentation	Sporulation
vnz_05405	*relA*	-1.30	-0.72	-1.06
vnz_27065	*rshA*	**2.45***	**-2.17***	-1.08
vnz_05890	*glnA4*	**2.84***	**-5.48***	**2.19***
vnz_09130	*glnA*	**-4.87***	0.34	-0.19
vnz_09185	*glnII*	**-7.45***	**3.57***	**3.88***
vnz_09195	*glnRII*	0.85	2.56	3.16
vnz_09440	*glnA2*	-1.63	**2.45***	1.02
vnz_11080	*nasA*	1.93	**8.22***	**11.95***
vnz_11140	*nirB*	0.00	**10.18***	**11.26***
vnz_11145	*nirB*	-0.63	**9.16***	**10.28***
vnz_11150	*nirC*	0.00	**8.46***	**9.85***
vnz_13340	*nnaR*	-2.57	**6.42***	**8.02***
vnz_13345	*narK*	0.40	**4.81***	**8.28***
vnz_26110	*amtB*	-4.01	**5.24***	**5.20***
vnz_26115	*glnK*	-1.76	**6.01***	**5.54***
vnz_26120	*glnD*	-0.04	**4.99***	**4.13***
vnz_34930	N/A	0.56	**6.36***	**9.11***
vnz_07320	*pitH2*	**-3.25***	0.30	**-2.17***
vnz_08450	*phoD*	-0.29	**-2.53***	**-2.02***
vnz_09625	*phoA*	-2.07	1.87	**-2.13***
vnz_19250	*pstB*	**-3.46***	-0.50	0.09
vnz_19255	*pstA*	**-4.47***	**-2.30***	-1.13
vnz_19260	*pstC*	**-4.54***	**-2.31***	-1.62
vnz_19265	*pstS*	**-4.55***	-1.50	-1.17
vnz_19575	*phoU*	**-4.55***	-1.41	-0.61

[1]Vegetative/Fragmentation/Sporulation columns contain the $\log_2$(Fold Change) values from wild type to the Δ*rnj* mutant at each of those developmental stages. Green highlights indicate nitrogen assimilation-related genes and orange highlights indicate phosphate-related genes. Bolded cells with a * indicate the $\log_2$(FC) value is significant (P-adj <0.05); positive values indicate higher transcript abundance in the mutant strain and negative values indicate lower transcript abundance in the mutant. The full data for these genes is available in the supplemental data.

Table 5.4: Differential transcript abundance in nitrogen assimilation and phosphate uptake genes between wild type and Δ*rnc* strains[1]

Gene ID	Name	Vegetative	Fragmentation	Sporulation
vnz_07320	*pitH2*	**-3.00***	**2.62***	0.90
vnz_08450	*phoD*	-0.82	-1.18	**-3.91***
vnz_09625	*phoA*	-1.50	**2.52***	**-4.42***
vnz_19250	*pstB*	**-4.51***	1.98	-1.74
vnz_19255	*pstA*	**-5.25***	-0.18	**-2.91***
vnz_19260	*pstC*	**-5.08***	0.35	**-3.76***
vnz_19265	*pstS*	**-5.06***	1.79	**-4.25***
vnz_19575	*phoU*	**-4.01***	1.65	-1.18
vnz_05890	*glnA4*	0.78	**-8.26***	**3.49***
vnz_09130	*glnA*	**-2.72***	-0.63	-1.29
vnz_09185	*glnII*	**-5.73***	-0.02	1.90
vnz_09195	*glnRII*	-1.33	-1.00	-1.21
vnz_09440	*glnA2*	-0.35	0.56	0.09
vnz_11080	*nasA*	-1.56	1.93	**7.82***
vnz_11140	*nirB*	0.00	**3.44***	**8.31***
vnz_11145	*nirB*	-1.02	**3.56***	**7.81***
vnz_11150	*nirC*	1.00	3.10	**7.55***
vnz_13340	*nnaR*	**-4.87***	1.47	**4.70***
vnz_13345	*narK*	-0.25	-0.18	**4.99***
vnz_26110	*amtB*	-2.67	0.55	2.91
vnz_26115	*glnK*	-1.30	0.84	3.65
vnz_26120	*glnD*	0.64	1.62	2.57
vnz_34930	N/A	0.40	**3.06***	**6.31***
vnz_05405	*relA*	-0.71	0.96	0.33
vnz_27065	*rshA*	2.08	-1.82	**-3.19***

[1]Vegetative/Fragmentation/Sporulation columns contain the $\log_2$(Fold Change) values from wild type to the Δ*rnc* mutant at each of those developmental stages. Green highlights indicate nitrogen assimilation-related genes and orange highlights indicate phosphate-related genes. Bolded cells with an asterisk (*) indicate the $\log_2$(FC) value is significant (P-adj <0.05); positive values indicate higher transcript abundance in the mutant strain and negative values indicate lower transcript abundance in the mutant. The full data for these genes is available in the supplemental data.

Table 5.5: Differential transcript abundance in TCA cycle genes and complex I genes between wild type and Δ*rnj* strains[1]

Gene ID	Name	Vegetative	Fragmentation	Sporulation
vnz_21055	*nuoA*	**3.00***	-0.90	-0.23
vnz_21060	*nuoB*	**3.91***	-1.30	-0.02
vnz_21065	*nuoC*	**3.36***	**-2.29***	-1.03
vnz_21070	*nuoD*	**5.00***	**-2.79***	-0.71
vnz_21075	*nuoE*	**4.53***	**-2.95***	-0.79
vnz_21080	*nuoF*	**4.90***	**-3.05***	-0.92
vnz_21085	*nuoG*	**5.62***	**-2.43***	-0.42
vnz_21090	*nuoH*	**5.32***	**-3.53***	-0.93
vnz_21095	*nuoI*	**4.61***	**-2.29***	-0.36
vnz_21100	*nuoJ*	**5.16***	**-3.06***	-0.56
vnz_21105	*nuoK*	**4.63***	**-3.14***	-0.90
vnz_21110	*nuoL*	**5.03***	**-3.55***	-0.94
vnz_21115	*nuoM*	**5.83***	**-3.86***	-1.13
vnz_21120	*nuoN*	**5.38***	**-2.74***	-0.23
vnz_02070	*icd*	**-2.85***	-1.50	**-3.09***
vnz_08885	*cox1*	-1.68	**-2.53***	**-2.07***
vnz_09030	*pdhL*	**-2.11***	-1.62	-1.74
vnz_09045	*aceE1*	-1.41	**-2.18***	0.00
vnz_18250	*cydB*	**-3.02***	-1.08	**-2.00***
vnz_18335	Dihydrolipoamide dehydrogenase	**-2.14***	-1.53	-1.91
vnz_20755	Citrate synthase	-0.72	**-3.04***	**-2.25***
vnz_21240	2-oxoacid:ferredoxin oxidoreductase subunit beta	1.38	**-2.15***	-1.06
vnz_21245	2-oxoglutarate ferredoxin oxidoreductase subunit alpha	0.42	**-3.28***	**-2.82***
vnz_22160	*sucC*	-1.14	-1.89	**-2.04***
vnz_22230	*mdh*	**-2.06***	**-2.71***	**-2.53***
vnz_22395	*sdhA*	-1.43	**-2.15***	-1.79
vnz_22400	*sdhD*	-1.84	**-2.10***	**-2.02***
vnz_22405	*sdhC*	-1.71	**-2.44***	**-2.12***
vnz_23020	Phosphoenolpyruvate carboxykinase	0.06	-0.40	**-2.26***
vnz_28745	*acnA*	**-3.14***	0.62	-1.26

[1]Vegetative/Fragmentation/Sporulation columns contain the $\log_2$(Fold Change) values from wild type to the Δ*rnj* mutant at each of those developmental stages. Pink highlights indicate genes involved in complex I, non-highlighted genes are involved in the TCA

cycle. Bolded cells with an asterisk (*) indicate the log_2(FC) value is significant (P-adj <0.05); positive values indicate higher transcript abundance in the mutant strain and negative values indicate lower transcript abundance in the mutant. The full data for these genes is available in the supplemental data.

Table 5.6: Differential transcript abundance in TCA cycle genes and complex I genes between wild type and Δ*rnc* strains *

Gene ID	Name	Vegetative	Fragmentation	Sporulation
vnz_21055	*nuoA*	1.95	-1.08	-1.92
vnz_21060	*nuoB*	**3.01***	-1.24	-1.81
vnz_21065	*nuoC*	**2.73***	-1.67	**-2.75***
vnz_21070	*nuoD*	**4.20***	**-2.12***	**-2.34***
vnz_21075	*nuoE*	**3.79***	**-2.19***	**-3.31***
vnz_21080	*nuoF*	**4.11***	**-2.50***	**-2.77***
vnz_21085	*nuoG*	**4.56***	**-2.02***	**-2.36***
vnz_21090	*nuoH*	**4.48***	**-3.02***	**-3.09***
vnz_21095	*nuoI*	**3.65***	-1.64	**-2.30***
vnz_21100	*nuoJ*	**4.52***	**-3.10***	**-2.77***
vnz_21105	*nuoK*	**4.13***	**-2.25***	**-2.39***
vnz_21110	*nuoL*	**4.60***	**-2.93***	**-2.54***
vnz_21115	*nuoM*	**5.60***	**-3.21***	**-2.84***
vnz_21120	*nuoN*	**5.10***	**-2.88***	**-2.26***
vnz_02070	*icd*	-1.45	-0.88	**-3.18***
vnz_08885	*cox1*	-0.59	-1.07	**-4.88***
vnz_09030	*pdhL*	-1.46	0.10	-1.84
vnz_09045	*aceE1*	-1.90	-1.83	-0.52
vnz_18250	*cydB*	-0.97	-0.59	-1.72
vnz_18335	Dihydrolipoamide dehydrogenase	-1.05	0.07	**-2.23***
vnz_20755	citrate synthase	-0.79	**-2.37***	-1.38
vnz_21240	2-oxoacid:ferredoxin oxidoreductase subunit beta	-0.24	-1.86	**-2.54***
vnz_21245	2-oxoglutarate ferredoxin oxidoreductase subunit alpha	-0.49	-1.73	**-2.59***
vnz_22160	*sucC*	-0.64	-0.10	**-2.71***
vnz_22230	*mdh*	-0.93	-1.43	**-4.29***
vnz_22395	*sdhA*	-0.66	-0.49	**-3.27***
vnz_22400	*sdhD*	-0.68	-0.95	**-3.40***

Gene ID	Name	Vegetative	Fragmentation	Sporulation
vnz_22405	*sdhC*	-0.70	-0.82	**-3.24***
vnz_23020	phosphoenolpyruvate carboxykinase	-0.77	1.41	0.96
vnz_28745	*acnA*	**-2.15***	0.12	-1.80

*Vegetative/Fragmentation/Sporulation columns contain the log2(FC) value from wild type to the Δ*rnc* mutant at each of those developmental stages. Pink highlights indicate genes involved in complex I, non-highlighted genes are involved in the TCA cycle. Bolded cells with an asterisk (*) indicate the $\log_2$(FC) value is significant (P-adj <0.05). Positive values indicate higher transcript abundance in the mutant strain and negative values indicate lower transcript abundance in the mutant. The full data for these genes is available in the supplemental data.

5.5.3 Δ*rnj* and Δ*rnc* mutants have increased transcript levels of genes within biosynthetic clusters during vegetative growth

We next investigated whether there were any changes in the transcript levels of genes within specialized metabolic clusters in the RNase mutants, based on a list of annotated clusters compiled through the antiSMASH program (89). Many of these clusters are transcriptionally inactive when wild type *S. venezuelae* is grown under standard laboratory conditions and the regulatory pathways involved in their expression are of particular interest (19). We found differential transcript abundance between the RNase mutants and wild type *S. venezuelae* in five of the thirty biosynthetic clusters annotated by antiSMASH in *S. venezuelae.* The general trend within these clusters was that regions of the cluster would have higher transcript abundance in the RNase mutants during vegetative growth and the levels were similar, or less, in the mutant at later stages of growth. The chloramphenicol cluster was particularly affected; the transcript abundance of genes in this cluster were 16 to 256-fold higher in the Δ*rnc* and Δ*rnj* mutants than the wild type during vegetative growth. The dramatic changes in the chloramphenicol cluster led us to suspect the involvement of Lsr2.

Lsr2 is a global regulatory protein that binds within multiple biosynthetic clusters and represses their transcription; it has a significant impact on the chloramphenicol cluster in *S. venezuelae* (88). In the biosynthetic clusters where we observed changes in

transcript levels in the RNase mutants, the genes with the most significant changes in transcript abundance were frequently proximal to documented Lsr2 binding sites (88). During vegetative growth the gene encoding Lsr2 (*lsr2*) was significantly lower in transcript abundance in the Δ*rnc* mutant (almost 8-fold reduction) and was also lower in the Δ*rnj* mutant as well (just under our significance threshold, with an approximately 3-fold reduction).

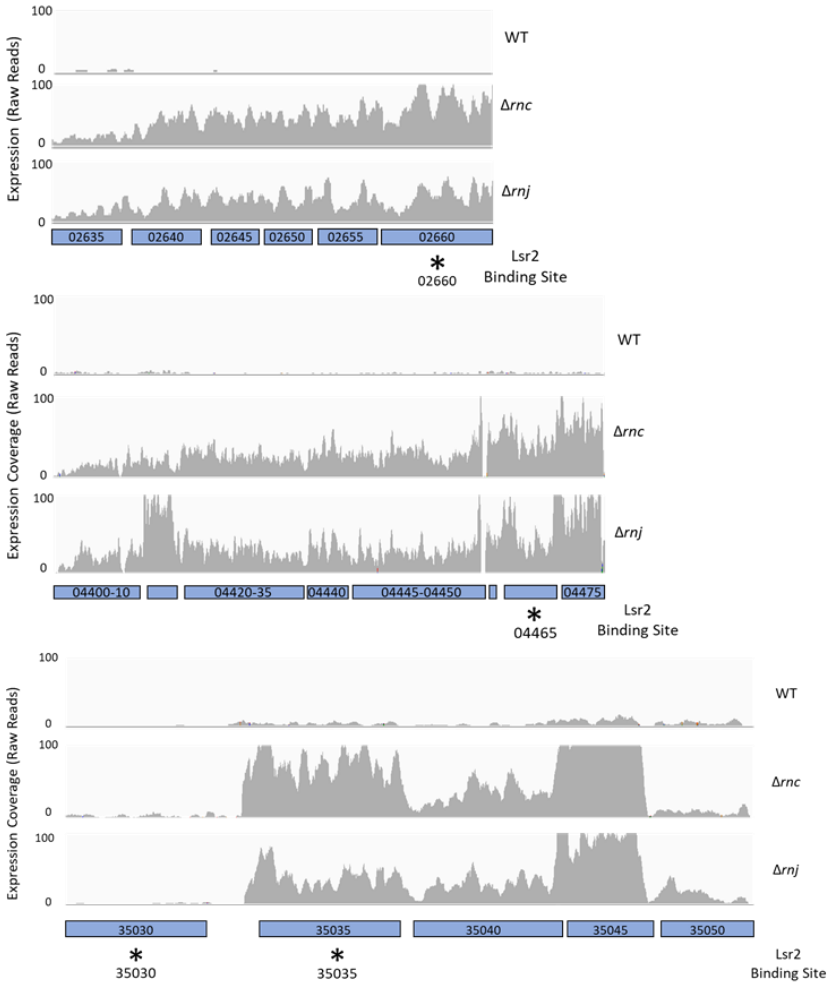

Figure 5.9. Visualization of read coverage for regions of three biosynthetic clusters in the wild type and RNase mutants during vegetative growth. * indicate Lsr2 binding sites within the highlighted gene. (**A)** Region of a lantipeptide cluster (cluster: *vnz_02575-vnz_02680;* pictured: *vnz_02635-vnz_02660*). **(B)** Chloramphenicol cluster (cluster: *vnz_04400-vnz_04475*). **(C)** Region of a terpene cluster (cluster: *vnz_34990-vnz_35080*; pictured: *vnz_35030-vnz_35050*).

Beyond the chloramphenicol cluster, we found significant differential transcript levels between the RNase mutants and wild type in a predicted lantipeptide cluster (*vnz_02585*-*vnz_02675*), a non-ribosomal peptide synthase (NRPS) cluster (*vnz_34650*-*vnz_34800*), a melanin cluster (*vnz*_22830-*vnz*_23040), and a predicted terpene synthesis cluster (*vnz_34995*-*vnz_35080*) (Figure 5.9). These clusters followed the same pattern as the chloramphenicol cluster, in that genes within them had higher transcript levels during vegetative growth relative to the wild type and lower or similar levels during the later stages of growth. The changes in expression were not always present across an entire cluster. For example, within the lantipeptide cluster, only the genes from *vnz_02640* to *vnz_02655* changed significantly.

5.6 Laying the foundation for differentiating direct and indirect RNase targets using FLAG-tagged catalytically inactive RNase III and RNase J enzymes

To follow up on the RNA-sequencing data, and to differentiate between direct and indirect targets of RNase III and RNase J, we created 3×FLAG-tagged variants of each protein. Specifically, we constructed a 3×FLAG-tagged variant with the wild type RNase sequence and a catalytically inactive variant (RNase III: E132Q; RNase J: H86A) bearing a point mutation in the active site that would allow binding, but not cleavage, of a target RNA (50, 84). These constructs were intended to be used to determine whether changes in the transcript abundance of a gene in a RNase mutant were the result of an RNase directly targeting that transcript. The FLAG-tag would allow us to 'pull down' the enzymes with their associated transcripts and the lack of catalytic activity would allow for transcript retention. We confirmed that the 3×FLAG-RNase III E132Q construct did not complement the Δ*rnc* mutant 'peeling' phenotype on solid MYM medium, while the 3×FLAG-wild type RNC construct was able to complement this phenotype (Figure 5.10).

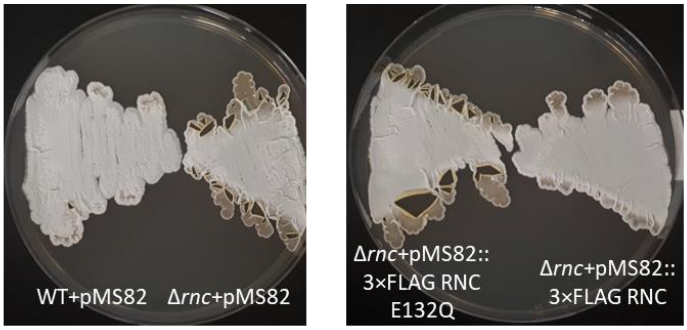

Figure 5.10. Image of wild type and Δ*rnc* mutant strains of *S. venezuelae* containing the constructs for FLAG-tagged RNase III. Five microlitres of an overnight culture for each strain were streaked on the MYM plate and then grown at 30°C for 6 days.

We also confirmed the expression of 3×FLAG-tagged RNase III E132Q and 3×FLAG-tagged wild type RNase III at each developmental stage using western blotting.

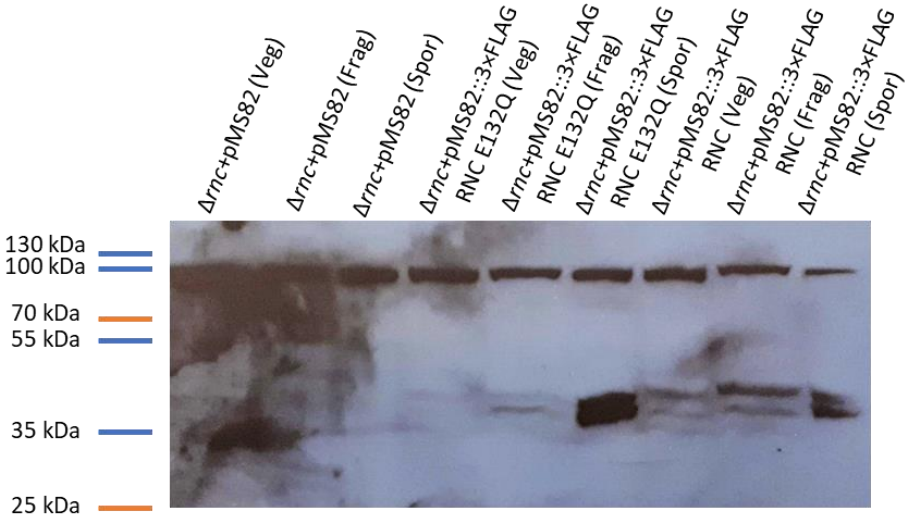

Figure 5.11. Western blot of 3×FLAG-tagged RNase III protein from vegetative, fragmentation, or sporulation stages of growth. Sixty micrograms of total protein extract from *S. venezuelae,* containing either the empty pMS82 vector or the pMS82 vector with 3×FLAG-tagged RNase III (E132Q or wild type) were run on a 12% SDS-PAG. The molecular weight of 3×FLAG-tagged RNase III is 31.3 kDa.

The bands at approximately 35 kDa in the lanes containing the FLAG-tagged constructs were indicative of FLAG-tagged RNase III. The presence of two bands may indicate processing or cleavage of RNase III (Figure 5.11). We were also able to confirm that the 3×FLAG-tagged RNase J H86A variant did not complement the developmental delay of the Δ*rnj* mutant when grown in liquid MYM, while the 3×FLAG-tagged wild type variant successfully restored development to wild type kinetics (Figure 5.12). However, we were unable to confirm the expression of the 3×FLAG-tagged RNase J H86A or 3×FLAG-tagged wild type RNase J enzymes through western blotting. The FLAG tag associated with RNase J may be inaccessible to the antibody, or it may be cleaved from the protein and degraded *in vivo*.

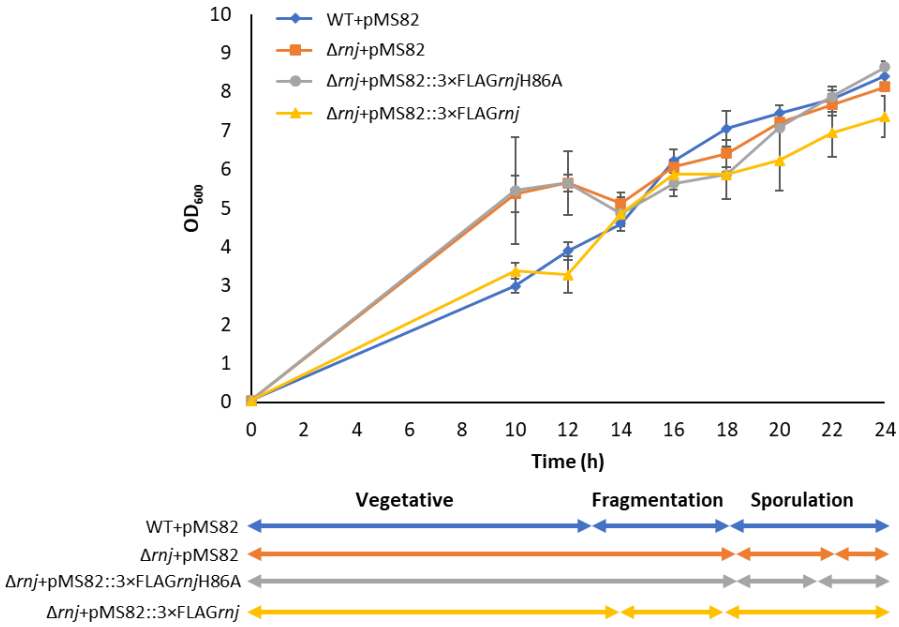

Figure 5.12. Growth of wild type and Δ*rnj S. venezuelae* containing constructs for FLAG-tagged RNase J (H86A or wild type). Strains were inoculated from an overnight culture to a starting OD_{600} of 0.05 and grown shaking at 30°C. OD_{600} was measured using a spectrophotometer and developmental stage was tracked using light microscopy. Error bars represent standard error of three biological replicates.

5.7 Conclusions

Overall, it is clear that the deletion of either *rnc* or *rnj* from *S. venezuelae* alters the behaviour of *S. venezuelae* and profoundly affects the transcript abundance of a diverse set of genes, including those that encode products involved in nutrient acquisition and usage. It is also apparent that these genes are connected through high level regulatory networks in *Streptomyces.* As of yet it remains unclear exactly how an RNase deletion triggers these changes, but future work with these strains and our FLAG-tagged RNase constructs will help us to elucidate direct and indirect effects of RNase J and III in these complex bacteria.

6. Discussion and Future Directions

In this work we investigated the roles of two components of gene regulation in *S. venezuelae*: G-quadruplex structures, and RNase enzymes. We were specifically interested in a potential interaction between the tRNA-methyltransferase TrmB and G-quadruplexes (GQs). While we were not able to draw conclusions about the relationship between TrmB and GQs in *S. venezuelae*, these structures remain of interest in *Streptomyces* and other GC rich organisms.

We also showed that the deletion of either *rnc* or *rnj* had significant effects on the global transcript levels in *S. venezuelae* and changed the transcript abundance of genes involved in primary metabolism, biosynthetic clusters, and other global regulators. Interestingly, several of the same genes and clusters were similarly affected in both mutants when compared to the wild type. These changes reveal a number of exciting future directions for investigating the roles of these enzymes in *Streptomyces*.

6.1 The role of TrmB in connection to G-quadruplexes in *S. venezuelae* is uncertain

TrmB, a tRNA methyltransferase that methylates guanine residues at the N7 position, was identified in previous work as a potential GQ-interacting protein in *S. venezuelae* (68). One proposed model explaining this interaction was that TrmB could bind and methylate the GQ sequence in the DNA probe used in the pull-down assays; methylation of these sequences could represent a novel form of gene regulation in bacteria (68). However, using a variety of experimental techniques, we were unable to confirm the ability of TrmB to bind DNA probes or to methylate these sequences.

Upon reflection, our initial proposed methylation model itself presents a paradox. TrmB was identified bound to an already formed GQ structure, but our working model proposed that TrmB might prevent GQ-structure formation through methylation. In a GQ structure, the N7 position (where TrmB would methylate a guanine residue) is involved in the non-canonical bonds that form the planar structures in the quadruplex.

This interaction is impervious to chemically-mediated methylation via dimethyl sulfate and the residue might also be inaccessible to a methylating enzyme (96). It seems unlikely that TrmB could methylate guanine residues already integrated into a G-quadruplex structure. An alternative explanation for the interaction of TrmB and G-quadruplex structures could be that the protein only recognizes the GQ structure and not the specific DNA sequence. In *Aquifex aeolicus* the most important tRNA features for TrmB binding are the T-loop and anticodon-loop structures (97). *A. aeolicus* TrmB also binds tRNA molecules that lack the specific G46 residue that TrmB methylates, demonstrating that the substrate specificity of TrmB is not necessarily linked to its methylation activity (86).

If TrmB only binds GQ structures and does not methylate the associated DNA, this would not necessarily preclude TrmB from exerting a regulatory effect on gene expression. GQ binding proteins are important in both eukaryotic and bacterial systems (67, 98). If future work reveals an interaction between TrmB and GQ structures in *S. venezuelae*, an interesting avenue to consider would be whether the transcription or transcript stability of genes containing GQ structures change in the presence or absence of TrmB.

6.1.1 Future directions regarding G-quadruplexes in *Streptomyces*

Given the technical issues encountered in pursuing these studies, the value in pursuing this particular line of investigation is unclear. However, GQs remain a relevant feature in *Streptomyces* and it is becoming increasingly clear that these structures have significant roles in bacteria (64). An alternative direction to pursue could include determining the prevalence of GQ formation in *Streptomyces in vivo*, given that all work to date has focused on bioinformatics analyses, and the presence of a GQ sequence does not necessarily mean that a GQ structure will form at that location *in vivo*. Given the high GC content of *Streptomyces* genomes, these bacteria represent an exciting model for investigating the biological roles of these structures in bacteria.

6.2 Phenotypic and transcript level changes in the Δ*rnj* and Δ*rnc* mutants

6.2.1 The Δ*rnj* mutant grows poorly on a complex medium containing glycerol

The changes we observed in the growth of the Δ*rnc* or Δ*rnj* mutant compared to their wild type parent *S. venezuelae* strain align with previous reports for these mutants and are similar to what has been observed in *S. coelicolor* and *B. subtilis* (44). In *S. coelicolor, rnj* and *rnc* single mutants exhibited altered antibiotic production while the deletion of *rnjA/B* from *B. subtilis* resulted in major sporulation and growth defects similar to the delayed sporulation we observed in Δ*rnj S. venezuelae* (53, 99).

Recent work has shown that standard *Streptomyces* growth medium (MYM), when supplemented with glycerol (MYMG), prompts a shift in *S. venezuelae* from its classical mode of development to a newly characterized mode of growth called exploration (Shepherdson, unpublished). We found that the *S. venezuelae* Δ*rnj* mutant grew poorly on MYMG medium and did not progress through either its classical life cycle (aerial hyphae formation and sporulation) or explore like the wild type strain. In *S. venezuelae,* glycerol use is controlled by products encoded in the glycerol operon (*vnz_06115-vnz_06130*). Although the genes in this operon did not significantly change in transcript abundance between the wild type and Δ*rnj* strain in our RNA-sequencing data, it is not possible to say whether a change in transcription of this operon is responsible for the MYMG phenotype since the RNA-sequencing data were collected from strains grown in liquid MYM medium and not on solid MYMG medium.

Exploring colonies of *Streptomyces* display a striking visual similarity to biofilms formed in other species such as *B. subtilis*. Interestingly, in some *B. subtilis* mutants a glycerol-induced biofilm defect has been documented that is similar to, but less severe than, the phenotype seen here for the Δ*rnj* mutant. Specifically, a *B. subtilis* mutant lacking *gltA* (encoding glutamate synthase) did not form biofilms when grown in rich medium containing high concentrations of glycerol (95). It was determined that at high glycerol concentrations, the *B. subtilis gltA* mutant accumulated excess amounts of

citrate, which then sequestered iron away from the phosphorelay system involved in triggering biofilm formation (95). We noted significant changes in the transcript abundance of several genes encoding TCA cycle enzymes in our RNase mutants, but it is not clear if these changes would lead to an accumulation of citrate or other intermediates that could impair *S. venezuelae* growth on a medium containing glycerol. Additionally, the changes in TCA enzyme transcripts were also observed in the Δ*rnc S. venezuelae* strain, which is not deficient in growth on MYMG. The occurrence of the same genetic changes in the Δ*rnc* strain without the same phenotype on MYMG suggests that the genetic underpinning of the Δ*rnj* MYMG phenotype may be the result of other factors.

The distinct impairment in growth and the specificity of this phenotype to the Δ*rnj* mutant make it a promising tool for further investigations into the factors impacting *S. venezuelae* development, particularly exploratory growth. A targeted comparison of the transcript abundance of the glycerol operon and other glycerol metabolism genes between the Δ*rnj* mutant, the escaper strain we collected, the Δ*rnc* mutant, and the wild type when grown on MYMG could reveal if differences in the transcript abundance of these genes are connected to the Δ*rnj* growth defects on MYMG. Additionally, sequencing the genome of this escaper strain is another possible direction to determine what suppressor mutations are responsible for the reversion of the phenotype and what genes are important for growth on MYMG medium.

6.2.2 RNA fragment(s) unique to the Δ*rnj* mutant

Another phenomenon unique to the Δ*rnj* mutant was the consistent appearance of a small RNA fragment in RNA extracted from this strain. One candidate was identified as a fragment within the central region of the coding sequence of the gene *vnz_15980*, which is annotated as encoding a hypothetical protein. Initial northern blots showed that this transcript was indeed more abundant in the Δ*rnj* mutant compared to the wild type, but this observation could not be replicated. Given that the control probe showed

that RNA was present on the membrane in this situation, it may be a matter of further troubleshooting to properly detect the RNA fragment. Transcription start site data for *S. venezuelae* did not show any internal transcription start sites within *vnz_15980* which may indicate, along with the size of the RNA visible on an agarose gel, that the band we are observing is a stable degradation product.

We are also considering the possibility that the abundant band may represent stable tRNA cleavage products. In *S. coelicolor*, mature tRNA molecules are cleaved in the anticodon loop, starting during the transition from vegetative to aerial growth under nutrient limited conditions (100). This cleavage produces two fragments that are 5′ and 3′ of the anticodon loop. The 5′ fragment is then accessible for degradation by 3′-5′ RNases and the 3′ fragment is exposed to degradation in the 5′-3′ direction. As RNase J is the only documented bacterial RNase with 5′-3′ directionality, the deletion of *rnj* could significantly stabilize the 3′ tRNA fragments from these cleavage events. Additionally, this tRNA cleavage phenomenon is observed when *S. coelicolor* is grown in nutrient-limited medium. Transcriptional data from our *S. venezuelae* Δ*rnj* mutant showed significant changes in many genes related to primary metabolism and nutrient uptake and usage (discussed further in section 6.2.3). These transcriptional changes may indicate that the mutant is experiencing nutrient stress, a condition in which tRNA cleavage is prompted. A future direction for this project will be to use RNA extracts from our Δ*rnj* mutants and wild type strains to investigate if this tRNA cleavage phenomenon is also present in *S. venezuelae*, and if so, whether the 3′ fragments are significantly stabilized in the Δ*rnj* mutant.

6.2.3 Deletion of *rnj* or *rnc* from *S. venezuelae* leads to changes in the transcript abundance of genes involved in nitrogen and phosphate acquisition and usage

In addition to investigating the phenotypes of the RNase mutants, we also used RNA-sequencing to compare the transcript profiles of the Δ*rnj,* Δ*rnc,* and wild type *S. venezuelae* strains. We observed the most significant changes in transcript abundance in

genes related to nitrogen assimilation during middle and late stages of growth. For example, transcript levels for *nirB*—encoding a nitrite reductase subunit— increased >200 fold in abundance in the RNase mutants relative to the wild type at sporulation. Other genes whose transcript levels were significantly increased in abundance included genes encoding nitrate transporters and reductases, an ammonium transporter (*amtB*), one of the two major glutamine synthetases in *S. venezuelae,* and several nitrogen assimilation regulatory proteins (*glnK, glnD, nnaR*). Although we observed similar changes for the same sets of genes in both the Δ*rnc* and Δ*rnj* mutants, the trend was more dramatic in the Δ*rnj* mutant. A visual summary of the relationship between the differentially abundant genes and their regulators is shown in Figure 6.1.

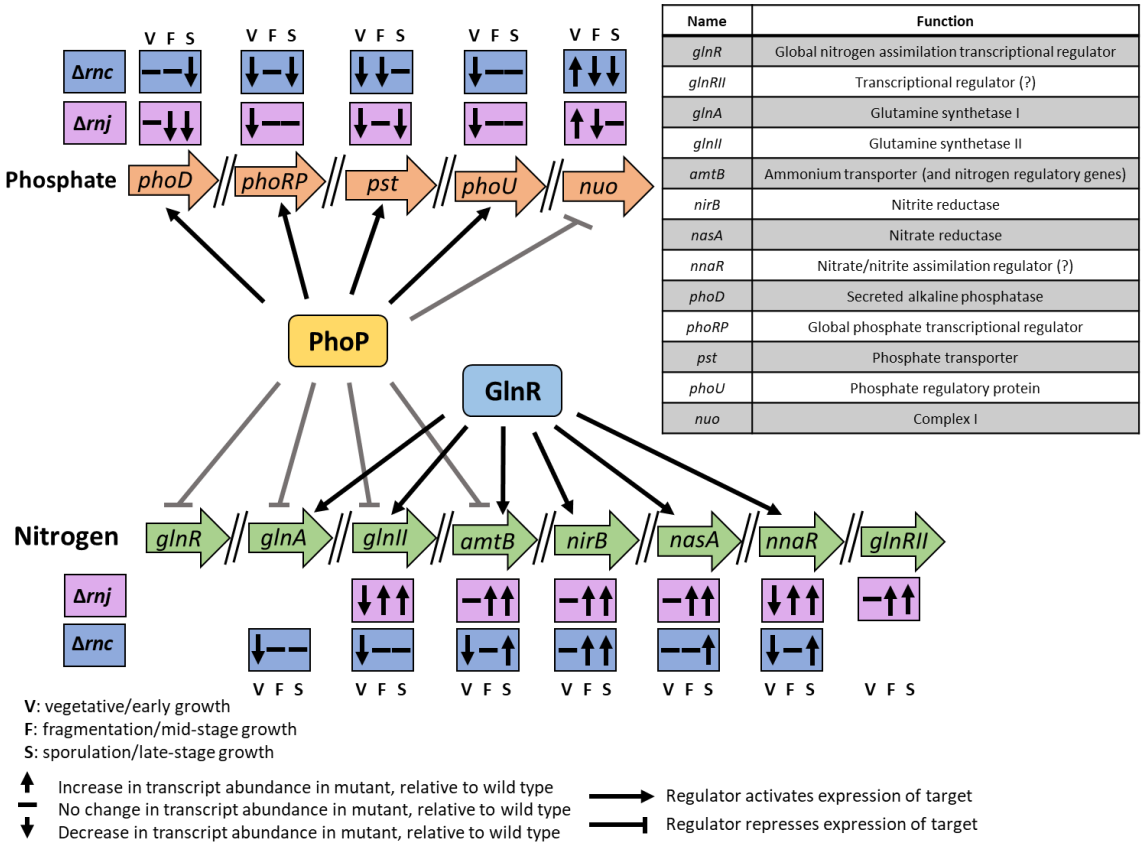

Name	Function
glnR	Global nitrogen assimilation transcriptional regulator
glnRII	Transcriptional regulator (?)
glnA	Glutamine synthetase I
glnII	Glutamine synthetase II
amtB	Ammonium transporter (and nitrogen regulatory genes)
nirB	Nitrite reductase
nasA	Nitrate reductase
nnaR	Nitrate/nitrite assimilation regulator (?)
phoD	Secreted alkaline phosphatase
phoRP	Global phosphate transcriptional regulator
pst	Phosphate transporter
phoU	Phosphate regulatory protein
nuo	Complex I

Figure 6.1. Schematic of phosphate and nitrogen regulatory relationships and changes in transcript abundance of genes between the wild type and RNase mutant strains.

Further investigation revealed that almost all of the nitrogen assimilation genes whose transcript abundance was altered were part of the GlnR regulon. Under nitrogen-limited growth conditions, GlnR activates the expression of genes involved in nitrogen assimilation, including those encoding nitrate and ammonium transporters, assimilatory nitrate/nitrite reductases, and glutamine synthetases (26). The increase in transcript abundance observed for the GlnR-regulated genes found in the RNase mutants is not the result of increased *glnR* transcript levels and increased GlnR, as *glnR* transcript abundance did not change significantly in either mutant across the developmental timepoints relative to the wild type. One possibility is that the activity of GlnR is modulated post-translationally under these conditions in *S. venezuelae*.

There is evidence for the post-translational modification of GlnR in *S. coelicolor,* where GlnR is phosphorylated on serine and threonine residues under nitrogen-rich conditions and is dephosphorylated under nitrogen-limited conditions (15). When GlnR is phosphorylated, it is unable to bind its target promoters (15). Of the eight phosphorylated residues in *S. coelicolor* GlnR, five are conserved and located in the predicted DNA-binding domain of *S. venezuelae* GlnR, suggesting that phosphorylation may also impact GlnR activity in *S. venezuelae*. However, at this point it is not known what protein might be responsible for phosphorylating GlnR. There are at least 45 proteins with annotated serine/threonine kinase domains in *S. venezuelae*, several of which are conserved in *S. coelicolor* (where the GlnR phosphorylation work was done). Further work assessing differences in the expression and behaviour of these kinases, and in GlnR phosphorylation patterns in the wild type and RNase mutant *S. venezuelae* strains, would provide valuable insight into the regulation of GlnR and its targets.

Changes in the transcript abundance of the nitrogen assimilation regulatory gene *nnaR* (*vnz_13340*) may also contribute to the observed changes in other nitrogen assimilation genes. In *S. coelicolor nnaR* is both a target of GlnR and a co-activator of nitrate/nitrite assimilation genes, specifically *nirB, nasA,* and *narK* (101). In *S.*

venezuelae, the *nnaR* promoter region is associated *in vivo* with GlnR, but is not directly bound by the protein *in vitro* (93). *nnaR* transcripts were significantly more abundant relative to the wild type in both of our RNase mutants during later stages of growth, but from the RNA-sequencing data alone it is not possible to determine if this is one of the causes of increased abundance of the other nitrogen assimilation genes. We have deleted *nnaR* separately in the *S. venezuelae* wild type, Δ*rnc,* and Δ*rnj* backgrounds (Table 3.1 and Supplemental Methods) and will be using these strains in future experiments to investigate the potential effects of *nnaR* in the context of RNase III and J.

We did not observe changes in transcript abundance between the wild type and RNase mutant strains in *relA*, which encodes the major ppGpp producing enzyme in *Streptomyces.* We did observe changes in the transcript levels of *rshA*. In *S. coelicolor,* increased transcription of *rshA* is linked to the accumulation of ppGpp during later stages of growth (102). Although it is not possible to tell from just the RNA-sequencing data whether the increased transcript abundance of *rshA* during vegetative growth (and the decreased abundance during late stage growth) is due to stabilization effects or changes in transcription, the connection is intriguing. Reporter assays with the *rshA* promoter and stability assays for the *rshA* transcript in the wild type and RNase mutant *S. venezuelae* strains could shed light on the mechanism underlying its increased and decreased transcript levels.

Another factor that must be considered within this regulatory network is the global phosphate regulator, PhoP. Of all the metabolic and developmental regulators that we investigated in our RNA-sequencing data, the genes with the most significantly altered transcript levels from the wild type to the RNase mutants were the two genes that encode the PhoRP two-component system. This system responds to phosphate-limited growth conditions by upregulating genes involved in phosphate uptake (29). PhoR is a kinase that auto-phosphorylates under low phosphate growth conditions and then transfers the phosphate group to the transcriptional regulator PhoP (29). In both of

the RNase mutants we found *phoR* and *phoP* had significantly lower transcript levels relative to the wild type during vegetative growth. PhoP competes with GlnR to bind the promoters of several nitrogen assimilation genes and, when bound, represses their expression; its target promoters include *glnR*, *glnA* and *glnII* (glutamine synthetases), and *amtB* (ammonium transporter) (30). If PhoP was less abundant in the RNase mutants, as is suggested by the RNA-sequencing data, then GlnR would have less competition in binding to their shared targets, potentially leading to a concomitant increase in transcription of these shared target genes.

We are in the process of creating a *phoP* overexpression construct that can be integrated into the chromosome of the Δ*rnj*, Δ*rnc,* and wild type *S. venezuelae* strains. If a loss of competition between GlnR and PhoP is responsible for the dysregulation of downstream genes like *nirB* and *glnII*, then overexpression of *phoP* should return the transcript levels of these genes in the mutants to near wild type levels. This will also help us to determine what effects are the result of changes in *phoP* and what is specific to the loss of RNase J or III.

There is evidence for a connection between the PhoP regulon and RNase J in *B. subtilis.* In a *B. subtilis* strain where the two paralogs of *rnj* were either deleted (*rnjB*) or depleted (*rnjA*), transcripts for 14 genes in the PhoP regulon (excluding *phoP* itself) were more abundant in the mutant compared to the wild type (47). Interestingly, this is the opposite trend of what we observed in our data from the Δ*rnj S. venezuelae* strain, where *phoP* and genes in the PhoP regulon were significantly lower in transcript abundance.

Work in *S. coelicolor* has also linked RNase III with phosphate and nitrogen metabolism. RNA-sequencing data comparing a Δ*rnc* strain of *S. coelicolor* with the wild type revealed that a gene encoding a glutamine synthetase, and genes in the PhoP regulon, both had higher transcript levels in the *rnc* mutant (103). RNA-sequencing was coupled with RNA-immunoprecipitation using a catalytically inactive RNase III protein to

identify specific transcripts targeted by RNase III in *S. coelicolor* (103). *phoR*, *pstS,* and *glnA* were all transcripts associated with RNase III in the immunoprecipitation assays and were more abundant in the *rnc* mutant (103). If RNase III directly targeted *phoR, pstS* and *glnA* in *S. venezuelae* then we would expect their transcript abundance to increase in the Δ*rnc* strain. What we found, however, was that *phoR* and *pstS* transcript levels both decreased in our *S. venezuelae* Δ*rnc* strain, which indicates that these transcripts are more likely indirectly affected by RNase III in *S. venezuelae.*

6.2.4 The deletion of *rnj* or *rnc* from *S. venezuelae* affects the transcript levels of genes in biosynthetic clusters

We also investigated transcript level changes in genes within annotated biosynthetic clusters in *S. venezuelae.* We found five biosynthetic clusters that contained regions with altered transcript abundance, as well as changes in the transcript levels of multiple regulators of specialized metabolism, including the gene for the nucleoid-associated protein Lsr2.

Lsr2 is a global repressor of biosynthetic clusters, so the decrease in *lsr2* in the RNase mutants during vegetative growth might account for the early increase in the transcript abundance of genes in Lsr2-targeted biosynthetic clusters (88). The fact that most biosynthetic cluster genes that had altered transcript levels were located near known Lsr2 binding locations adds support to this hypothesis. However, the specific connection between the loss of RNase III or J and the decrease in *lsr2* remains elusive; perhaps *lsr2* is connected to other metabolic and biosynthetic regulators that we observed changing in the RNase mutants.

Inorganic phosphate availability is also linked to specialized metabolism in *Streptomyces,* where abundant phosphate represses the production of specialized compounds (104). As discussed in section 5.5.1, we found that there were major changes in the transcript abundance of genes that regulate and participate in phosphate uptake. In *S. coelicolor,* PhoP (active under phosphate limitation) activates the

expression of *afsS*, which in turn activates pathway specific regulators for the antibiotic clusters that produce actinorhodin and undecylprodigiosin (105). The *afsS* promoter is also bound by the regulator AfsR, which responds to *S*-adenosylmethionine concentrations (105). AfsR and PhoP are both activators of *afsS*, but they compete for binding in the *afsS* promoter region (105). We did not observe any significant changes in the transcript abundance of *afsR,* while *afsS* transcript abundance was only significantly lower at one time point in the Δ*rnc* mutant. The molecular mechanisms of the phosphate effect in *S. venezuelae* are not as well defined as in *S. coelicolor*. However, if PhoP and AfsR share a similar relationship in *S. venezuelae* as they do in *S. coelicolor,* then perhaps a change in PhoP abundance affects the competitive balance between PhoP and AfsR, with downstream effects on antibiotic production.

A final consideration is whether or not the chloramphenicol compound (which is the product of the most dramatically and consistently affected cluster in the RNase mutants) is actually produced in excess in the RNase mutants compared with the wild type. Screening for inhibitory activity from the Δ*rnc* and Δ*rnj* strains using bioassays against indicator organisms, coupled with HPLC analyses, would allow us to determine whether increased transcription of the chloramphenicol cluster is associated with increased production of the chloramphenicol molecule in the RNase mutants.

6.2.5 The specific roles of RNase J or III in mediating transcriptional and metabolic change

Previous work has reported on the various phenotypic and biosynthetic effects of deleting *rnj* or *rnc* from *Streptomyces* species (43, 44, 53). We have shown here that these phenotypic changes are accompanied by a dramatic alteration in the transcript abundance of genes involved in primary and specialized metabolism in the RNase mutants. And while we are beginning to unravel the relationships between these metabolic genes and their regulators, the question remains: why does the loss of RNase J or III from *S. venezuelae* result in these specific changes?

With just our time course data, it is difficult to say whether changes in the transcript abundance of specific genes are the result of direct or indirect RNase effects. However, in the context of the many metabolism-associated genes we identified as being more abundant in the mutants (*nirB, nasA, glnII, amtB,* etc.), it seems unlikely that all these changes are the result of direct transcript stabilization due to the deletion of RNase J or III. In the case of *phoRP* and several genes in the PhoP regulon that were less abundant in the RNase mutants, the effect of RNase III or J is certainly indirect.

Beyond rRNA precursors, several direct targets have been identified each for RNase J and RNase III in common model organisms. In *B. subtilis,* RNase J was originally identified for its ability to cleave *thrS* (threonyl-tRNA synthetase) leader RNA; cleavage in the leader region of this transcript stabilizes the downstream transcript (48). RNase J also targets *glmS* RNA in *B. subtilis* (106). The 5' UTR of the *glmS* transcript forms a ribozyme that is activated by glucosamine-6-phosphate to self-cleave and the downstream fragment is then accessible for degradation by RNase J (106). RNase III targets a hairpin structure in its own mRNA transcript to autoregulate its expression (107). It has also been implicated in mediating multiple toxin antitoxin systems. For example, in *E. coli,* RNase III targets the *lstR-1/tisAB* complex and degrades the *tisB* toxin mRNA (108). As discussed in section 6.2.3, RNA-immunoprecipitation assays in *S. coelicolor* have also identified many RNase III-associated target RNA molecules, with the expectation that some are directly cleaved by RNase III while others may only be bound by RNase III (103).

One tool that will help us elucidate the direct effects of RNase J and III in *S. venezuelae* is the FLAG-tagged catalytically inactive and active RNase constructs that we created. RNA-immunoprecipitation with catalytically inactive RNases has been used successfully in *S. coelicolor* to identify targets of RNase III and it is a technique that will allow us to clarify the specific and direct effects of RNase J and III in *S. venezuelae* (103). Transcripts that are identified in these immunoprecipitation assays can be correlated

with our RNA-sequencing data to determine if RNase J or III directly target them. We have not yet been able to confirm the expression of our FLAG-tagged RNase J construct by western blot in *S. venezuelae,* but we know that introducing the active and inactive RNase J constructs into a Δ*rnj S. venezuelae* background resulted in the expected phenotypes so our attention will be focused on optimizing tag detection.

The link between deleting these RNases and the associated changes in transcript levels of various genes may also stem from changes in RNA polymerase activity or ribosome availability. In both the Δ*rnj* and Δ*rnc* strains, there is an accumulation of inactive ribosome dimers (44). Actively translating ribosomes help to stabilize most mRNA transcripts (by occluding RNase access to this RNA substrate) and a reduction in the number of active ribosomes could decrease transcript stability (37). Furthermore, recent work in *B. subtilis* revealed that RNase J has an additional quality control function where it can help dislodge stalled RNA polymerase (RNAP) complexes; a Δ*rnj* mutant in *B. subtilis* had increased coverage of RNAP on DNA, but decreased transcript abundance for several genes as a result of stalling RNAP (41). The “torpedo effect” by which RNase J functions to remove stalled RNAP complexes in *B. subtilis* depends on its 5’-3’ exonuclease activity (41). As this activity and directionality have been shown for RNase J in *Streptomyces,* it is conceivable that RNase J may have a similar quality control role in *S. venezuelae* (41, 53). In this case, loss of RNase J from *S. venezuelae* could lead to decreased transcriptional activity and reduced transcript abundance, which could impact downstream metabolic responses. Perhaps these indirect effects could explain the decrease in transcript abundance of *phoR* and *phoP*, which in turn could affect the activity of other global metabolic regulators and the expression of their targets.

7. Conclusion

In this work, we explored two components of gene regulation in *S. venezuelae*, namely G-quadruplex structures and RNases. We were unable to draw conclusions about an interaction between TrmB and GQs in *S. venezuelae*, but these structures remain of interest in GC-rich bacteria like *Streptomyces*. Our work to define the transcript profiles of Δ*rnj* and Δ*rnc S. venezuelae* mutants revealed surprising changes in the transcript levels of genes whose products are involved in multiple metabolic networks and in the regulation of many biosynthetic clusters. Taken together this work highlights the interconnected nature of development and both primary and specialized metabolism in *S. venezuelae*. It demonstrates a central role for RNases in the regulation of these major cellular functions and presents many exciting directions for future investigation.

References

1. Browning DF, Busby SJW. 2004. The regulation of bacterial transcription initiation. Nat Rev Microbiol 2:57–65.

2. Perez-Rueda E. 2000. The repertoire of DNA-binding transcriptional regulators in *Escherichia coli* K-12. Nucleic Acids Res 28:1838–1847.

3. Maeda H, Fujita N, Ishihama A. 2000. Competition among seven *Escherichia coli* sigma subunits: relative binding affinities to the core RNA polymerase. Nucleic Acids Res 28:3497–3503.

4. Barker MM, Gaal T, Gourse RL. 2001. Mechanism of regulation of transcription initiation by ppGpp. II. Models for positive control based on properties of RNAP mutants and competition for RNAP. J Mol Biol 305:689–702.

5. Hajnsdorf E, Régnier P. 2000. Host factor Hfq of *Escherichia coli* stimulates elongation of poly(A) tails by poly(A) polymerase I. Proc Natl Acad Sci U S A 97:1501–1505.

6. Santiago-Frangos A, Woodson SA. 2018. Hfq chaperone brings speed dating to bacterial sRNA. Wiley Interdiscip Rev RNA 9:1–16.

7. Fröhlich KS, Papenfort K, Fekete A, Vogel J. 2013. A small RNA activates CFA synthase by isoform-specific mRNA stabilization. EMBO J 32:2963–2979.

8. Massé E, Escorcia FE, Gottesman S. 2003. Coupled degradation of a small regulatory RNA and its mRNA targets in *Escherichia coli*. Genes Dev 17:2374–2383.

9. Soper T, Mandin P, Majdalani N, Gottesman S, Woodson SA. 2010. Positive regulation by small RNAs and the role of Hfq. Proc Natl Acad Sci U S A 107:9602–9607.

10. Geissmann T, Marzi S, Romby P. 2009. The role of mRNA structure in translational control in bacteria. RNA Biol 6:153–160.

11. Ito K, Chiba S, Pogliano K. 2010. Divergent stalling sequences sense and control cellular physiology. Biochem Biophys Res Commun 393:1–5.

12. Bedouelle H, Bassford PJ, Fowler A V., Zabin I, Beckwith J, Hofnung M. 1980. Mutations which alter the function of the signal sequence of the maltose binding protein of *Escherichia coli*. Nature 285:78–81.

13. Keiler KC, Waller PRH, Sauer RT. 1996. Role of a peptide tagging system in degradation of proteins synthesized from damaged messenger RNA. Science (80-) 271:990–993.

14. Fink D, Weißschuh N, Reuther J, Wohlleben W, Engels A. 2002. Two transcriptional regulators GlnR and GlnRII are involved in regulation of nitrogen metabolism in *Streptomyces coelicolor* A3(2). Mol Microbiol 46:331–347.

15. Amin R, Franz-Wachtel M, Tiffert Y, Heberer M, Meky M, Ahmed Y, Matthews A, Krysenko S, Jakobi M, Hinder M, Moore J, Okoniewski N, Macek B, Wohlleben W, Bera A. 2016. Post-translational serine/threonine phosphorylation and lysine acetylation: A novel regulatory aspect of the global nitrogen response regulator GlnR in *S. coelicolor* M145. Front Mol Biosci 3:1–14.

16. Flärdh K, Buttner MJ. 2009. *Streptomyces* morphogenetics: dissecting differentiation in a filamentous bacterium. Nat Rev Microbiol 7:36–49.

17. Jones SE, Ho L, Rees CA, Hill JE, Nodwell JR, Elliot MA. 2017. *Streptomyces* exploration is triggered by fungal interactions and volatile signals. elife 6:1–21.

18. Bentley S, Chater K, Cerdeño-Tárraga A-M, Challis GL, Thomson NR, James KD, Harris DE, Quail MA, Kieser H, Harper D, Bateman A, Brown S, Chandra G, Chen CW, Collins M, Cronin A, Fraser A, Goble A, Hidalgo J, Hornsby T, Howarth S, Huang C-H, Kieser T, Larke L, Murphy L, Oliver K, O'Neil S, Rabbinowitsch E, Rajandream M-A, Rutherford K, Rutter S, Seeger K, Saunders D, Sharp S, Squares R, Squares S, Taylor K, Warren T, Wietzorrek A, Woodward J, Barrell BG, Parkhill J, Hopwood DA. 2002. Complete genome sequence of the model actinomycete *Streptomyces coelicolor* A3(2). Nature 417:141–147.

19. Nett M, Ikeda H, Moore BS. 2009. Genomic basis for natural product biosynthetic diversity in the actinomycetes. Nat Prod Rep 26:1362–1384.

20. Merrick MJ, Edwards RA. 1995. Nitrogen Control in Bacteria. Microbiol Rev 59:1–19.

21. Snyder L, Henkin TM, Peters JE, Champness W. 2013. Molecular Genetics of Bacteria, 4th Edition, 4th ed. American Society of Microbiology, Washington, D.C. 83, 536-544.

22. Fink D, Falke D, Wohlleben W, Engels A. 1999. Nitrogen metabolism in *Streptomyces coelicolor* A3(2): Modification of glutamine synthetase I by an adenylyltransferase. Microbiology 145:2313–2322.

23. Wohlleben W, Mast Y, Reuther J. 2011. Regulation of Nitrogen Assimilation in *Streptomyces* and other Actinobacteria., p. 125–136. *In* Dyson, P (ed.), Streptomyces Molecular Biology and Biotechnology. Caister Academic Press, Norfolk. 1-14

24. Rexer HU, Schäberle T, Wohlleben W, Engels A. 2006. Investigation of the functional properties and regulation of three glutamine synthetase-like genes in *Streptomyces coelicolor* A3(2). Arch Microbiol 186:447–458.

25. Hesketh A, Fink D, Gust B, Rexer HU, Scheel B, Chater K, Wohlleben W, Engels A. 2002. The GlnD and GlnK homologues of *Streptomyces coelicolor* A3(2) are functionally dissimilar to their nitrogen regulatory system counterparts from enteric bacteria. Mol Microbiol 46:319–330.

26. Tiffert Y, Supra P, Wurm R, Wohlleben W, Wagner R, Reuther J. 2008. The *Streptomyces coelicolor* GlnR regulon: Identification of new GlnR targets and evidence for a central role of GlnR in nitrogen metabolism in actinomycetes. Mol Microbiol 67:861–880.

27. Sola-Landa A, Rodríguez-García A, Franco-Domínguez E, Martín JF. 2005. Binding of PhoP to promoters of phosphate-regulated genes in *Streptomyces coelicolor*: Identification of PHO boxes. Mol Microbiol 56:1373–1385.

28. Santos-Beneit F. 2015. The Pho regulon: A huge regulatory network in bacteria. Front Microbiol 6:1–13.

29. Sola-Landa A, Moura RS, Martin JF. 2003. The two-componenet PhoR-PhoP system controls both primary metabolism and secondary metabolite biosynthesis in *Streptomyces lividans*. Proc Natl Acad Sci 100:6133–6138.

30. Rodríguez-García A, Sola-landa A, Apel K, Santos-Beneit F, Martín JF. 2009. Phosphate control over nitrogen metabolism in *Streptomyces coelicolor*: Direct and indirect negative control of *glnR, glnA, glnII* and *amtB* expression by the response regulator PhoP. Nucleic Acids Res 37:3230–3242.

31. Sola-Landa A, Rodríguez-García A, Amin R, Wohlleben W, Martín JF. 2013. Competition between the GlnR and PhoP regulators for the *glnA* and *amtB* promoters in *Streptomyces coelicolor*. Nucleic Acids Res 41:1767–1782.

32. Zhu Y, Zhang P, Zhang J, Xu W, Wang X, Wu L, Sheng D, Ma W, Cao G, Chen X lan, Lu Y, Zhang YZ, Pang X. 2019. The developmental regulator MtrA binds GlnR boxes and represses nitrogen metabolism genes in *Streptomyces coelicolor*. Mol Microbiol 112:29–46.

33. Hong SK, Kito M, Beppu T, Horinouchi S. 1991. Phosphorylation of the AfsR product, a global regulatory protein for secondary-metabolite formation in *Streptomyces coelicolor* A3(2). J Bacteriol 173:2311–2318.

34. Lee PC, Umeyama T, Horinouchi S. 2002. *afsS* is a target of AfsR, a transcriptional factor with ATPase activity that globally controls secondary metabolism in *Streptomyces coelicolor* A3(2). Mol Microbiol 43:1413–1430.

35. Santos-Beneit F, Rodríguez-García A, Martín JF. 2012. Overlapping binding of PhoP and AfsR to the promoter region of *glnR* in *Streptomyces coelicolor*. Microbiol Res 167:532–535.

36. Santos-Beneit F, Rodríguez-García A, Sola-Landa A, Martín JF. 2009. Cross-talk between two global regulators in *Streptomyces*: PhoP and AfsR interact in the control of *afsS, pstS* and *phoRP* transcription. Mol Microbiol 72:53–68.

37. Arraiano CM, Andrade JM, Domingues S, Guinote IB, Malecki M, Matos RG, Moreira RN, Pobre V, Reis FP, Saramago M, Silva IJ, Viegas SC. 2010. The critical role of RNA processing and degradation in the control of gene expression. FEMS Microbiol Rev 34:883–923.

38. Durand S, Gilet L, Bessières P, Nicolas P, Condon C. 2012. Three essential ribonucleases-RNase Y, J1, and III-control the abundance of a majority of *Bacillus subtilis* mRNAs. PLoS Genet 8:1–14.

39. Li Z, Deutscher MP. 2002. RNase E plays an essential role in the maturation of *Escherichia coli* tRNA precursors. RNA 8:97–109.

40. Jacob AI, Köhrer C, Davies BW, RajBhandary UL, Walker GC. 2013. Conserved Bacterial RNase YbeY Plays Key Roles in 70S Ribosome Quality Control and 16S rRNA Maturation. Mol Cell 49:427–438.

41. Šiková M, Wiedermannová J, Převorovský M, Barvík I, Sudzinová P, Kofroňová O, Benada O, Šanderová H, Condon C, Krásný L. 2020. The torpedo effect in *Bacillus subtilis*: RNase J1 resolves stalled transcription complexes. EMBO J 39:1–17.

42. Sohlberg B, Huang J, Cohen SN. 2003. The *Streptomyces coelicolor* polynucleotid phosphorylase homologue, and not the putative poly(A) polymerase, can polyadenylate RNA. J Bacteriol 185:7273–7278.

43. Price B, Adamidis T, Kong R, Champness W. 1999. A *Streptomyces coelicolor* antibiotic regulatory gene, *absB*, encodes an RNase III homolog. J Bacteriol 181:6142–6151.

44. Jones SE, Leong V, Ortega J, Elliot MA. 2014. Development, antibiotic production, and ribosome assembly in *Streptomyces venezuelae* are impacted by RNase J and RNase III deletion. J Bacteriol 196:4253–4267.

45. Mathy N, Bénard L, Pellegrini O, Daou R, Wen T, Condon C. 2007. 5′-to-3′ Exoribonuclease Activity in Bacteria: Role of RNase J1 in rRNA Maturation and 5′ Stability of mRNA. Cell 129:681–692.

46. Mathy N, Hébert A, Mervelet P, Bénard L, Dorléans A, Li De La Sierra-Gallay I, Noirot P, Putzer H, Condon C. 2010. *Bacillus subtilis* ribonucleases J1 and J2 form a complex with altered enzyme behaviour. Mol Microbiol 75:489–498.

47. Mäder U, Zig L, Kretschmer J, Homuth G, Putzer H. 2008. mRNA processing by RNases J1 and J2 affects *Bacillus subtilis* gene expression on a global scale. Mol Microbiol 70:183–196.

48. Even S, Pellegrini O, Zig L, Labas V, Vinh J, Bréchemmier-Baey D, Putzer H. 2005. Ribonucleases J1 and J2: Two novel endoribonucleases in *B.subtilis* with functional homology to *E.coli* RNase E. Nucleic Acids Res 33:2141–2152.

49. Durand S, Tomasini A, Braun F, Condon C, Romby P. 2015. sRNA and mRNA turnover in Gram-positive bacteria. FEMS Microbiol Rev 39:316–330.

50. Britton RA, Wen T, Schaefer L, Pellegrini O, Uicker WC, Mathy N, Tobin C, Daou R, Szyk J, Condon C. 2007. Maturation of the 5′ end of *Bacillus subtilis* 16S rRNA by the essential ribonuclease YkqC/RNase J1. Mol Microbiol 63:127–138.

51. Mäder U, Zig L, Kretschmer J, Homuth G, Putzer H. 2008. mRNA processing by RNases J1 and J2 affects *Bacillus subtilis* gene expression on a global scale. Mol Microbiol 70:183–196.

52. Condon C. 2010. What is the role of RNase J in mRNA turnover? RNA Biol 7:316–321.

53. Bralley P, Aseem M, Jones GH. 2014. SCO5745, a Bifunctional RNase J Ortholog, affects antibiotic production in *Streptomyces coelicolor*. J Bacteriol 196:1197–1205.

54. Nicholson AW. 2014. Ribonuclease III mechanisms of double-stranded RNA cleavage. Wiley Interdiscip Rev RNA 5:31–48.

55. Court DL, Gan J, Liang Y-H, Shaw GX, Tropea JE, Costantino N, Waugh DS, Ji X. 2013. RNase III: Genetics and Function; Structure and Mechanism. Annu Rev Genet 47:405–431.

56. Blaszczyk J, Tropea JE, Bubunenko M, Routzahn KM, Waugh DS, Court DL, Ji X. 2001. Crystallographic and modeling studies of RNase III suggest a mechanism for double-stranded RNA cleavage. Structure 9:1225–1236.

57. Gegenheimer P, Apirion D. 1980. Precursors to 16S and 23S ribosomal RNA from a ribonuclease III- strain of *Escherichia coli* contain intact RNase III processing sites. Nucleic Acids Res 8:1873–1891.

58. Srivastava AK, Schlessinger D. 1990. Mechanism and Regulation of Bacterial Ribosomal RNA Processing. Annu Rev Microbiol 44:105–29.

59. Viegas SC, Silva IJ, Saramago M, Domingues S, Arraiano CM. 2011. Regulation of the small regulatory RNA MicA by ribonuclease III: A target-dependent pathway. Nucleic Acids Res 39:2918–2930.

60. Gravenbeek ML, Jones GH. 2008. The endonuclease activity of RNase III is required for the regulation of antibiotic production by *Streptomyces coelicolor*. Microbiology 154:3547–3555.

61. Bochman ML, Paeschke K, Zakian VA. 2012. DNA secondary structures: Stability and function of G-quadruplex structures. Nat Rev Genet 13:770–780.

62. Han H, Hurley LH, Salazar M. 1999. A DNA polymerase stop assay for G-quadruplex-interactive compounds. Nucleic Acids Res 27:537–542.

63. Shao X, Zhang W, Umar MI, Wong HY, Seng Z, Xie Y, Zhang Y, Yang L, Kwok CK, Deng X. 2020. RNA G-Quadruplex Structures Mediate Gene Regulation in Bacteria. mBio 11:1–15.

64. Saranathan N, Vivekanandan P. 2018. G-Quadruplexes: More Than Just a Kink in Microbial Genomes. Trends Microbiol 27:148–163.

65. Patel DJ, Phan AT, Kuryavyi V. 2007. Human telomere, oncogenic promoter and 5'-UTR G-quadruplexes: Diverse higher order DNA and RNA targets for cancer therapeutics. Nucleic Acids Res 35:7429–7455.

66. Waller ZAE, Pinchbeck BJ, Buguth BS, Meadows TG, Richardson DJ, Gates AJ. 2016. Control of bacterial nitrate assimilation by stabilization of G-quadruplex DNA. Chem Commun 52:13511–13514.

67. Kuryavyi V, Cahoon LA, Seifert HS, Patel DJ. 2012. RecA-binding pilE G4 sequence essential for pilin antigenic variation forms monomeric and 5' end-stacked dimeric parallel G-quadruplexes. Structure 20:2090–2102.

68. Colameco S. 2018. Characterizing G-quadruplexes, a novel regulatory element, in Streptomyces bacteria. McMaster University.

69. De Bie LGS, Roovers M, Oudjama Y, Wattiez R, Tricot C, Stalon V, Droogmans L, Bujnicki JM. 2003. The *yggH* Gene of *Escherichia coli* Encodes a tRNA (m 7 G46) Methyltransferase. J Bacteriol 185:3238–3243.

70. Kou Y, Koag MC, Lee S. 2015. N7 Methylation Alters Hydrogen-Bonding Patterns of Guanine in Duplex DNA. J Am Chem Soc 137:14067–14070.

71. Rana AK, Ankri S. 2016. Reviving the RNA world: An insight into the appearance of RNA methyltransferases. Front Genet 7:1–9.

72. Gust B, Challis GL, Fowler K, Kieser T, Chater KF. 2003. PCR-targeted *Streptomyces* gene replacement identifies a protein domain needed for biosynthesis of the sesquiterpene soil odor geosmin. Proc Natl Acad Sci U S A 100:1541–1546.

73. MacNeil DJ, Gewain KM, Ruby CL, Dezeny G, Gibbons PH, MacNeil T. 1992. Analysis of *Streptomyces avermitilis* genes required for avermectin biosynthesis utilizing a novel integration vector. Gene 111:61–68.

74. Bush MJ, Chandra G, Al-Bassam MM, Findlay KC, Buttner MJ. 2019. BldC delays entry into development to produce a sustained period of vegetative growth in *Streptomyces venezuelae*. mBio 10:1–16.

75. Gregory M a, Smith MCM. 2003. Integration Site for Phage ΦBT1 and Development of Site-Specific Integrating Vectors. J Bacteriol 185:5320–5323.

76. Bolger AM, Lohse M, Usadel B. 2014. Trimmomatic: A flexible trimmer for Illumina sequence data. Bioinformatics 30:2114–2120.

77. Andrews S. 2010. FastQC: a quality control tool for high throughout sequence data.

78. Langmead B, Salzberg SL. 2012. Fast gapped-read alignment with Bowtie 2. Nat Methods 9:357–359.

79. Li H, Handsaker B, Wysoker A, Fennell T, Ruan J, Homer N, Marth G, Abecasis G, Durbin R. 2009. The Sequence Alignment/Map format and SAMtools. Bioinformatics 25:2078–2079.

80. James T Robinson, Thorvaldsdóttir H, Winckler W, Guttman M, Lander ES, Getz G, Mesirov JP. 2011. Integrative genomics viewer. Nat Biotechnol 29:24–26.

81. Anders S, Pyl PT, Huber W. 2015. HTSeq-A Python framework to work with high-throughput sequencing data. Bioinformatics 31:166–169.

82. Love MI, Huber W, Anders S. 2014. Moderated estimation of fold change and dispersion for RNA-seq data with DESeq2. Genome Biol 15:1–21.

83. Pall GS, Hamilton AJ. 2008. Improved northern blot method for enhanced detection of small RNA. Nat Protoc 3:1077–1084.

84. Sun W, Nicholson AW. 2001. Mechanism of action of *Escherichia coli* ribonuclease III. Stringent chemical requirement for the Glutamic acid 117 side chain and Mn2+ rescue of the Glu117Asp mutant. Biochemistry 40:5102–5110.

85. Bradford MM. 1976. A Rapid and Sensitive Method for the Quantification of Microgram Quantities of Protein Utilizing the Principle of Protein-Dye Binding. Anal Biochem 72:248–254.

86. Tomikawa C, Takai K, Hori H. 2017. Kinetic characterization of substrate-binding sites of thermostable tRNA methyltransferase (TrmB). J Biochem 163:133–142.

87. Rhodes D, Lipps HJ. 2015. G-quadruplexes and their regulatory roles in biology. Nucleic Acids Res 43:8627–8637.

88. Gehrke EJ, Zhang X, Pimentel-Elardo SM, Johnson AR, Rees CA, Jones SE, Hindra, Gehrke SS, Turvey S, Boursalie S, Hill JE, Carlson EE, Nodwell JR, Elliot MA. 2019. Silencing cryptic specialized metabolism in *Streptomyces* by the nucleoid-associated protein Lsr2. elife 8:1–28.

89. Medema MH, Blin K, Cimermancic P, De Jager V, Zakrzewski P, Fischbach MA, Weber T, Takano E, Breitling R. 2011. antiSMASH: Rapid identification, annotation and analysis of secondary metabolite biosynthesis gene clusters in bacterial and fungal genome sequences. Nucleic Acids Res 39:339–346.

90. Swiercz JP, Nanji T, Gloyd M, Guarné A, Elliot MA. 2013. A novel nucleoid-associated protein specific to the actinobacteria. Nucleic Acids Res 41:4171–4184.

91. Yang YH, Song E, Lee BR, Kim EJ, Park SH, Kim YG, Lee CS, Kim BG. 2010. Rapid functional screening of *Streptomyces coelicolor* regulators by use of a pH indicator and application to the MarR-Like regulator AbsC. Appl Environ Microbiol 76:3645–3656.

92. Martín JF, Liras P. 2020. The balance metabolism safety net: integration of stress signals by interacting transcriptional factors in *Streptomyces* and related actinobacteria. Front Microbiol 10:1–19.

93. Pullan ST, Chandra G, Bibb MJ, Merrick M. 2011. Genome-wide analysis of the role of GlnR in Streptomyces venezuelae provides new insights into global nitrogen regulation in actinomycetes. BMC Genomics 12:1–14.

94. Allenby NEE, Laing E, Bucca G, Kierzek AM, Smith CP. 2012. Diverse control of metabolism and other cellular processes in *Streptomyces coelicolor* by the PhoP transcription factor: genome-wide identification of *in vivo* targets. Nucleic Acids Res 40:9543–9556.

95. Kimura T, Kobayashi K. 2020. Role of glutamate synthase in biofilm formation by *Bacillus subtilis*. J Bacteriol 202:1–17.

96. McManus SA, Li Y. 2008. A Deoxyribozyme with a Novel Guanine Quartet-Helix Pseudoknot Structure. J Mol Biol 375:960–968.

97. Okamoto H, Watanabe K, Ikeuchi Y, Suzuki T, Endo Y, Hori H. 2004. Substrate tRNA recognition mechanism of tRNA (m7G46) methyltransferase from *Aquifex aeolicus*. J Biol Chem 279:49151–49159.

98. Tauchi T, Shin-Ya K, Sashida G, Sumi M, Okabe S, Ohyashiki JH, Ohyashiki K. 2006. Telomerase inhibition with a novel G-quadruplex-interactive agent, telomestatin: In vitro and in vivo studies in acute leukemia. Oncogene 25:5719–5725.

99. Figaro S, Durand S, Gilet L, Cayet N, Sachse M, Condon C. 2013. *Bacillus subtilis* mutants with knockouts of the genes encoding ribonucleases RNase Y and RNase J1 are viable, with major defects in cell morphology, sporulation, and competence. J Bacteriol 195:2340–2348.

100. Haiser HJ, Karginov F V, Hannon GJ, Elliot MA. 2008. Developmentally regulated cleavage of tRNAs in the bacterium *Streptomyces coelicolor*. Nucleic Acids Res 36:732–741.

101. Amin R, Reuther J, Bera A, Wohlleben W, Mast Y. 2012. A novel GlnR target gene, *nnaR*, is involved in nitrate/nitrite assimilation in *Streptomyces coelicolor*. Microbiology 158:1172–1182.

102. Sun J, Hesketh A, Bibb MJ. 2001. Functional analysis of *relA* and *rshA*, two *relA/spoT* homologues of *Streptomyces coelicolor* A3(2). J Bacteriol 183:3488–3498.

103. Gatewood ML, Bralley P, Ryan Weil M, Jones GH. 2012. RNA-Seq and RNA immunoprecipitation analyses of the transcriptome of *Streptomyces coelicolor* identify substrates for RNase III. J Bacteriol 12:2228–2237.

104. Martín JF. 2004. Phosphate control of the biosynthesis of antibiotics and other secondary metabolites is mediated by the PhoR-PhoP system: an unfinished story. J Bacteriol 186:5197–5201.

105. Santos-Beneit F, Rodríguez-García A, Martín JF. 2011. Complex transcriptional control of the antibiotic regulator *afsS* in *Streptomyces*: PhoP and AfsR are overlapping, competitive activators. J Bacteriol 193:2242–2251.

106. Collins JA, Irnov I, Baker S, Winkler WC. 2007. Mechanism of mRNA destabilization by the *glmS* ribozyme. Genes Dev 21:3356–3368.

107. Bardwell JCA, Regnier P, Chen SM, Nakamura Y, Grunberg-Manago M, Court DL. 1989. Autoregulation of RNase III operon by mRNA processing. EMBO J 8:3401–3407.

108. Vogel J, Argaman L, Wagner EGH, Altuvia S. 2004. The small RNA lstR inhibits synthesis of an SOS-induced toxic peptide. Curr Biol 14:2271–2276.

109. Livak KJ, Schmittgen TD. 2001. Analysis of relative gene expression data using real-time quantitative PCR and the 2-ΔΔCT method. Methods 25:402–408.

110. Huynh K, Partch CL. 2015. Analysis of protein stability and ligand interations by thermal shift assay. Curr Protoc Protein Sci 79:1–28.

Appendices

A1. Supplemental methods

Genetic modification of the *S. venezuelae* chromosome

The deletion of *nnaR* (*vnz_13340*) from the *S. venezuelae* chromosome (Table 3.1) was done using PCR targeting as previously described (72). Briefly, the cosmid Sv-5-A04, carrying *vnz_13340* was modified to replace *vnz_13340* with a hygromycin B selection marker and origin of transfer to create the cosmid Sv-5-A04 *vnz_13340::hygoriT* (Table 3.2). Successful replacement of *nnaR* with the resistance cassette was confirmed through PCR with primers located at the forward position of the cassette (vnz13340RED_F) and downstream of the wild type gene (vnz13340down_R) (Table 3.4). This cosmid was then introduced to wild type, Δ*rnj*, and Δ*rnc* strains of *S. venezuelae* via conjugation and colonies were screened for a double crossover event (hygromycin B resistance and kanamycin sensitivity) marking the replacement of the gene of interest with the antibiotic resistance cassette. Potential mutants for each background strain were then confirmed through colony PCR on *S. venezuelae* colonies. To confirm the presence and correct location of the cassette, the same PCR reaction with vnz13340RED_F and vnz13340down_R was conducted on the *S. venezuelae* colonies as on the mutant cosmid. Additionally, PCR was also conducted using a primer specific to the internal coding sequence of *vnz_13340* (vnz_13340int_F) and the downstream primer (vnz13340down_R) (Table 3.4). The presence of product from the first reaction and the absence of product from the second reaction confirmed the deletion of *vnz_13340* in each strain.

Collection of *S. venezuelae* for RNA stability assays

S. venezuelae strains were inoculated from overnight cultures to an OD_{600} of 0.05 in 100 mL of MYM medium in a 500 mL baffled flask and then grown for 16 hours. The flask was then removed from the incubator and samples for stability assays were collected by removing 14 mL of culture at each time point and transferring them to a

tube on ice containing 1.35 mL of 95% ethanol and 150 µL of phenol (pH 6.6) (stop growth solution). Samples were immediately vortexed to stop *S. venezuelae* growth. One sample was collected before the addition of rifampicin to the flask (designated 'time 0'), and then samples were collected at 2, 4, 6, 8, and 10 minutes post-rifampicin addition. Rifampicin (working concentration of 50 mg/mL) was added as 0.012 volumes of the amount of culture in the flask. Cells in each sample were collected by centrifugation and RNA was extracted as in section 3.4.

Assessing relative RNA stability with qPCR

Luna® Universal qPCR Master Mix (NEB) was used for qPCR with 2.5 µL of cDNA (1:4 dilution) as template, and primers for genes of interest at a final concentration of 5 pmol/µL. The BioRad CFX96™ Real-Time PCR machine was used for amplification and data were normalized to the 5S rRNA which is considered to be a stable RNA and was not expected to be profoundly impacted by the assay. Analysis of relative RNA abundance was done using the $2^{-\Delta\Delta Ct}$ method (109).

FLAG-tagged immunoprecipitation of FLAG-RNase J constructs

When FLAG-tagged constructs could not be detected within total protein extracts we used immunoprecipitation to pull-down the tagged protein specifically for subsequent blotting. Anti-FLAG® M2 Affinity Gel (Sigma) was used to purify FLAG-tagged RNase J and RNase J H86A from *S. venezuelae* cell lysate. Cells were sub-cultured in liquid MYM medium and 50 mL of culture was collected at 12, 18, and 20 hours of growth then lysed (as described for protein purification). The affinity gel was prepared as per manufacturer's instructions and 20 µL of the gel was added per 1 mL of cell lysate. The samples were mixed overnight on a roller shaker at 4°C and then washed with 1×TBS. Tagged protein was eluted with the addition of 4× SDS-loading dye and boiling at 95°C, as described in the manufacturer's instructions. The supernatant from the boiled protein was then used in subsequent western blotting experiments.

Protein stability assays

A thermal shift assay with fluorescent dye was used to test the stability of TrmB protein in different buffers (110). Approximately 40 µg of protein was mixed with 30 µL of the buffer of interest, either methylation buffer at pH 7.6 or 8.5 (50 mM Tris-HCl, 5 mM $MgCl_2$, 6 mM β-mercaptoethanol, 50 mM KCl), or TrmB storage buffer (5 mM Tris-HCl pH 8.5, 50 mM NaCl, 10% glycerol) and 6 µL of SYPRO Orange. The final volume was brought to 60 µL with MilliQ water and then split into three technical triplicate reactions of 20 µL. Fluorescence values were observed in the BioRad CFX96™ Real-Time PCR machine as the temperature of the sample increased by 1°C intervals from 4°C-95°C.